INTEGRATED HYDROLOGICAL MODELING OF GROUNDWATER RECHARGE AND GROUNDWATER RESOURCES IN THE AUOB CATCHMENT (NAMIBIA)
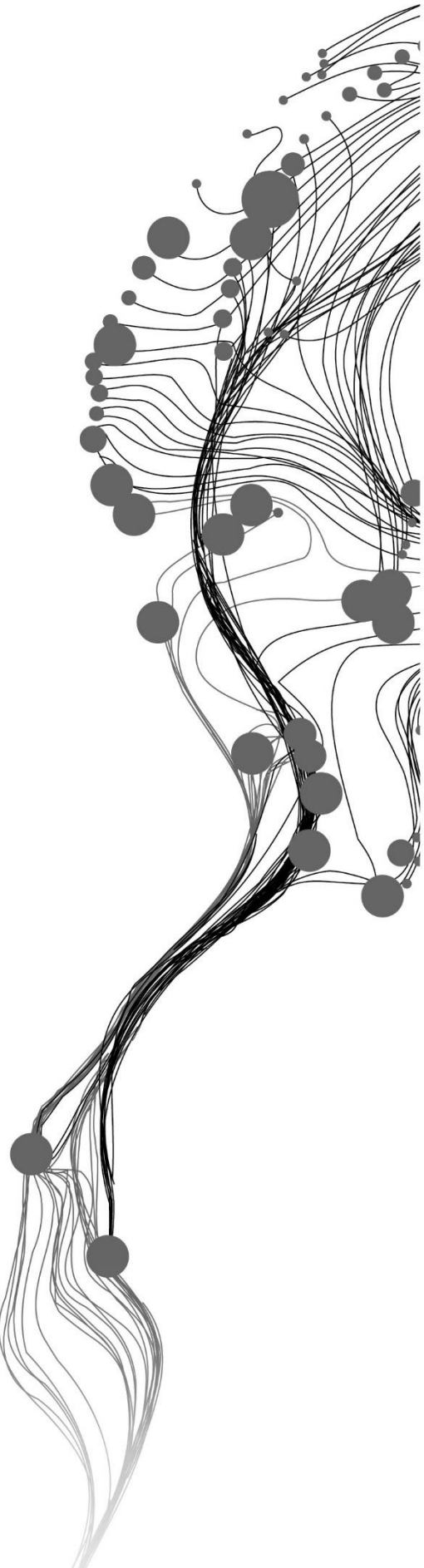
KAMUIIUA KAMUNDU [S1956817]
February 2019

SUPERVISORS:
Dr.Ir. M.W. Lubczynski
Ir. G. Parodi

INTEGRATED HYDROLOGICAL MODELING OF GROUNDWATER RECHARGE AND GROUNDWATER RESOURCES IN THE AUOB CATCHMENT (NAMIBIA)

KAMUIIUA KAMUNDU
Enschede, The Netherlands, February 2019

SUPERVISORS:
Dr. M.W. Lubczynski
Ir. G. Parodi

PROPOSAL ASSESSMENT BOARD:
Dr.Ir. C. van der Tol (Chair)
Dr.P.Gurwin (External Examiner, University of Wraclow)

Abstract

 Part of the Auob Catchment is suited within the Stampriet artesian basin. The basin is experiencing a decline in the water levels, which triggered a proposed reduction of up to 50% water use in the area. There is a burning need for the implementation of intervention methods such as artificial recharge. The current study aims at understanding the spatio-temporal distribution of natural groundwater recharge of the system and groundwater resources distribution as well as at identifying potential artificial recharge zones (by injection wells) that can further be used in scenario analysis. In order to account for the spatio-temporal distribution of groundwater fluxes, MODFLOW-NWT model was created. This model was calibrated in trial and error manner.

The 5-year model simulation (1/09/2012-31/08/2017) show that 94.44% of precipitation (P) is distributed over the catchment as effective precipitation while 67.53% of P percolates as gross recharge. Most of the water is lost via groundwater evapotranspiration (ET_g), which accounts for 68.74% of P, unsaturated zone evapotranspiration (ET_{uz}) contributing 24.01% of P and groundwater exfiltration (Exf_g) which represents 19.74% of P. Thus, creating a negative net recharge (R_n) of -20.95 % of P. The abstraction in the area accounts for 0.17% of P. Potential recharge zones and injection well locations have been proposed based on the analysis of natural recharge processes on the model solution.

Acknowledgment

INTEGRATED HYDROLOGICAL MODELING OF GROUNDWATER RECHARGE AND GROUNDWATER RESOURCES IN THE AUOB CATCHMENT (NAMIBIA)

DISCLAIMER

This document describes work undertaken as part of a programme of study at the Faculty of Geo-Information Science and Earth Observation of the University of Twente. All views and opinions expressed therein remain the sole responsibility of the author, and do not necessarily represent those of the Faculty.

**INTEGRATED HYDROLOGICAL MODELING OF GROUNDWATER RECHARGE AND GROUNDWATER RESOURCES
IN THE AUOB CATCHMENT (NAMIBIA)**

TABLE OF CONTENTS

LIST OF FIGURES

LIST OF TABLES

1. INTRODUCTION

1.1. Background

Namibia is an arid country and relies mainly on its groundwater resources. These resources do not only support the growing population but are also useful for the country's economic activities and ecosystems. The country is dominated by ephemeral rivers associated with more than 45 major catchments (Jacobson et al. 1995; Strohbach 2008; Sarma 2016). Just like many other catchments elsewhere, part of the water flowing in these rivers, mainly from rainfall, percolates and contribute to groundwater recharge. Australian Bureau of Meteorology (2018) defines groundwater recharge as the movement of water to the saturated area of a geological unit. Rainfall in this region is low and unevenly distributed in space and time. This affects groundwater recharge and it is difficult to predict respectively (Jacobson et al. 1995). Moreover, there are higher groundwater demands than what can be naturally replenished by recharge. Understanding groundwater recharge and discharge is imperative in such conditions. Various methods are used to measure groundwater recharge and for understanding its spatiotemporal distribution. The inability to directly measure recharge makes it one of the most complex components of water balance to quantify (Knowling and Werner 2017; Tashiro 2017). Several recharge estimation methods have been proposed, particularly for arid environments (Xu and Beekman 2003). These include the chloride mass balance (CMB), cumulative rainfall departure (CRD) and groundwater modelling (GM). These methods have their strength and weakness that need to be considered before use, depending on data availability and catchment characteristics. For example, the CMB method cannot be relied on in areas where the long-term atmospheric Sodium chloride (NaCl) deposition is unknown. The CRD method should be used for unconfined aquifer with known specific yield (Sy). For the GM method, well-defined boundary conditions should be considered and parameters such as transmissivity should be known (Xu and Beekman 2003). In the same line of thought, Knowling & Werner, (2017) observed that implementing better means of groundwater management is essential to accurately estimate recharge, for which numerical groundwater models can be adopted. Groundwater recharge can also be estimated as a residue using the soil water balance method (Anderson et al. 2015). This method is dependent on soil properties, precipitation, air temperature, root depths and land cover. The method is also applicable to domains of any spatial extent. There are a variety of catchment characteristics that influence the distribution of groundwater recharge.

Groundwater recharge distribution is influenced by different factors, such as land cover and land use, geology, slope, climatic conditions, soil types, topography (Francés and Lubczynski 2011; Anderson et al. 2015; Condon and Maxwell 2015; Adane et al. 2018; Li et al. 2018). Groundwater recharge is significantly affected by deep-rooted vegetation. Changes in land cover does not only influence the extinction depth, which eventually alters the recharge distribution. It also influences interception as a result of the change in leaf area index and changes the soil hydraulic properties (Adane et al. 2018; Li et al. 2018). Regarding soil types, recharge is said to occur more in sandy soil compared to clayey soil. This is due to the high water holding capacity of clay, which lowers the infiltration of water and exposes it to evapotranspiration (Anuraga et al. 2006; Francés and Lubczynski 2011). Soils that are dry for more prolonged periods are said to be well drained and they are mainly associated with high infiltration making them potential recharge zones. The drainage ability of the soil is influenced by land slope, soil texture, soil structure and water table depth (Tweed et al. 2007). The spatiotemporal variation of geomorphology, structural aspect and geology lead to uneven distribution of groundwater (Tweed et al. 2007). Geological structures such as fractures, faulting, joints, veins and folds influence the distribution of groundwater. Landscape topography is one of the most

important forces that drive the movement of groundwater (Marklund and Wörman 2007). Groundwater tables are mostly conceptualized as subdued replicas of topography (Haitjema and Mitchell-Bruker 2005; Condon and Maxwell 2015).

The relevant studies conducted on ephemeral catchments and recharge processes were conducted on the central to the western part of Namibia (Jacobson, Jacobson, & Seely, 1995). The current study is located in the south-eastern part of the country, aims at determining groundwater recharge and the spatial distribution and temporal variation of groundwater components in the Auob catchment.

Research problem

The only permanent water supply in Kalahari is groundwater from the aquifers that are associated with the ephemeral rivers. The Kalahari, Auob and Nossob aquifers supply 65%, 33% and 1% of the water consumed in this area respectively. Water in this area is used for domestic use (16%), stock watering (32%) and irrigation (52%) (GGRETA 2015). There has been a drastic decline in the water level, especially within the uppermost aquifer of the Auob Catchment which is estimated to be depleted within 30 years since 2002. Thus a 50% reduction in water use in this area was recommended, which the author's further state that is not feasible considering the socio-economic impact on this system (JICA 2002). For this reason, there is a burning need for understanding the natural aquifer recharge processes and find solutions on how to restore these declining heads by use of intervention methods such as artificial recharge.

The geohydrological structure of the Auob aquifer does not allow direct recharge from rainfall, because of the Riedmond member (impermeable layer) that overlays the aquifer. Recharge only occurs in areas where the Auob is in direct contact with the Kalahari which is around the central area of the Auob basin (JICA 2002). Groundwater in the eastern part of Namibia flow in the eastern direction and to date, it is not known how much of this water is flowing in this direction (FAO 2016). The Auob aquifer is overlain by the Kalahari which is an unconfined aquifer. Various studies have been carried out to try and conceptualize the aquifer behaviour and reasonably good work has been done. These studies have conceptualized the study area and recharge zones have been identified based on other methods such as the chloride mass balance (Stone & Edmunds, 2012; GGRETA, 2016; & JICA, 2002), but no numerical model has been carried out in this area. Numerical models have an advantage, due to their ability to quantify different water balance components and their spatio-temporal distribution.

1.2.   Justification

Upon successful completion of this study, it will be the first study that will:
- Organize hydrological database in the study area;
- Develop and calibrate an integrated hydrological model solution involving the use of MODFLOW NWT with the UZF package solution linking surface and groundwater domains to integrate climatic, hydrometeorological and hydrogeological data.
- provide advice for sustainable use of the groundwater resources within this area and propose artificial recharge zones and available potential injection wells.

1.3.   Research objectives and questions

1.3.1.   General objective

The main purpose of the study is to assess groundwater recharge from precipitation and evaluate groundwater resources within the Auob Catchment.

Specific objectives related to Auob Catchment are to:
- Organize hydrological database;
- Develop a conceptual model;
- Setup and calibrate a distributed numerical hydrological model with 5-year time series data;
- Evaluate the spatio-temporal distribution of groundwater recharge and groundwater resources for sustainable use of water resources.

1.3.2. General question

How much of the precipitation received within the Auob Catchment, recharges the saturated zone and how does it influence the spatiotemporal distribution of groundwater resources?

1.3.3. Specific questions
- What is the conceptual model of the Auob Catchment?
- What are the effects of catchment characteristics on the spatial distribution of groundwater resources?
- What is the spatio-temporal variability of groundwater resources?

1.4. Hypothesis and assumptions.

1.4.1. Hypothesis

- About 0.3-0.7% of the precipitation ends up as groundwater recharge in the Auob Catchment.

1.4.2. Assumptions

- If there are any lateral groundwater fluxes across the northwest to the southeast watershed boundaries, these fluxes are insignificant.
- During the model simulation period (1/9/2012-31/8/2017) and throughout the study area the groundwater has uniform density and it is not influenced by salinity.

2. STUDY AREA

2.1. Location

The Auob Catchment is located within the Stampriet Artesian Basin (SAB) in the southeastern part of Namibia. The catchment is about 74 081km² within the borders of Namibia (JICA 2002). For this study, only the part of the Auob Catchment that is situated within the SAB is considered and it covers about 40Mm². The national watershed boundary is situated on the northwest to the southeast of the study area. The basin in which the Auob Catchment is situated receives a small amount of recharge, as it is located in a dry part of the country and there is no permanent surface water (GGRETA 2015).
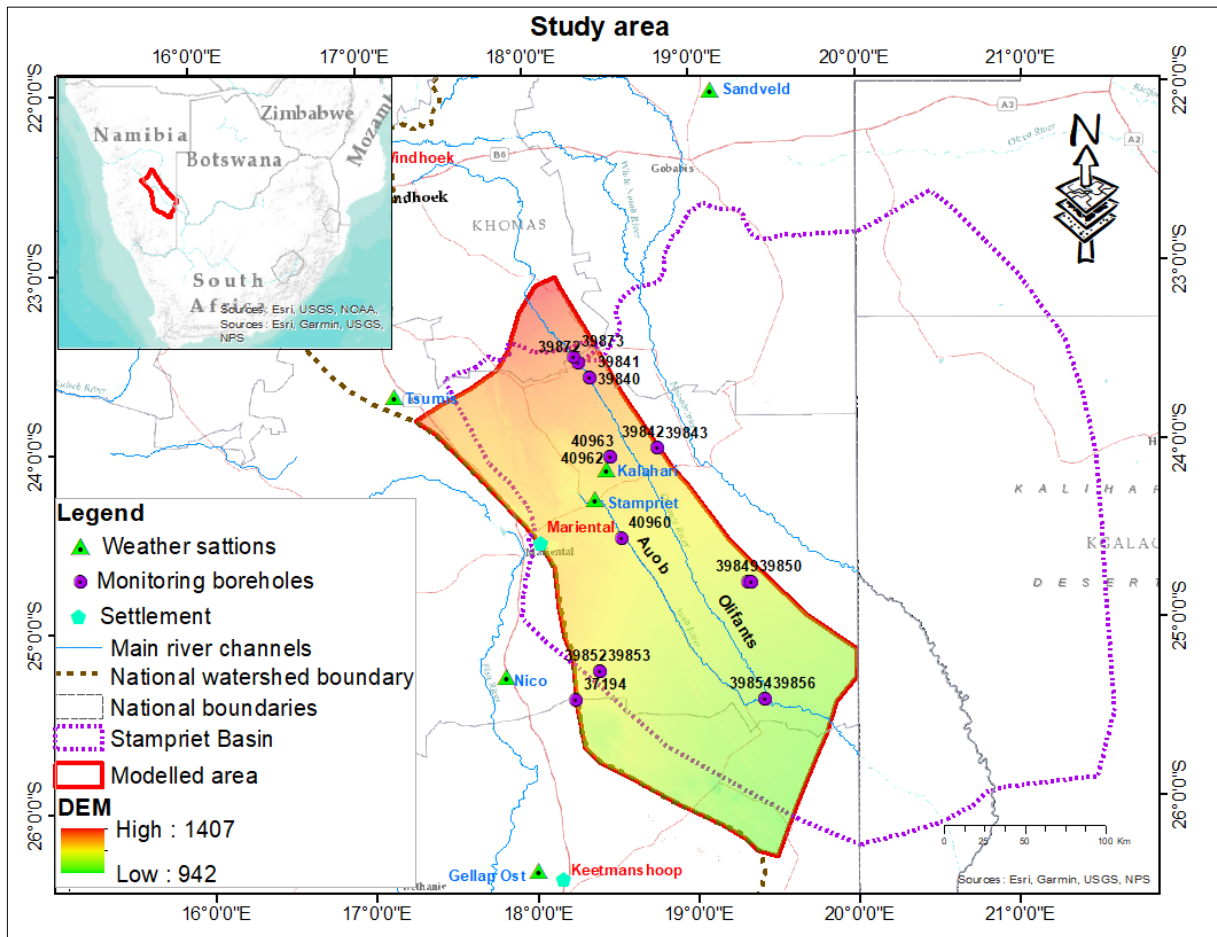
Figure 1: Study area and monitoring network map.

2.2. Topography

The topography of the study area is presented Figure 1. The highest elevation is 1407 m.a.s.l. at the north-western part of the study area. The lowest elevation is 942 m.a.s.l. at south-eastern part of the study area. The study is relatively flat with mountains in the north-western part.

2.3. Climate

Rainfall
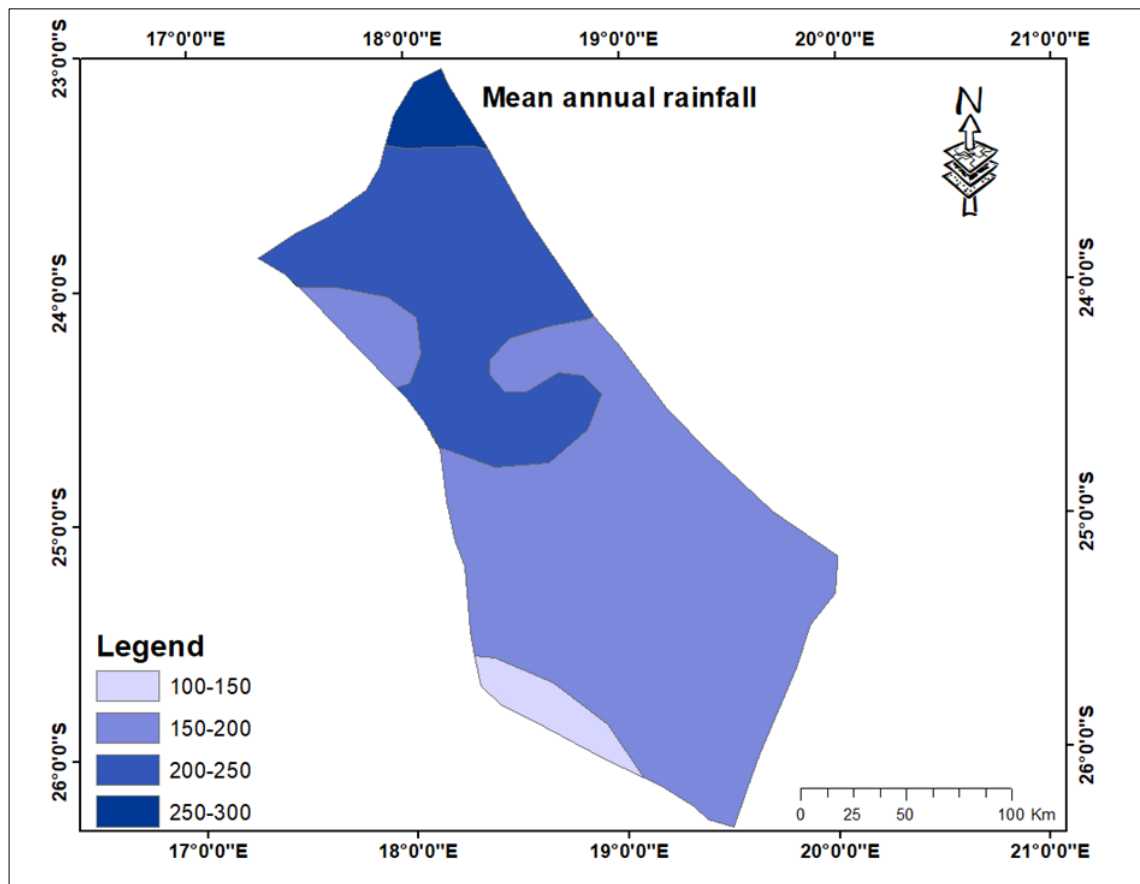
Figure 2: Annual average rainfall distribution in 1999 within the study area. Source: Atlas of Namibia derived from 300 stations.

Auob Catchment annual precipitation ranges from 100-400 mm, with an average of 249 mmyr[-1] (MAWF, 2000; JICA, 2002; Stone & Edmunds, 2012). Rainfall within the Stampriet Basin in which the Auob Catchment is located decreases from the north west towards the south (JICA 2002). The highest rainfall in the Auob area was experienced in 2010-2011, of which the farmers confirmed to have been approximately three times the recorded average. Other high rainfall events were recorded in the 1970s which accounted for 600 mm/year (Stone and Edmunds 2012).

Temperature

The temperature in the study area gets to about $40\,^{\circ}$C on very hot days. The hot days are associated with summer, which range from December to February. The temperatures also get as low as below freezing point in winter which range from June to August. On average the area experience a maximum temperature of 30 $^{\circ}$C and minimum of $2\,^{\circ}$C (JICA 2002).

Evapotranspiration

The potential evapotranspiration in the area is very high as a result of long sunshine hours and the overall climatic conditions. The annual pan evaporation is about 3700 mmyr[-1] (JICA 2002).
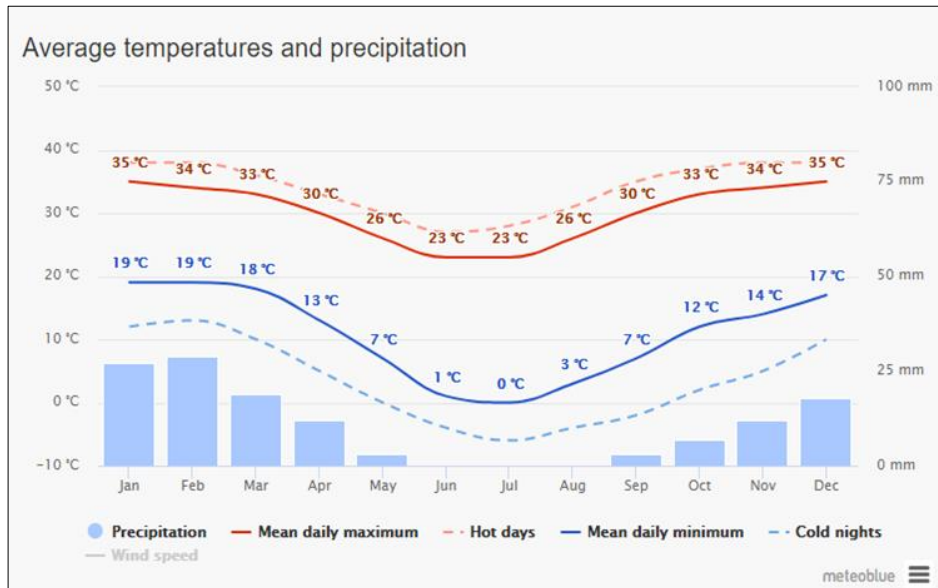
Figure 3: Average monthly temperature and precipitation over a 30 year (1988-2018) period at the Stampriet station (Metoeblue, 2018). For the location of the Stampriet station see Figure 1.

The climatic conditions of the study area over the five years of model simulation ranging from 1st September 2012 to 31st August 2017 are characterized in Figure 4. The rainfall is from the CHRIPS product (satellite rainfall estimate at the location of the Kalahari station). The temperature was taken from the Gallep Ost station as it had continuous data during the simulation period. The reference evapotranspiration (ET_o) was taken from the US-based GMAO GOES-5 model (at Kalahari station) due to its 20 km spatial resolution and its continuity in time during the simulation period as opposed to FEWSNET that have a spatial resolution of 111km and METREF that start from 2016 to present (Trigo and Debruin 2016). The performance of the US-based GMAO GOES-5 model was validated using the Pearson correlation, scatter plots and cumulative curves as indicated in section 4.2.2.1 of this study.
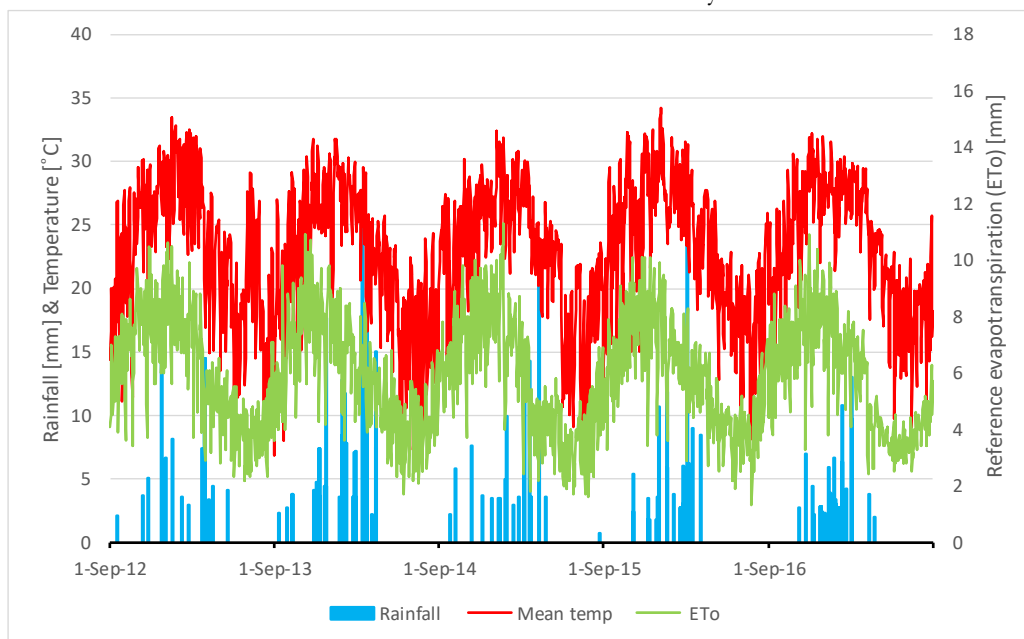
Figure 4: Daily meteorological data for the five year period at the Kalahari (rainfall was taken from the satellite pixel at the Kalahari station) and Gallep Ost weather stations (potential evapotranspiration was taken from the satellite pixel at the Gallep Ost station) and temperature came from the insitu Gallep Ost station as it had continuous data. For the location of these stations see Figure 1.

2.4. Land cover and land use
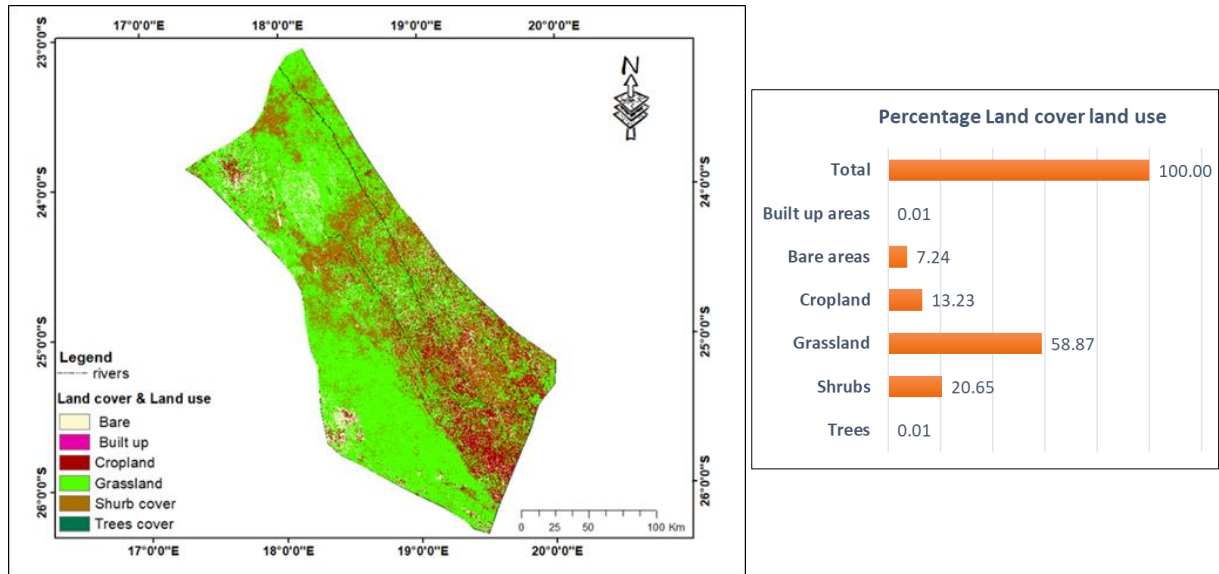
Figure 5: Reclassified land cover and land use map. Source: RCMRD geoportal, the map is a Sentinel II map of 2016 by (Serviresa 2018).

The study area is dominated by grass and shrublands, with few trees mainly along river channels. The southeastern part of the study area is covered by sparse vegetation and bare areas are found in the eastern region of the study area. The south and southwestern location of the study area is covered by grassland. In addition, the Auob river has channels that range between 100-500 m and comprised of fine-grained silts (February et al. 2017) and (Shadwell and February 2017). The river channels are dominated by plants species such as the *Vachellia erioloba* and *Vachellia haematoxylon*, low shrubs found in this area are *Rhigozum trichotomum* and grasses are *Schmidtia kalahariensis*, *Stipagrostis abtusa* and *Eragrostis porosa* (February et al. 2017). Other studies have indicated that trees such as *Acacia erioloba* and *Acacia haematoxylon* are found in the dry river beds and have the ability to withdraw deep underground water at depths of 56m (Shadwell and February 2017).

In the past alien species such as the *Prosopies* planting was encouraged due to their ability to thrive in this harsh conditions and their useful provisions (livestock fodder, fuelwood and shade) to the local communities (GGRETA 2015). The problem associated with this species at the moment is that they grow along the alluvial strips causing bush encroachment in these areas. Moreover, their roots have the ability to tap into the deep underground water of approximately 15m and mainly affects areas that have water tables ranging between 3-10m (GGRETA 2016). Even if the tapping depths of this trees are lower compared to *Acacia erioloba* and *Acacia haematoxylon* the concern is governed by the amount of water this trees can abstract (50l/day/tree) and their density is estimated to increase up to 18% per annum (GGRETA 2016).

2.5. Dominant soil types
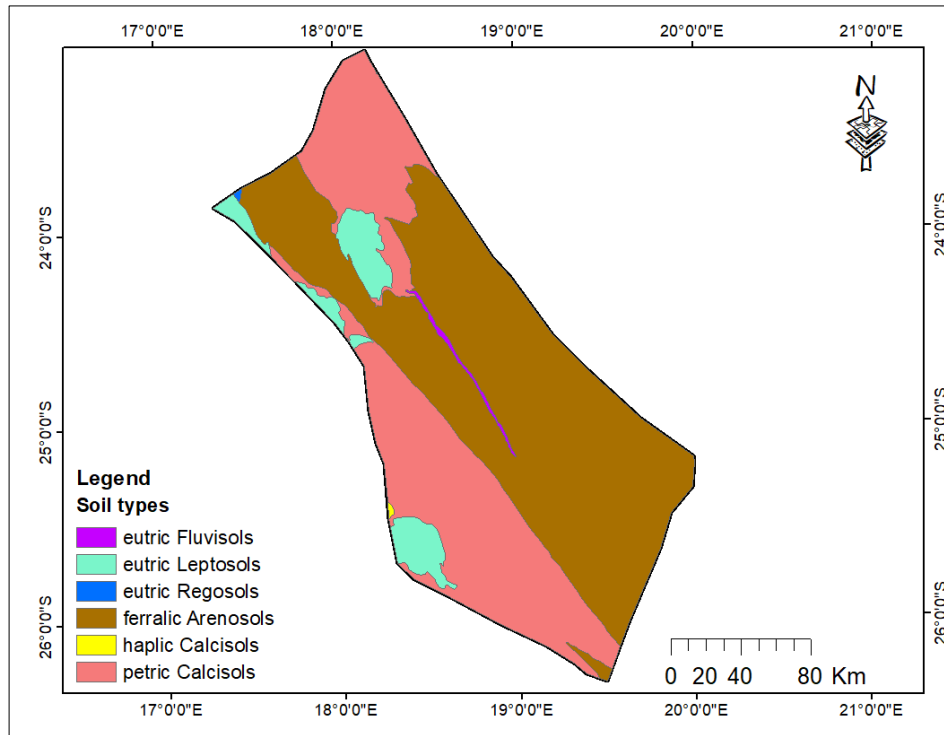
Figure 6: Soil map. This map depicts the different soil types in study area. Source: Atlas of
Namibia.

The study area is dominated by ferralic arenosols which are windblown; they cover the Kalahari Sandveld.
This sand material is high in iron and aluminum oxide, which is responsible for the red colour of the sand
(Alker 2008). Arenosols are sandy soils with a coarse texture. They have high permeability and low water
storage. Furthermore, they are said to have high percolation losses and are prone to erosion (World Soil
Resources 2006). The second dominant soil cover is the petric calcisols which have the potential to be fertile.
At shallow depths, these soils are associated with rocks that contain accumulations of calcium carbonate
(Alker 2008). Calcisols are associated with medium to fine texture and they have good water holding
capacity. Calcisols that are found on the surface, when they are silty and have the presence of slaking and
crust they may hinder infiltration from the rain. They are mainly common in semi-arid to arid parts of the
world (World Soil Resources 2006). Patches of eutric leptosols are also noticed in the study area. They are
caused by erosion and they are fertile (Alker 2008). Leptosols are shallow soils found on continuous rocks,
they are extremely stony and/or gravely. They are associated with excessive internal drainage and with the
ability to cause drought even in humid environments (World Soil Resources 2006). The eutric fluvisols are
a result of flood deposits (Alker 2008) and they are noticed in the channels of the fossil river as indicated in
Figure 6.

2.6. Geology

The Auob catchment is separated into 12 geological units as indicated in Table 1, which include the Kalahari
beds, the upper and lower Rietmond member, 5 layers of the Auob, upper and lower Mukorob, Nossob
member and Pre Ecca-group (basement). These geological units are separated into 6 hydrogeologic layers
containing three aquifers (Kalahari, Auob and Nossob) and three impermeable layers (lower Rietmond,
lower Mukorob member and basement).

Table 1: Geological and hydro-stratigraphical classification of the study area modified from Stone & Edmunds, (2012).

Stratigraphy of the Stampriet Basin (after Miller, 2000;2008) and corresponding hydrogeological classification (modified from JICA,2002)			
Geological stratigraphy			**Hydrogeological classification**
Kalahari beds Tertiary to Quaternary	Linear dunes (~10-20 m)		Unsaturated (Vadose) zone
	Sands, gravels and calcretes overlying calcrete-cemented conglomerate		
Karoo	Kalkrand Basalt (in NW of basin) *Jurassic* to *Triassic*		Kalahari Aquifer
	Rietmond member *Permian*	Sandstone, shale (and in east Whitehill black shale and limestone)	
		Shale (yellow and grey)	Impermeable layers
	Auob member *Permian*	Upper sandstone	Auob Aquifer
		Upper coal and black shale	
		Medium sandstone	
		Lower coal and black shale	
		Lower sandstone	
	Mukorob member *Permian*	Upper sandstone	
		Mukorob shale (grey-black)	Impermeable layer
	Nossob member *Permian*	Upper sandstone	Nossob Aquifer
		Upper siltstone-shale	
		Lower sandstone	
		Lower siltstone-shale	Impermeable layer
	Dwyka member *Carboniferous*	Mudstone	
		Tillite	
Pre Karoo *Cambrian*	Upper Nama red sandstone, shale		
	Lower Nama grey shale, sandstone		
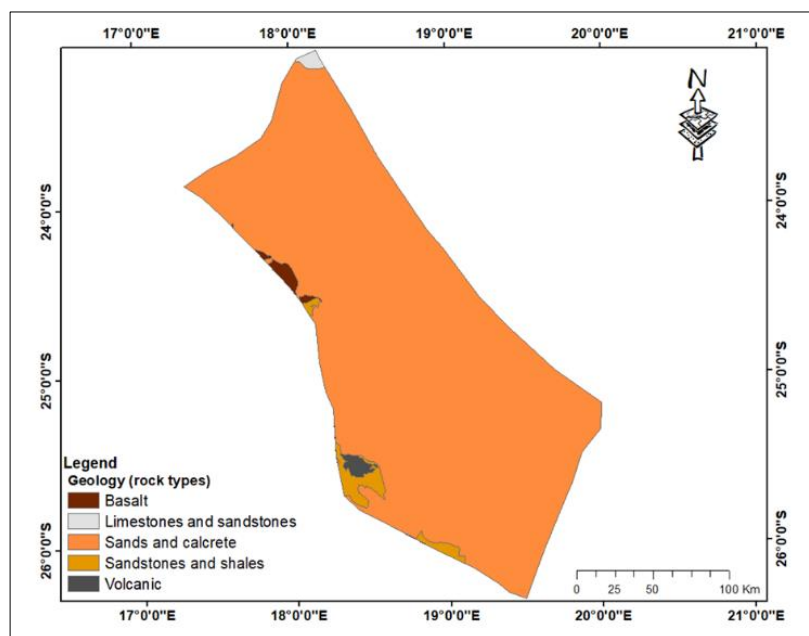
Figure 7: Surface geology of the study area. Source: Atlas of Namibia
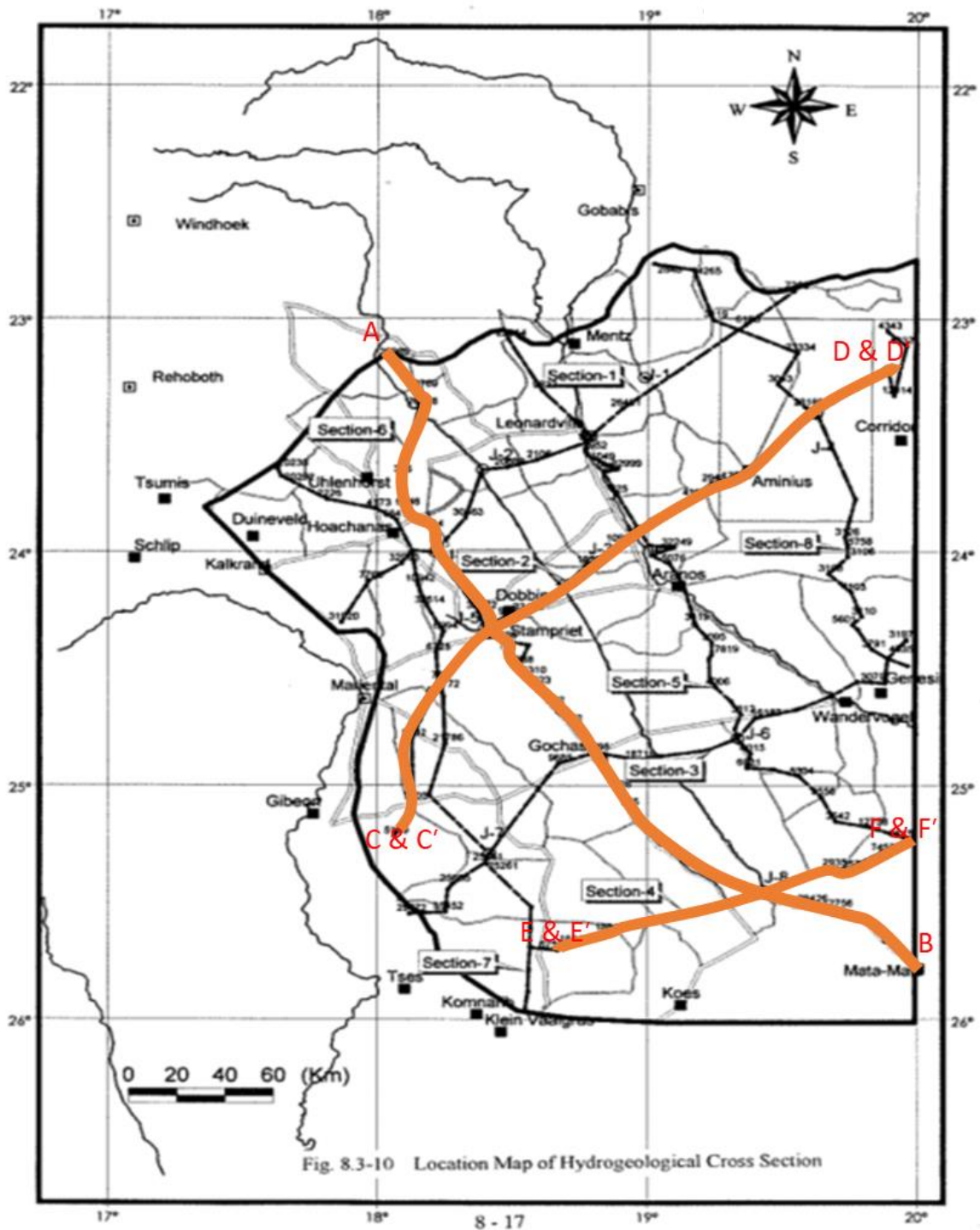
Figure 8: A map depicting the different cross-sections along the study area, relating to Figure 9 and Figure 10 (JICA, 2002). Cross sections A-B, C-D,E-F represent geology and C'-D', E'- F' represent, the hydrogeology of the Auob Catchment.
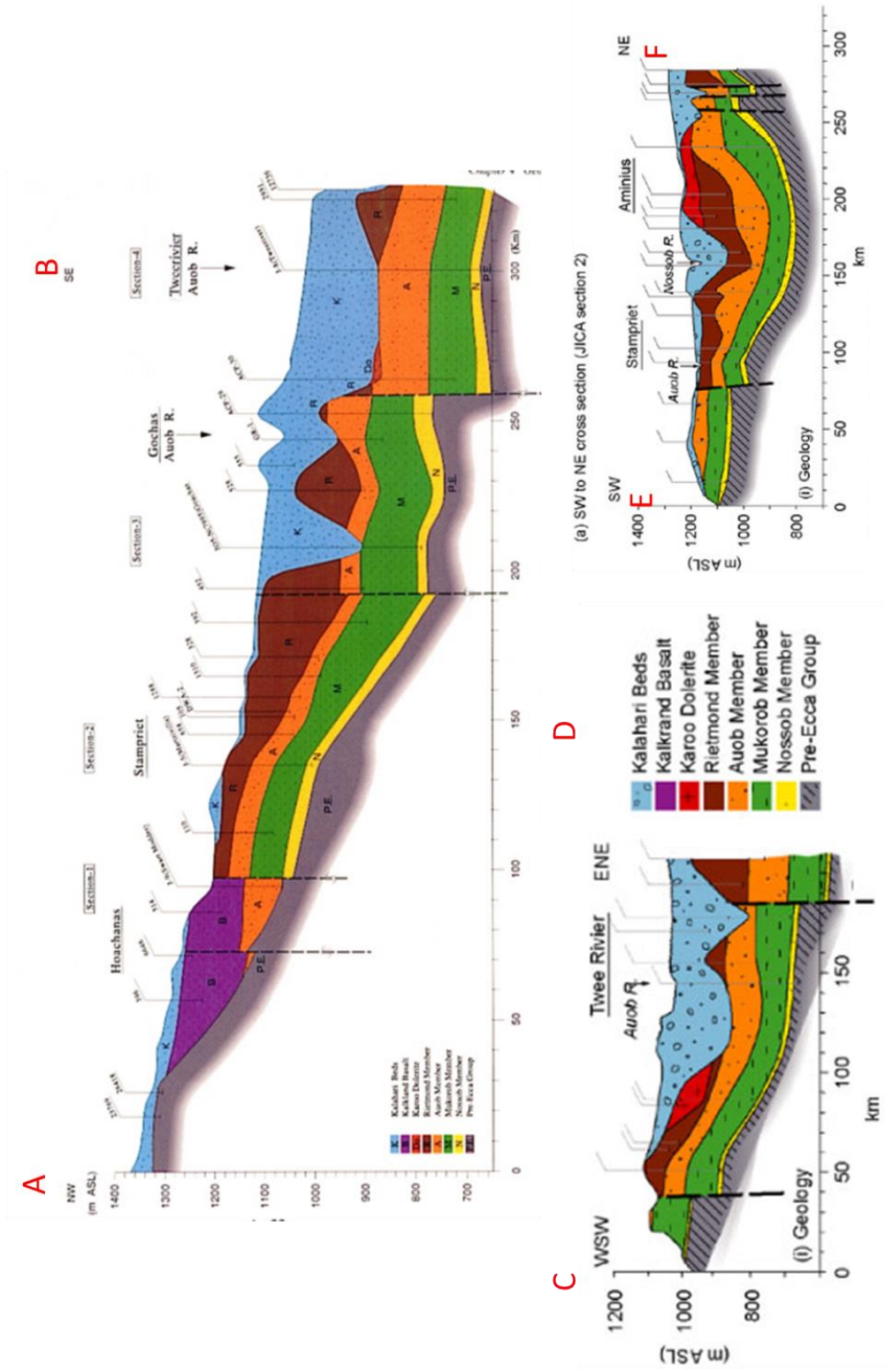
Figure 9: Geological cross-section map of the different cross-sections depicted in Figure 8 (JICA, 2002)

2.7. Hydrology and hydrogeology

All the rivers that originate within Namibia are ephemeral. They flow only during and/or after the period of high rainfall and the Auob river is no exception (Goudie and Viles 2015). The Auob (bitter water) River originates from the Anas mountain near Windhoek (Smith et al. 2014). The river flows into South Africa into the Orange River (Stone and Edmunds 2012). The Auob river drains the Kalahari Basin, which is a flat sandy plateau, with little runoff as most of the precipitation is absorbed by thick sand layers (Strohbach 2008). On average the catchment experiences runoff that ranges from 5.23-8.60 Mm³yr^{-1} along Stampriet and Gochas respectively (MAWF 2000). The Auob river is very active in the upstream reaches, but as it reaches the sandy Kalahari the water seeps into the sand. In the past, it was fed by the Stampriet artisan spring since the infestation of the Prosopis tress the river has dried up completely (Strohbach 2008). The river is currently referred to as a fossil river because it has been long since it last flooded, which was in 1933 and 1934 (Smith et al. 2014).

In terms of hydrogeology, the Auob Catchment is composed of three aquifers namely the Kalahari, Auob and the Nossob. The details about the aquifers will be discussed below based (JICA 2002; OBASECOM 2009; Stone and Edmunds 2012; Mulokoshi 2016):
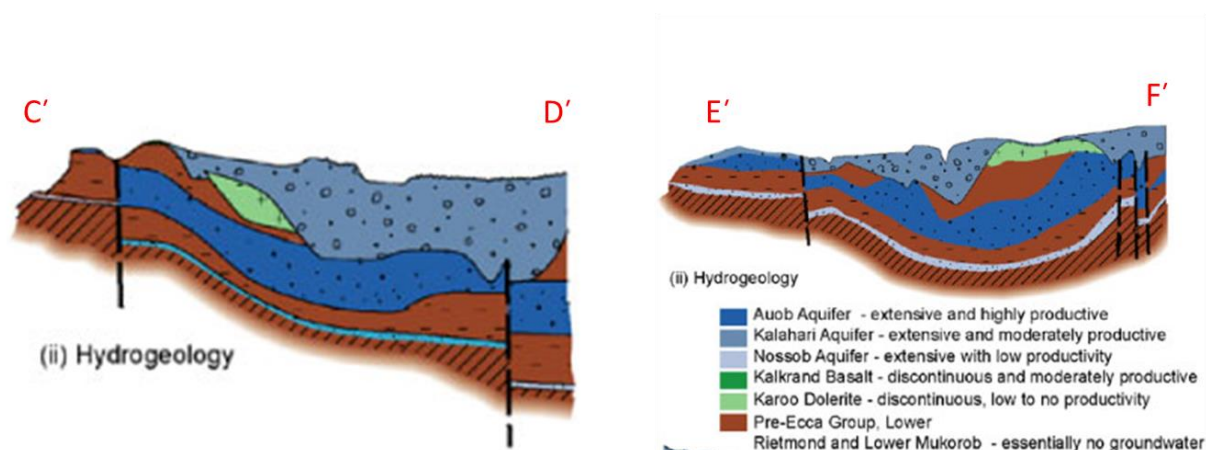
Figure 10: Hydrogeology map of the different cross-section shown in Figure 8. The legend is arranged in their order of productivity and their spatial coverage (JICA 2002).

Kalahari aquifer and Rietmond member (aquitard):

The Kalahari aquifer is underlain by the Reitmond member which is composed of the upper and the lower Rietmond. The lower Rietmond is impermeable and the upper is merged with the Kalahari making it a single hydro-stratigraphic unit. The Kalahari sands have undergone massive erosion, which is also evident in the Pre-Kalahari valley. In the central part of the Auob Catchment, the erosion has reached the Auob aquifer. This erosion runs along the Auob river within the study area and joins the orange river area. Therefore, the distribution of the Rietmond member is not noticed in this area, making this layer spatially discontinuous. Figure 10 shows the hypothetical distribution of the different layers in the Auob Catchment. In the areas were the Rietmond is not present the Kalahari and the Auob aquifers are directly connected and there could also be a probable upward leakage of the Auob aquifer into the Rietmond Member and Kalahari aquifer. The Kalahari aquifer is said to be moderately productive.

Auob aquifer and Mukorob member (aquitard):

The Auob aquifer is the most productive in the study area, it is hydraulically connected with the Kalahari aquifer (Figure 10). The Auob member is classified into five geological units. The units have horizontally changeable lithofacies, thus making it a single aquifer. The Auob members crop out at the east of Mariental and extend towards the south of Mariental. The Mukorob member underlies the Auob member. The upper Mokorob is permeable and the lower is impermeable, for this reason, the Auob and the upper Mukorob member are considered as a single hydrogeological entity. The lower Mukorob is spatially continuous as it can be seen from Figure 10; thus it acts as a separating entity between the Auob and the Nossob aquifer. Regarding thickness, it decreases in the south-eastern direction from the northwest.

Nossob Aquifer and pre-Ecca basement:

The Nossob aquifer is located between the Mukorob member and the Pre-Ecca group. The Pre-Ecca is composed of the Dwyka, Nama group and the Damara sequence this forms the basement of the catchment. This aquifer follows the same thickness decline trend as the Auob aquifer. The Nossob is overlain by the Mukorob layer which is spatially continuous thus separating it from the two above aquifer and making them hydraulically disconnected. The aquifer is said to have fossil water and does not receive recharge and it is considered the least productive aquifer.

The different layers within the study area can be visualized using Table 1 and Figure 10. The area has shallow depressions or pans that are typical globally in areas of low relief, which are arid to semi-arid. The pans hold water only during the rainy seasons (JICA 2002; Smith et al. 2014). There is some connection between the aquifers in areas where erosion channels, faults, dolerite intrusions occur and through the aquitard leakage (Stone and Edmunds 2012).

3. METHODOLOGY

This chapter presents the methodology undertaken during this study. The main intention of the study was to determine groundwater recharge from precipitation, the spatio-temporal distribution of groundwater resources and the effects of catchment characteristics on the distribution of fluxes. Satellite products such as rainfall and potential evapotranspiration were adapted due to the limited availability of the in-situ data. In- situ data in this study were used for the validation of the satellite products or as complementary data together with archived and ancillary data to understand the spatial distribution of land cover and land use components within the study area. To account for the spatio-temporal distribution of groundwater resources, the MODFLOW-NWT was used, it was calibrated in transient mode via trial and error. The steps and the details undertook will be discussed in the different sections of this chapter.
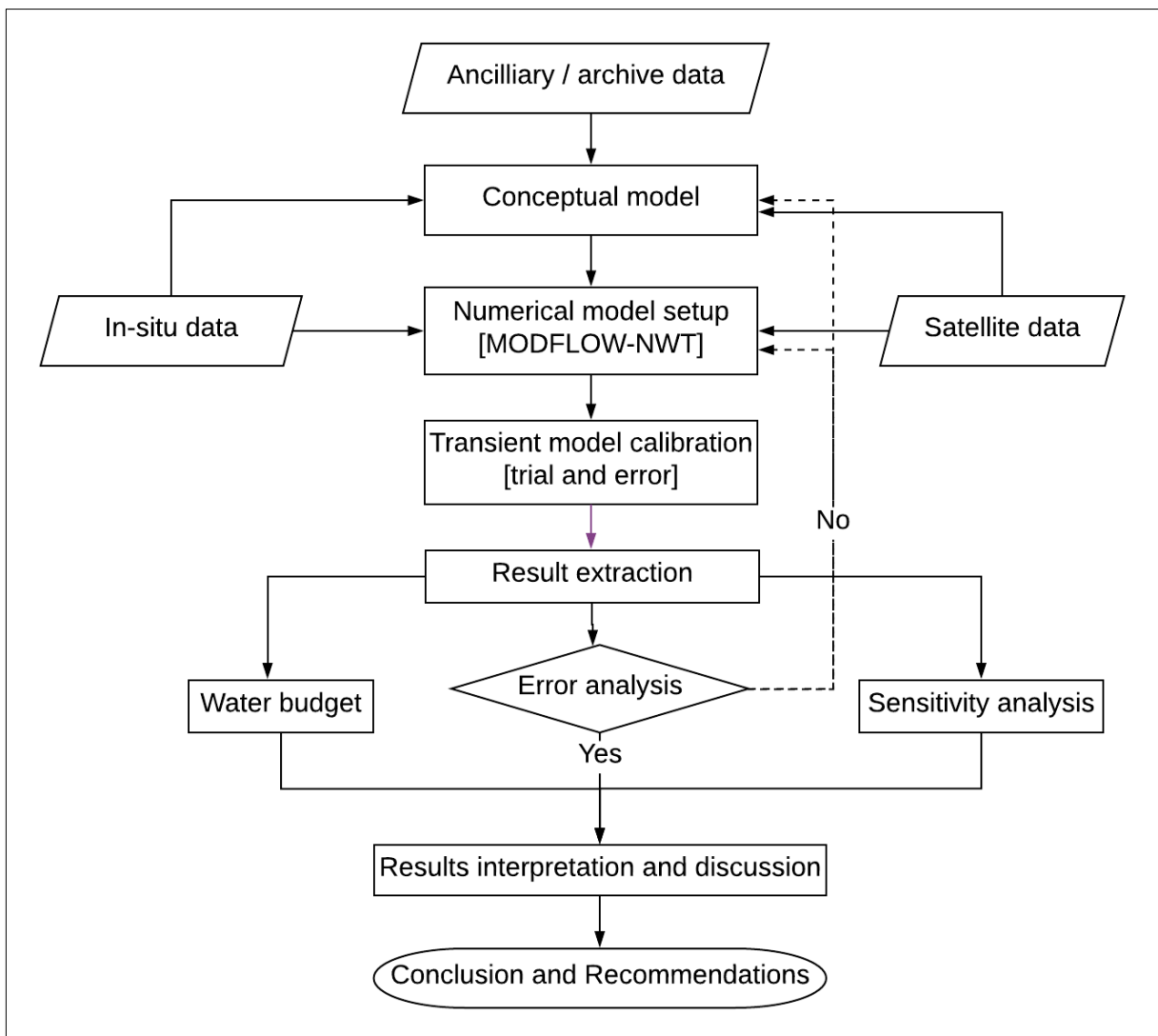
Figure 11: Research plan

3.1. Data collection and processing

The first step in groundwater studies consists of collecting existing geological and hydrological data at the catchment of interest. These data include; surface and subsurface geology, water tables, stream flows, evapotranspiration, precipitation, pumped abstractions, soil, vegetation, land use, irrigation, aquifer characteristic and boundaries (Kumar 2015). Their availability and quality often hamper the input data. The provided data sets for this study were evaluated for their quality before using them for the modelling process.

3.1.1. Ancillary/archived data

Ancillary or archived data included the land cover & land use map, surface geology, soil types, mean rainfall distribution. Geology and hydrogeology maps.

3.1.1.1. Land cover and land use map
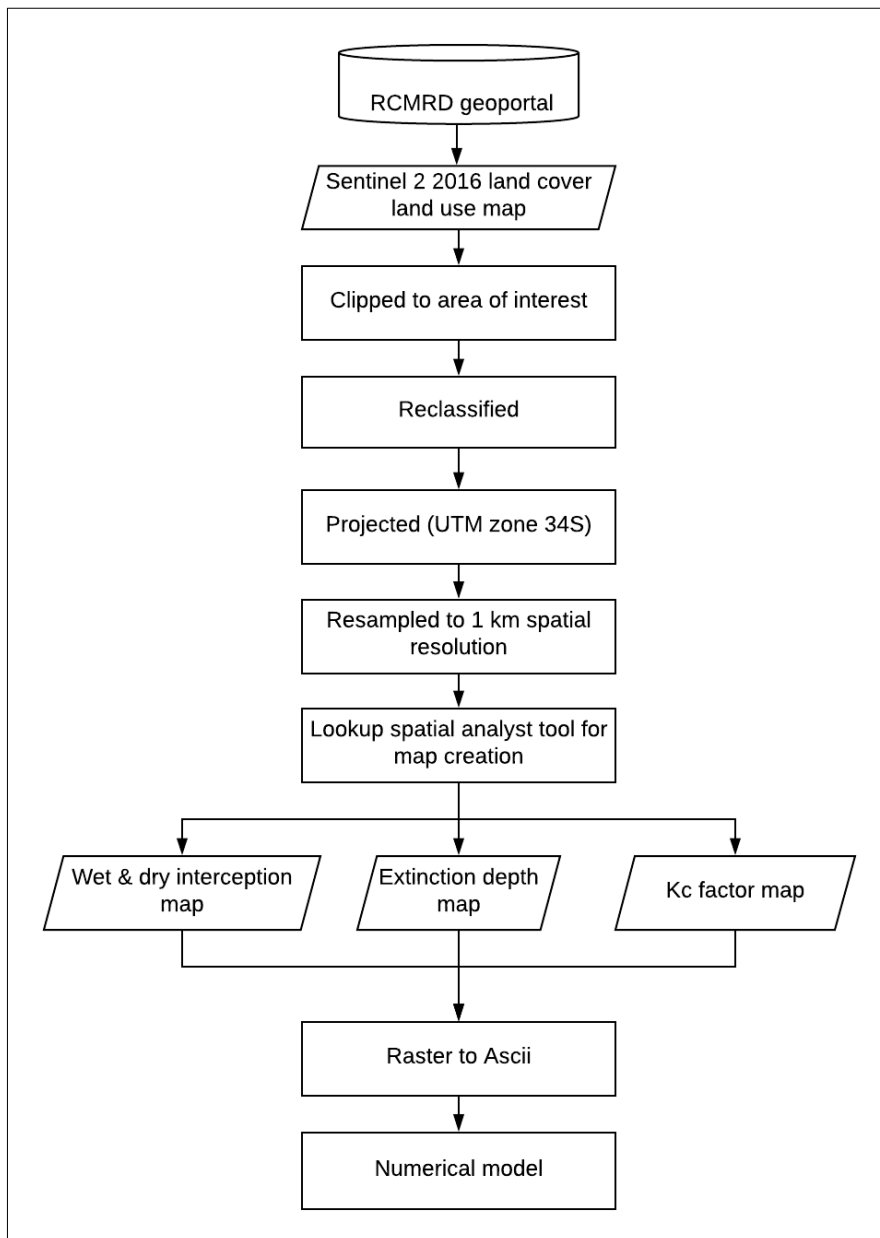
Figure 12: Land cover and land use flow chart. It indicates processes that were carried out on the original landcover map before it was used as input for the numerical model.

A 2016 land cover and land use map was used for this study, with the assumption that land cover and land use features were reasonably stable during the simulation period. This assumption can be further supported by Figure 49 in the Appendix that shows the NDVI maps at the beginning of the simulation and the end of the simulation period. The land cover and land use map was obtained from the RCMRD geoportal; geoportal.rcmrd.org/layers/servir%3Anamibia_sentinel2_lulc2016 compiled by (Serviresa 2018). The map was clipped to the area of interest. The original map had 10 classes of land cover types. These classes where reclassified and narrowed down to 6, henceforth the small amount of coverage by certain features such as standing water bodies, mosses and aquatic vegetation. After reclassification, the map was projected to the UTM zone 34 south, which is the UTM zone of the study area. Than it was resampled to 1 km spatial resolution to fit the model grid. The interception, Kc factor and extinction depth map were created using the lookup spatial analyst tool in ArcMap. The created maps were converted to Ascii and used as input into the numerical model, as indicated in Figure 12 above.

3.1.1.2. Surface geology, soil and annual mean rainfall.
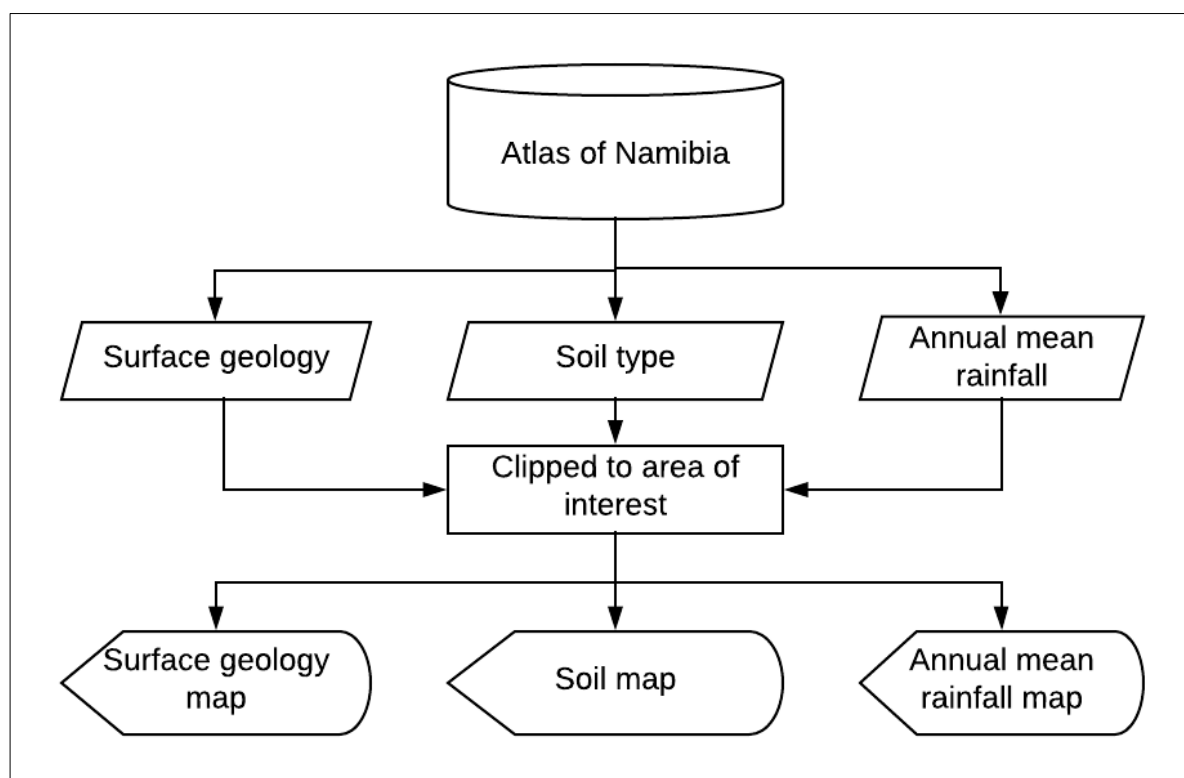
Figure 13: The flow chart presenting construction of soil, geology and annual rainfall distribution maps. Source: Atlas of Namibia.

The shapefiles of soil, geology and general rainfall trend was obtained from the Atlas of Namibia: (https://www.google.nl/search?q=atlas+of+namibia&oq=atlas+&aqs=chrome.2.69i57j35i39l2j0l3.7423j0 j7&sourceid=chrome&ie=UTF-8). All these features were clipped to the study area as indicated in Figure 13. No further processing was done on these maps. They were displayed and used in the understanding of the spatial extent of surficial geology, soil types and which areas are likely to receive more rainfall. The rainfall map according to (Mendelsohn, Jarvis, Roberts & Robertson, 2002) was created from a network of ~300 stations all over Namibia in 1999. Due to the large time lapse between the moment of map creation and the study simulation time and the fact that it is a one-year average, it was not used in any of the decision making process of this study. Thus, it was treated as archive data for trend display.

3.1.2. In-situ data

3.1.2.1. Microclimatic data

The microclimatic data was obtained from the Sasscal weather net network. This data was used for understanding rainfall distribution within the study area and calculation of reference evapotranspiration. To allow the eventual data gap filling, the variables were analysed using the correlation method to determine the relationship between the different meteorological variables at the various stations.

Table 2: Microclimatic variables within and around the study area measured daily. For the location of the below listed station, see Figure 1.

Station_id	Latitude	Longitude	Altitude	Rainfall	Tmax	Tmin	Relative humidity	Solar Radiation [W/m²]	Wind Speed [m/s]	Pressure in [kpa]
Kalahari	-24.163	18.477	1229	✓	✓	✓	✓	✓	✓	✓
Gellap Ost	-26.401	18.007	1080	✓	✓	✓	✓	✓	✓	✓
Sandveld	-22.045	19.132	1058	✓	✓	✓	✓	✓	✓	✓
Nico	-25.313	17.835	1527	✓	✓	✓	✓	✓	✓	✓
Tsumis	-23.730	17.194	1376	✓	✓	✓	✓	✓	✓	✓

A threshold of 0.6 coefficient of determination was used. For anything above the threshold, an averaging method was used. This was applicable to variables such as maximum and minimum temperature, relative humidity, barometric pressure. Due to the spatial uniformity of these variables and for anything below the threshold, the inverse distance weighting (IDW) method was used. Consequently, the IDW method was applicable to variables such as solar radiation and wind speed (which were found to be spatially non-uniform), except for rainfall.

In-situ rainfall

Rainfall data had not undergone data filling using any of the above mentioned methods. Due to it's spatio-temporal variability, made the averaging or the IDW method not viable as the insitu stations were ~ 250 km apart. Instead, the Gallep Ost station had the highest continuous data with minimal gaps. For the continuity of this data set, it was assumed that there is no much variation in seasonal rainfall at the same location. For instance, rainfall recorded at the Kalahari station is likely to be of the same intensity over different years. On the day that had missing data, the values recorded for different years were averaged and used to fill the gap on that particular day. The full data set was used in comparison with the satellite data for determination of the most suitable bias correction scheme. The details on the bias correction scheme and the decision of the implementation of the bias correction factor is discussed in section 4.2.1.2 of this study. For all the insitu stations, scatter plots were created to reveal the relationship between the satellite and gauge products. This was done on the days when both the satellite and rainfall recorded rain.

In-situ reference evapotranspiration

The in-situ reference evapotranspiration (ET$_o$) was calculated with the microclimatic variables indicated in Table 2. Variables were used as input into the FAO Penman-Monteith formula as indicated in equation (12). The method was chosen due to its large use and approval by the scientific community, as being the best method in estimating PET which is associated with minimum errors (Wang et al., 2012). The provided data set from the various station as indicated in Figure 1 and Table 2 the majority of these stations, had data gaps and required gap filling as stipulated in section 3.1.2.1 of this study. An exception was noticed with the Gallep Ost station which had continuous data during the whole simulation period. After the gap filling and before this data was used in the satellite product validation, it was checked for consistency using the double mass curve technique. The technique was used for screening the data and to ensure that if there is any variation in the data, it is a result of meteorological causes and not due to changes in observational methods or station location (Bhatti et al. 2016). The double mass curve technique uses the cumulative of one station

in relation to the cumulative of other stations in order to compare the data behaviour of one station in relation to several other stations in the area (Searchy and Hardison 1960). The result should be a straight line if the relationship between the variables is a fixed ratio. The double mass curve technique is used for the adjustment of inconsistency in the data in case there is any (Searchy and Hardison 1960). In case of any inconsistency in the data after applying the double mass curve technique, then the following formula is implemented and used for the correction of the data set;

$$ETo_{c(u)} = ETo_u \frac{M_c}{M_a}$$

<div align="right">(1)</div>

where $ETo_{c(u)}$ is the corrected ET$_o$ at the station of interest, ETo_u is the original recorded ET$_o$ at other station. M_c is the corrected slope of the double mass curve and M_a is the original slope of the double mass curve.

The calculated insitu data was not used as input into the numerical model but it was used for the validation of the satellite product. Since the Gallep Ost station had continuous data it was used as a reference station for the validation of the satellite products performance at this location and overtime. This information was further used to infer on the performance of this product over the whole study area. Moreover, different evaluation method such as the Pearson correlation, scatter plots and cumulative curves were used for the validation of the performance of the product in relation to the Gallep Ost station as indicated in section 3.1.3.3.

3.1.2.2. Piezometric data

Table 3: Aquifer parameters (K- hydraulic conductivity, T- Transmissivity, Sy- Specific yield, Ss- Specific storage). For the location of the boreholes see Figure 1.

WW_NO	Aquifer	latitude	longitude	Kh [m/day]	T [m²/day]	Sy	Ss
37194	?	-25.44600	18.26319	-	-	-	-
39840	Auob	-23.64725	18.38976	0.13824	3.42	0.089	-
39841	Nossob	-23.64783	18.38970	0.12096	2.94	-	0.085
39842	Kalahari	-24.04592	18.79340	0.1296	6.42	-	0.143
39843	Auob	-24.04792	18.79312	5.7024	194	-	-
39849	Kalahari	-24.80014	19.33485	0.12096	6.23	-	0.145
39850	Auob	-24.80056	19.35511	2.8512E-06	8.44	-	0.166
39852	Kalahari	-25.29163	18.41678	1.0368	30	-	0.761
39853	Nossob	-25.29117	18.41650	0.00058752	0.01	0.0043	0.005
39854	Kalahari	-25.46122	19.43266	0.0061344	0.27	0.24	0.016
39856	Nossob	-25.46148	19.43324	0.00076032	0.02	-	-
39872	?	-23.56042	18.31644	-	-	-	-
39873	?	-23.52892	18.29247	-	-	-	-
40960	Kalahari	-24.55006	18.56227	-	-	-	-
40962	Auob	-24.09088	18.50235	-	-	-	-
40963	?	-24.09057	18.50329	-	-	-	-

The monitoring borehole data was obtained from the Ministry of Agriculture, Water and Forestry (MAWF) in Namibia. Some of the data used in this study was obtained from UNESCO based on studies conducted in this area under the approval of the Namibian MAWF. The data was available at a daily time step. The aquifer parameters for the respective boreholes was obtained from the JICA report. The piezometric data obtained from MAWF had undergone data cleaning before it was used as input into the head observation (HOB) package in the numerical model. There were various factors that called for model data correction before its use. This was likely due to misplacement of the sampler installation depth during field visits that caused an unrealistic shift in groundwater heads. Issues as such where manually corrected as indicated in Figure 14.

Borehole data processing

About 48 boreholes were acquired from the MAWF in Namibia. These were the monitoring wells for the SAB basin. A shapefile of these boreholes was created, and they were clipped to the area of interest. Thus, resulting in 23 boreholes. After data cleaning, 16 monitoring boreholes were kept for data processing. Of these boreholes 6 where taping into the Kalahari aquifer, 4 into the Auob, 3 into the Nossob and 3 where unknown. The boreholes that tap into the Nossob were discarded and not used as input into the model, because of the hydraulic discontinuity of this aquifer from the rest of the system as a result of the spatially continuous Mukorob impermeable layer. Hence, this resulted into 13 boreholes that were used for this study. The obtained piezometric heads from the MAWF were in the form of pressure heads with units of either pounds per square inch (PSI) or bar. They were converted to kilopascal and then to the water column (WK) or pressure heads, above the automatically recording electronic sensor as presented in Figure 14. Due to 'strange' appearance of the raw data water levels, they were further adjusted to find a more representative trend of what was happening in the field. The figures 14a-c below, outline the process that was carried out in order to arrive at the final pressure heads.
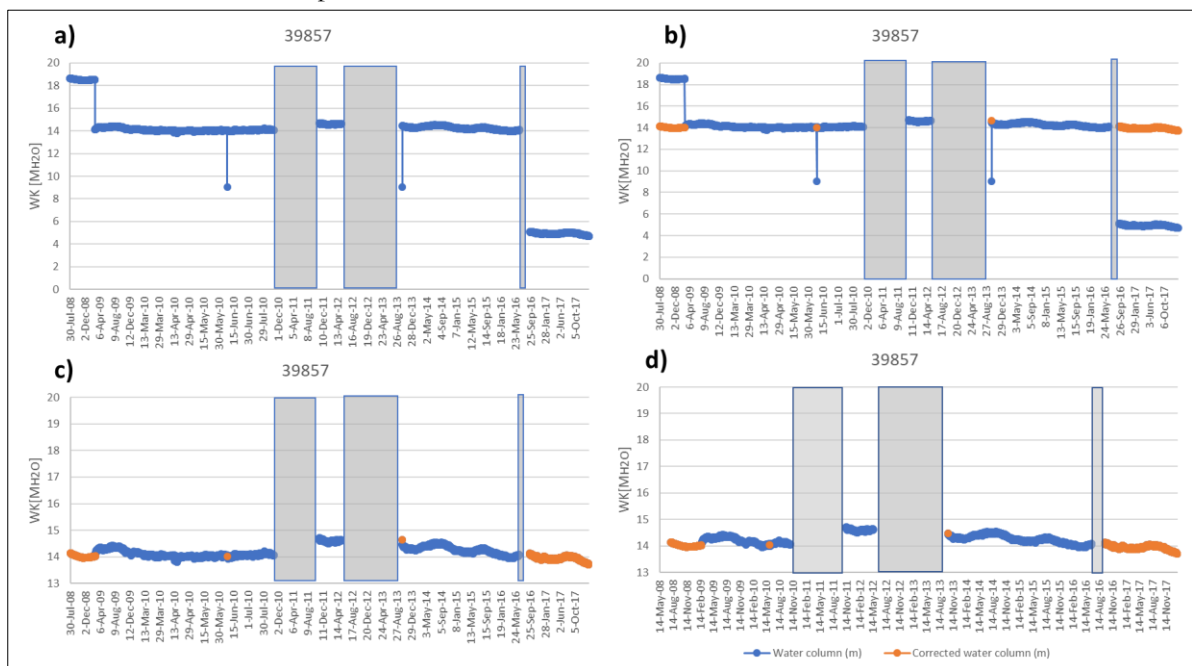
Figure 14: The data cleaning process of the piezometers located in the Auob Catchment; sequence of figures from a to d, represent sequence of correction steps.

During the data cleaning process, it was realised that boreholes had multiple values recorded on the same day at different times of the day. The daily observed values were analysed for outliers, the identified outliers were adjusted to follow a similar trend as most of the observed values on that day. During the adjustment process, the main purpose was to find a reasonable trend as the heads in the Kalahari aquifer are not much very variable in time. Therefore, the change of more than several to several tenths of centimetres of WK within few hours of data download was considered unlikely so the correction targeted in connecting such WK offsets.

The provided data set had undergone barometric effect testing with the intention of doing barometric correction of the data set. However, it was realised that after subtracting barometric pressure from the total head, the corrected heads still had a drift similar to the uncorrected record as indicated in Figure 15, because of one or more of the specified below reasons: i) the long distance between the barometric and pressure head measurement; ii) lack of synchronisation of logging time between groundwater level and barometric pressure; iii) barometric pressure attenuation (Obakeng 2006). For that reason, the barometric correction was not applied and the processed WK were directly converted to hydraulic heads based on local estimate of borehole altitude and finally averaged into daily time step required by the head observation (HOB) package of the numerical model.
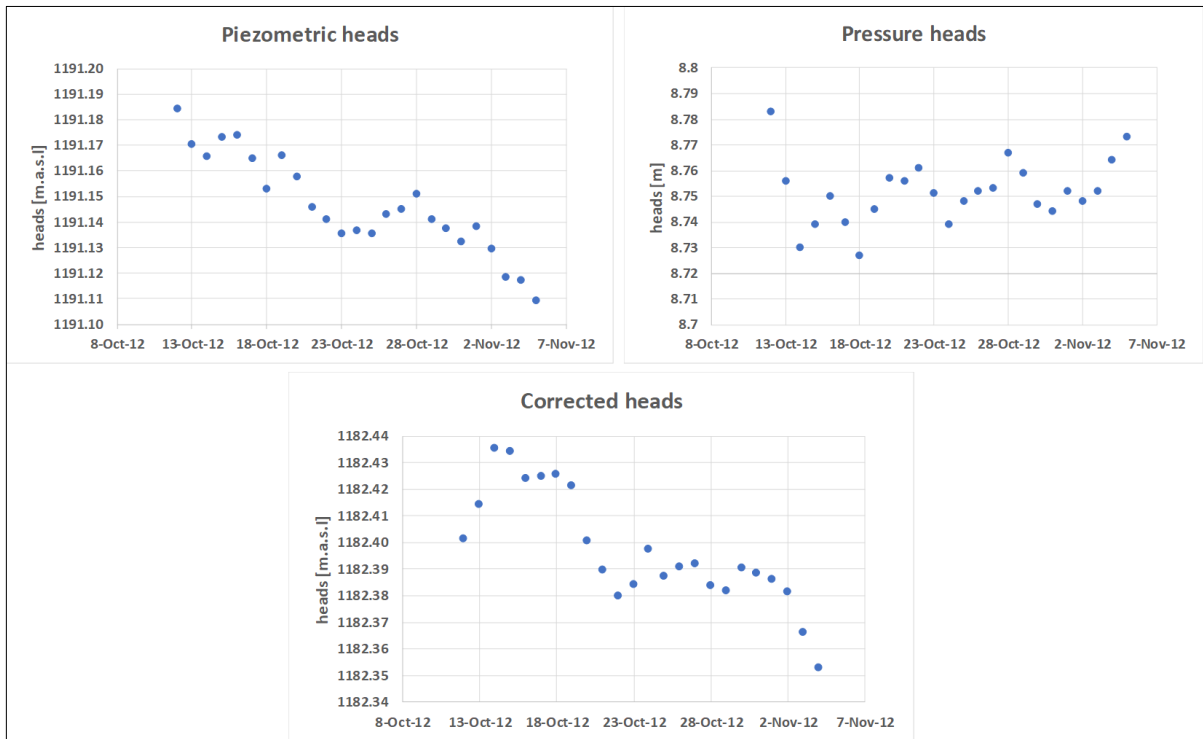
Figure 15: Uncorrected piezometric heads, pressure heads and corrected heads. Used to test the effect of barometric correction on the measured heads.

3.1.2.3. Abstractions
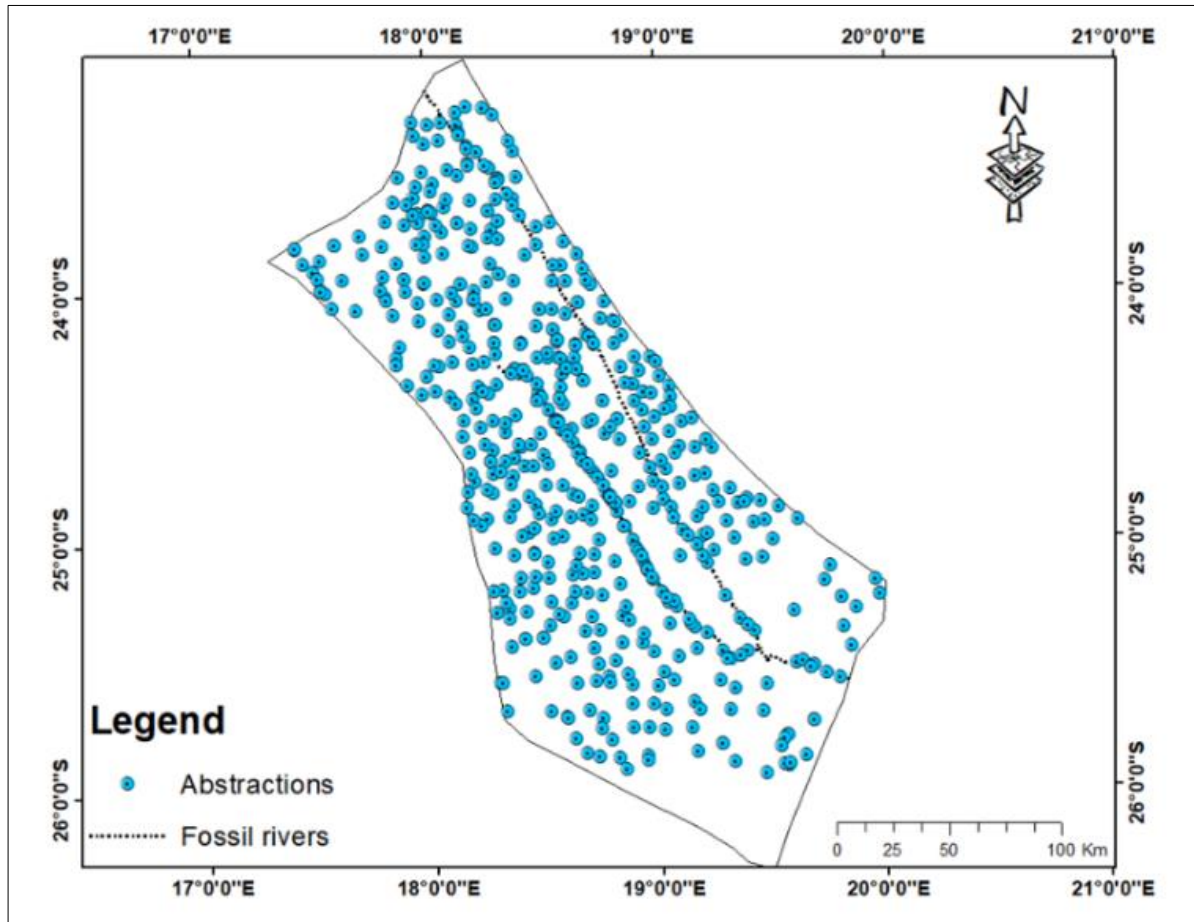
Figure 16: Abstraction borehole map. The map depicts the spatial distribution the 564 abstraction wells within the study area.

Figure 16 indicates the distribution of abstraction boreholes within the study area. The boreholes that had abstraction values with no coordinates where discarded, which resulted in 564 abstraction boreholes within the demarcated study area. Some boreholes had abstraction values, these boreholes account for 538 of the above-mentioned boreholes. The remaining 26 boreholes had no abstraction (0 m³ per day).

3.1.3. Satellite data

3.1.3.1. Digital elevation model.
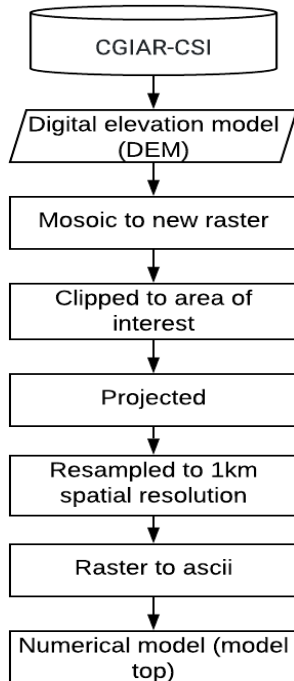
The DEM with 90m spatial resolution (SRTM 90m DEM Version 4) was downloaded by using this link: **http://srtm.csi.cgiar.org/download.** From the CGIAR- Consortium for Spatial information. After the processing of the DEM, it was used as a model top in the numerical model. The DEM was also used in the understanding of the topography of the area and treated as one of the factors that plays a role in catchment characteristics and the comprehending the topographic effect on the distribution of recharge in the Auob catchment.

Figure 17: DEM processing flow chart. Depicts the processes that were used for the processing of the DEM before it was imported into the model.

3.1.3.2. Precipitation

Precipitation is the most important model inputs especially for groundwater recharge estimates. Land surface precipitation is partitioned into runoff, infiltration, evapotranspiration, unsaturated-zone storage and recharge (Niswonger et al. 2006). Precipitation in integrated hydrogeological modelling is regarded as a driving force. Therefore, its continuity time is of great importance. The available insitu data had gaps, as discussed in section 3.1.2 of this study. Before the adoption of the gap filling method (such as the IDW method), a correlation of rainfall between different stations was carried out as indicated in section 4.1.2.1. There was a low correlation between the gauges within and around the study area. Thus, it was decided that the gauge rainfall estimates were not feasible to use in the gap filling process and as input into the model. Therefore, satellite products were evaluated and incorporated into this study.

The CHIRPS rainfall product was chosen for this study due to its high spatial resolution and lengthy records. Other products such as FEWSNET RFE, CMORPH and TRMM have a low spatial resolution of 11, (8,27) and 27 km respectively (Lekula et al. 2018; Kimani et al. 2018). CHIRPS have a spatial resolution of 5 km. It was preferred for this study since the model used was set to a spatial resolution of 1km. Making the resampling processes not too widespread compared to the other satellite rainfall estimates (SRE's). In terms of performance, the previously mentioned products were studied by Lekula et al., (2018) in an area of nearly the same terrain and climatic conditions (in relatively flat lands and semi-arid to arid environments) where he concluded that FEWSNET RFE performed better than the rest of the products.

During their study, they did not look at the performance of CHIRPS in relation to the other products. Another study was carried out in the same area and it mainly compared CHIRPS to FEWSNET RFE. That study preferred the performance of CHIRPS over FEWSNET RFE (Kipyegon, Lubczynski, Parodi, & Lekula, 2018). Which even further motivated the choice of this product. Apart from the good performance of this product over the others in this area; CHIRPS has undergone global bias correction using in-situ data. However, in most cases, these stations are spares and may not adequately represent the rainfall variability over the whole study area (Kimani et al. 2018). Hence, calling for some application of more ground-based bias correction schemes. It is further acknowledged that SRE's are associated with some errors and require even further correction.

Prior to the choice of the bias factor that will be implemented in this study, priority was given to the Kalahari station which is the main station within the study area. The available data set was evaluated based on their frequency of recording. It was noticed that this station had data gaps and due to the spatio-temporal variability nature of rainfall the implementation of data filling methods was not feasible as already discussed in section 3.1.2 of this study. During the correction data set evaluation between the satellite and the Kalahari station reading in terms of their accumulative rainfall, the following trend was noticed as indicated in Figure 18. This trend and its response to the space fixed and temporal variable bias factor is acceptable. However, due to the large gaps that were present during the analysis, this trend could not be used for the whole simulation period. Therefore, other bias factors where evaluated in the attempted of finding the most suitable bias correction factor as indicated in section 4.2.1.2 this study.

Cumulative precipitation
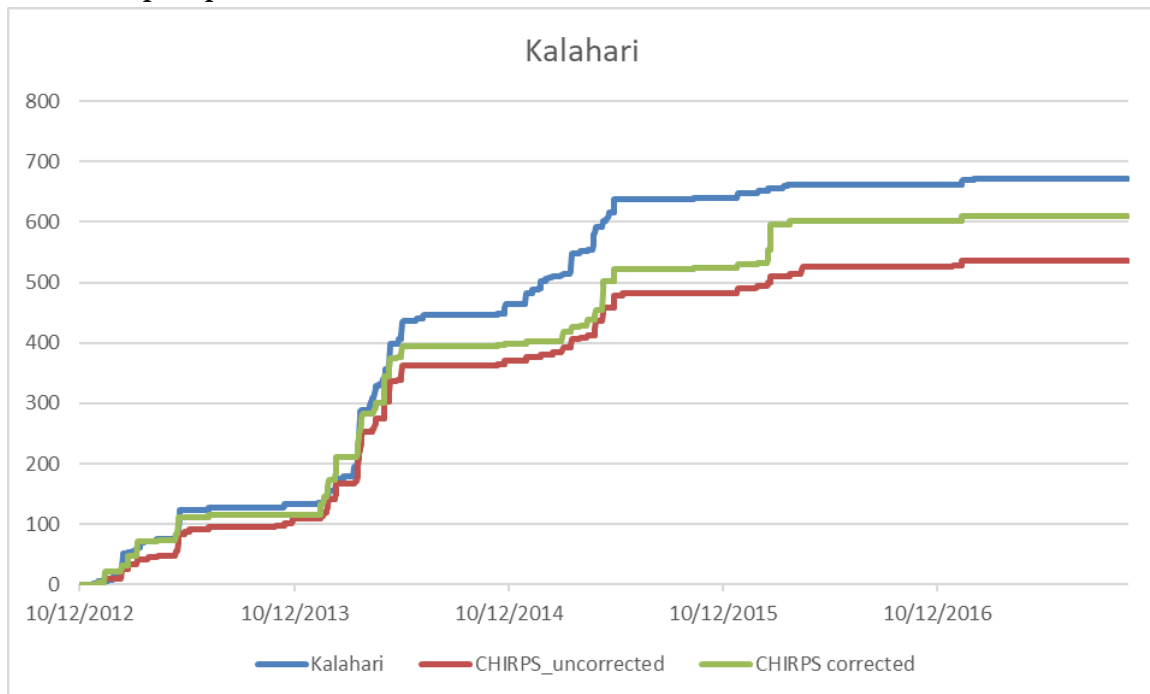
Figure 18:: The Kalahari station data in instances where both satellite and the gauge had recorded rainfall (no gap filling) as well as the CHIRPS bias corrected rain during that period.

The rainfall products were assessed for bias detection and decomposition. For bias detection the probability of detection (POD), false alarm ratio (FAR) and critical success index (CSI). All the bias detection schemes have a value range between 0-1, the POD a value close to 1 is preferred. Since it indicates that all or most of the rainfall occurrences were correctly detected. On the contrary for FAR, a value close to 0 is preferred. As this indicated that out of the occurrences during the satellite detections, the satellite did not have many

false detections. For the CSI a value of 1 is preferred as it indicated that in most of the cases the satellite correctly identified rain. Bias detection schemes were calculated based on the formula indicated below:

$$POD = \frac{hits}{Hits + miss}$$
(2)

$$FAR = \frac{false\ alarm}{hits + false\ alarm}$$
(3)

$$CSI = \frac{hits}{hits + miss + false\ alarm}$$
(4)

The satellite estimates were compared with the in-situ measurement to determine the bias at the pixel level. The bias was analyzed by decomposing it into three different components; hit, miss and false rainfall. The hit rain is when both the satellite and the gauge detect rainfall. The miss the satellite does not detect rainfall but the gauge recorded rain. The false rain is when the satellite detects rain and the gauge does not detect rainfall (Haile et al. 2013). When these conditions are encountered the following conditions were executed to decompose the bias;

$$Hit\ bias = \sum (R_s - R_g)|(R_s > 0\ \&\ R_g > 0)$$
(5)

$$Missed\ bias = \sum R_g|(R_s = 0\ \&\ R_g > 0)$$
(6)

$$False\ bias = \sum R_s|\left(R_s > 0\ \&\ R_g = 0\right)$$
(7)

$$Total\ bias = \sum_{i=1}^{n} R_s - \sum_{i=1}^{n} R_g$$
(8)

where: Rs is the satellite estimated rainfall [mm], Rg is rainfall from rain gauges [mm].

After bias decomposition, different bias correction schemes are used such as the BF_{TSF} (time and space fixed bias factor), BF_{SFTV} (space fixed and time variable) and BF_{TSV} (time and space variable) (Habib et al. 2014). The different bias factors were considered as indicated in section 4.2.1.2 of this study. The calculated bias factors were based on the below listed formula;

The two bias factors that were used for the bias scheme assessment for this study is indicated in the formula below;

$$BF_{TSF} = \frac{\sum_{t=1}^{t=T} G(i,t)}{\sum_{t=1}^{t=T} S(i,t)}$$

(9)

$$BF_{SFTV} = \frac{\sum_{t=d}^{t=d-l} G(i,t)}{\sum_{t=d}^{t=d-l} S(i,t)}$$

(10)

where: S is the satellite rainfall estimate, G is the rain gauge estimate, T is the full duration of the study period, t is the Julian day number, i refers to the gauge location, l refers to the length of the time window.

A comparison between the BF_{TSF} and BF_{SFTV} was made, regarding the space fixed and time variable bias factor a window of 7, 14 and 30 days was used. The outcome where compared to the time and space fixed bias factor as outlined in section 4.2.1.2 of this study. The use of other bias factors such as the BF_{TSV} require high gauge density within the area of interest as it uses interpolation methods which are prone to instability (Lekula et al. 2018). Especially when executed in areas of low gauge density (such as 5 stations within and around an area of ~40Mm²) such as the Auob catchment.

3.1.3.3. Potential evapotranspiration

Potential evaporation (PET) is defined as "the rate at which evapotranspiration would occur from a large area completely and uniformly covered with growing vegetation which has access to an unlimited supply of soil water, and without advection or heating effect" (McMahon et al. 2013). Potential evapotranspiration is mostly calculated using the FAO Penman-Monteith method, it is applicable when data (temperature, wind speed, atmospheric pressure, relative humidity, relative sunshine duration) is available at daily time scale.

The above mention data was available from the Sasscal weather net, but this data depended on the distribution of stations within the study area. Due to the low density of stations within the study area satellite products (US-based GMAO GOES-5 model) were incorporated into the study. The satellite products provided ET_o for the study area. The satellite ET_o was used together with the Kc factor map, for the calculation of PET using the Penman-Monteith method as indicated below:

$$PET = ET_0 * K_c$$

(11)

where ET_0 is the reference evapotranspiration [mm day $^{-1}$] and K_c is the crop coefficient [-].

Insitu ET_o was calculated using the microclimatic variables as listed in Table 2. The in-situ calculated ET_0 was compared to the ET_o from the satellite product. The reference evapotranspiration formula indicated below was used in the calculation of insitu ET_o which was further used on the validation of the ET_o product.

$$ET_0 = \frac{0.408 * \Delta * (R_n - G) + \gamma * \frac{900}{T + 273} \mu_2 (e_s - e_a)}{\Delta + \gamma(1 + 0.34 U_2)}$$

(12)

where Rn is the net radiation at the crop surface, G- soil heat flux [MJ m^{-2}day^{-1}], γ- psychrometric constant shanon [kPa$^°$C^{-1}], T- mean daily air temperature at 2m height [$^°$C], μ_2 -windspeed at 2 m height [ms^{-1}], e$_s$-

saturation vapour pressure [kPa], e_a-actual vapour pressure [kPa], Δ- slope of vapour pressure curve [kPa$^\circ$C^{-1}], e_s-e_a is the saturation vapour pressure deficit [kPa].

The satellite obtained ET$_o$ was be validated using the ET$_o$ calculated from the microclimatic data obtained from the met stations within and around the study area. For the validation process, the Pearson correlation coefficient was used based on equation (13). Scatter plots and cumulative curves were used to visualize and indicate the correlation between the in-situ and satellite ET$_o$ as indicated in section 4.2.2.

$$r = \frac{\sum(x - \bar{x})(y - \bar{y})}{\sqrt{\sum(x - \bar{x})^2 \sum(y - \bar{y})^2}}$$

(13)

where x- calculated ET$_o$ [mm day^{-1}] and y- is the satellite ET$_o$ [mm day^{-1}] and $\bar{x}$ and $\bar{y}$ are mean values.

Kc can be represented either as a single crop coefficient or a dual crop coefficient. The dual crop coefficient approach is more data demanding compared to the single crop coefficient. Moreover, the obtained Kc value could vary in time as well as space. The details on how time variant Kc and how it could be used in hydrological modelling are described in (Mehreteab et al. 2016). This study adapted the single crop coefficient approached, due to lack of data and detail description of plants as well as soil type. The Kc factor for this study was space variable and time fixed. The land cover land use (LCLU) Kc factor values were selected based on (Allen et al. 1998) and (García Petillo and Castel 2007). The selected Kc factors where imported into the model as a map derived from the landcover map following the steps shown in Figure 12.

Table 4: The land cover and land use classes as well as their Kc factors. The Kc factor values were selected based on (Allen et al. 1998) and (García Petillo and Castel 2007). The Kc factor was spatially variable and temporally in variant.

Land cover & land use	Kc factor
Trees	1.15
Shrubs	1.05
Cropland (Lucerne and wheat)	0.85
Grass	1
Bare areas	1.03
Built-up areas	0

According to the authors only Lucerne and wheat showed temporal variation and the others land cover features were reasonability stable in time. Thus all the land cover features were assumed to be variable in space and invariant in time.

Interception and infiltration rate

Infiltration is the difference between received rainfall and interception, due to the presence of the thick Kalahari sands and the fact that the catchment under observation has a fossil river, runoff in this study will be regarded as neglectable. Interception is the portion of rain that fall on vegetation, but never reach the ground and evaporates from the wet canopy (Van Dijk et al., 2015). The infiltration is calculated using the below mention formula and it should be noted that the infiltration rate is influenced by the vertical hydraulic

conductivity and the soil saturation degree. It is one of the requirements for the UZF1 package (Niswonger et al. 2006).

$$P_e = P - I$$

where Pe- infiltration rate per grid cell [m day⁻¹], P-precipitation [m day⁻¹] and I- canopy interception per grid cell [m day⁻¹].

The study area is covered by shrublands, grasslands, trees, cropland, built-up areas and bare land. The interception in the study area will be based on the formula below (Teketel et al. 2017);

$$I = P * \left(I_s * A_s + I_g * A_g + I_t * A_t + I_c * A_c * I_{bt} + A_{bt} \right)$$

where I- canopy interception per grid cell [m day⁻¹], P-precipitation [m day⁻¹], I_s, I_g, I_t, I_c, and I_{bt} – interception loss rates by shrubs lands, grasslands, trees, croplands and built up areas respectively in % of precipitation and A_s, A_g, A_t, A_c and A_{bt}, – spatial coverage per grid for shrubs lands, grasslands, trees, cropland and built up areas respectively.

Interception loss is strongly dependent on the vegetation structure, meteorological conditions, intensity and timing of rainfall (Kozak et al. 2007; Toba and Ohta 2008; Muzylo et al. 2009). In terms of rainfall timing for the Auob Catchment, simulation were based on the hydrological year which starts on 1st September and ends on the 31 August. The wet season ranges from the 1st September to 31st April and the dry season from the 1st May to the 31st August. These represents the variation in the climatic conditions within the simulated domain. The interception losses were obtained from literature as indicated in the Table 5 below:

Table 5: Landcover types and rate of interception during the wet (1st September to 31st April) and dry (1st May and 31st August) seasons. The interception rates were both spatially and temporally variable.

Land cover	Wet interception (dry season interception) [%]	Literature
Trees	12(8)	(Le Maitre et al., 1999)
Shrubs	4(2)	(Werger et a., 1973)
Grassland	5 (2)	(Corbett 1968)
Crop land (wheat & Lucerne)	1.3(1.3)	(Kang et al. 2005)
Built up area	6(1.9)	(Van Der Linden 2010)
Bare land	0	-

3.2. Model conceptualization

A conceptual model is a hypothesis that shows how a system or process operates (Konikow and Bredehoeft 1992). A hydrogeological conceptual model simplifies and summarizes hydrogeological information in the form of tables, graphs, flowcharts or written text. It expresses the past and current state of the system based on field information or similar sites and provides a framework for designing the numerical model (Anderson et al. 2015).

3.2.1. Hydro-stratigraphic units

The geological classification of these structures, as well as the hydrogeological classification, are indicated in Figure 9 and Figure 10 in section 2.7 of this study. Hydro-stratigraphic units are composed of geological

units that have similar hydrogeologic properties. Thus, some geological units can be combined into one hydro stratigraphic unit and while one geological unit may be separated into several hydro stratigraphic units with confining layers between them (Anderson and Woessner, 1992).
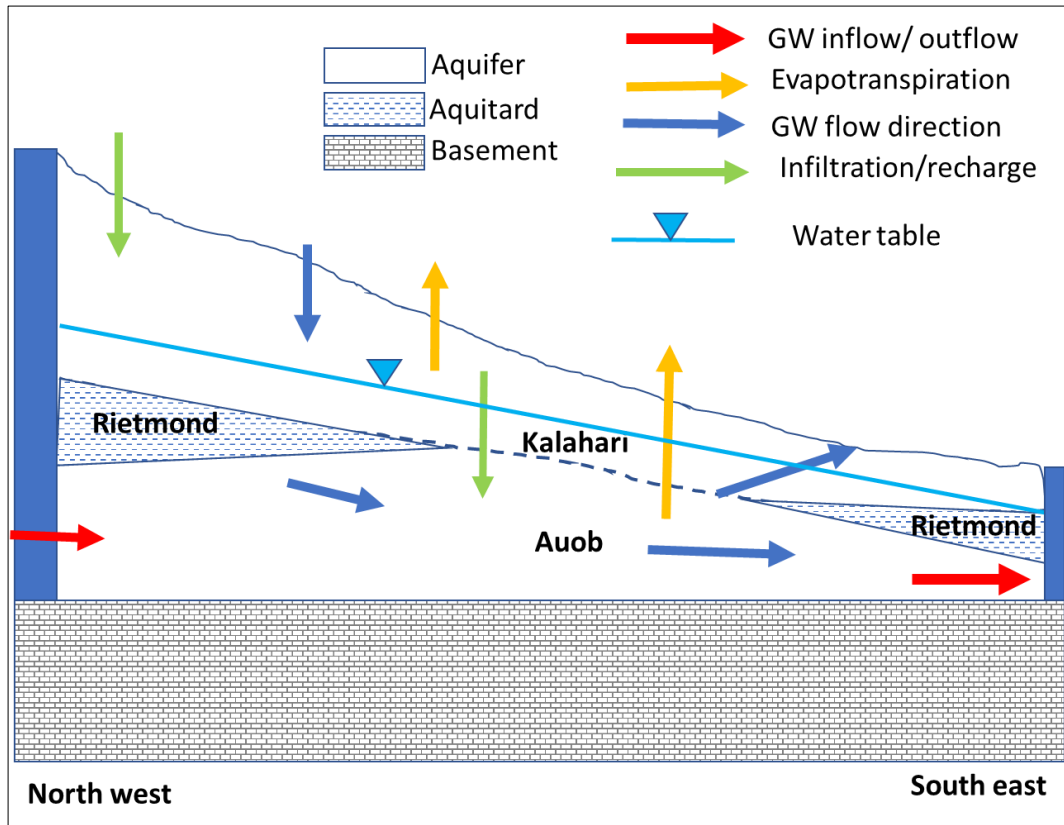
Figure 19: Conceptual model of the Auob Catchment (not to scale).

The layer discretization is influenced by the objective of the study and data availability. For this study, the model was treated as a single unconfined aquifer, by uniting the Kalahari and the Auob aquifers and treaing them as a single hydrostratigraphic unit. The layers from the lower Mukorob to pre-Ecca were treated as a basement or aquiclude as in Figure 19. The simplification of the model was due to the primary purpose of the study which is to account for the spatial distribution of the groundwater recharge from the precipitation received in the area and based on the various reasons as stipulated in section 2.7 of this study.

3.2.2. Flow direction

The Auob Catchment ranges along the highlands that are situated in the north-western part of the study area. The study area's topography gradually decreases towards the south east where relatively low lands are found. The groundwater generally flows from the high hydraulic heads in the northwest to the low hydraulic heads in the southeast Figure 20. Following the topographic surface of the study area.

3.2.3. Sources and sinks

Rainfall is the primary source of water in the Auob Catchment. The received rainfall is partitioned into an interception by plants and the remaining part called effective rainfall seeps into the thick Kalahari sands were some of the water is evaporated. The remaining water percolates deeper into the groundwater table as gross recharge, which is the groundwater recharge without the effect of groundwater evapotranspiration and exfiltration. After groundwater evapotranspiration and exfiltration has taken place, then net recharge is

experienced which under normal rainfall years is relatively low considering rather horizontal pattern of the Kalahari hydraulic heads (JICA 2002; Obakeng 2007; Alker 2008; Lekula 2018).

Studies have revealed that there are small, shallow depressions that are a result of the calcrete dissolution. These depressions acts as sinkholes, that collect water and further distribute it into permeable layers (Alker 2008). Apart from the sinkholes recharge is also said to occur in fractures, which are located within the SAB. These are evident due to the rising water table several kilometers from the identified recharge zones, after heavy rainfall events. The lower end (south-eastern) of the Auob catchment is known as the salt block area (JICA 2002). In this area, groundwater flows out of the deeper aquifers into the thick Kalahari sands where it is lost via evapotranspiration. Most of the water in the Kalahari aquifer is lost through evapotranspiration and very little discharges from springs. Apart from evapotranspiration and spring loses other sinks are experienced in the study area; these include abstraction wells and lateral groundwater outflow via the south eastern boundary. Storage changes could also have an influence in the gain or losses of the aquifer and they only happen over a specified period such as within a given year.

The different components of the groundwater were quantified during the simulation period. In simple terms the water balance components can be quantified based on the equation indicated below;

$$Inflow = Outflow \pm change\ in\ storage \qquad (16)$$

whereby, whatever comes into the model domain, should be approximately equivalent to whatever goes out of the model domain; the eventual differences are related to changes of water storage. With either gains or losses of the aquifer. Equation (16) was adapted from Anderson et al., (2015). The details on the individual water components and how they were accounted for is stipulated in section 3.3.9 of this study.

3.2.4. Boundary conditions
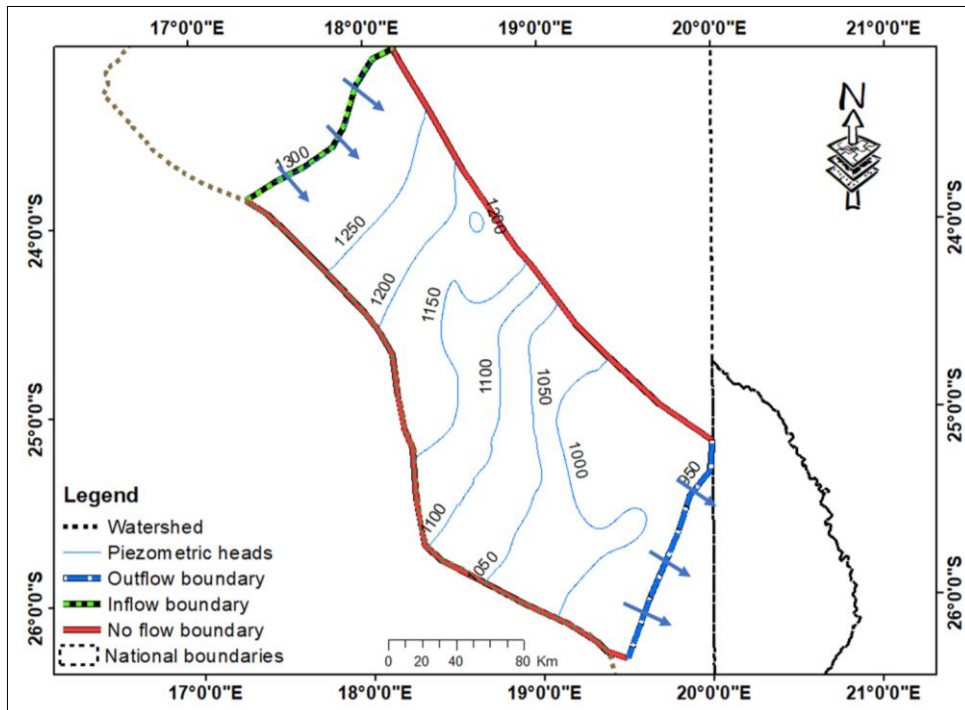
Figure 20: Model boundary conditions map. The map represents the different boundary conditions which were assigned during the model conceptualization.

The study area is ~40 Mm² and the whole south-western boundary extends along the national watershed boundary which separates flows discharging directly into the Atlantic Ocean and those towards Botswana-South Africa, discharging indirectly to Atlantic Ocean, through the Orange River. Thus, the whole of the north west to the south east area will be assigned a no-flow boundary. Meaning there is no groundwater flux exchange taking place in this area. The water in the study area flows from the northwest to the southeast. Thus, creating streamlines in the upper part of north-western to the south eastern part of the study area, hence, this area is assigned a no-flow boundary. The water flows to the south-eastern part of the study area and drains into South Africa. For this reason, an outflow boundary is assigned in the south-eastern part of the study area. The north-western region of the study area is receiving water from the high lands along the watershed into the study area. Thus, an inflow boundary was assigned in this zone.

3.3.   Numerical model

The numerical model is representation of reality that replaces objects, events and forces with a mathematical expression. Today most numerical models are deterministic models which are based on the conservation of mass, energy and momentum, by balancing different fluxes of these quantities (Konikow and Bredehoeft 1992). Numerical models are becoming more popular due to their flexibility as well as their capabilities to handle complex problems, especially at the catchment scale (Baalousha 2016). Numerical models yield approximate solution based on governing equation(s). It should be noted that numerical models only provide approximated solutions (Konikow & Bredehoeft, 1992). Konikow & Bredehoeft, (1992) further states that it is imperative that the user of the model is aware of the derivative approximation, scale of discretization and matrix solution techniques. In order to avoid the introduction of significant errors to these already approximated solutions.

3.3.1 Software selection

The selection of software is dependent on the objectives and the environment which is being modelled. For this study, the MODFLOW-NWT was used. MODFLOW-NWT is the Newton formulation of MODFLOW-2005. The unconfined groundwater flow equation has problems with the drying and rewetting nonlinearities, MODFLOW-NWT is a standalone program that is designed to solve these problems. The MODFLOW-NWT should always be used in conjunction with the Upstream-Weighting (UPW) package (Niswonger and Panday, Sorab. Motomu 2006). The UPW package is used for calculating intercell conductance and use a continuous function of groundwater head to treat nonlinearities of cell drying and rewetting. Thus, enabling the application of the Newton formulation for unconfined groundwater flow equation because of smooth conductance derivatives over the full range of head for a model cell (Niswonger & Panday, 2006). Further, it was used for the inputting of the parameters that control the flow between the cells in MODFLOW-NWT (Niswonger and Panday 2011).

3.3.2. System discretization

Numerical models require discretisation of both, time and space. The approximation of the variable internal properties, stresses and boundary of the system area carried out within the discretized format (Konikow & Bredehoeft, 1992). The choice of an appropriated spatial discretization is depended on the objectives of the study, data availability, dominant hydrological processes and the spatial resolution of the data set (Dehotin and Braud 2008). (Dehotin and Braud 2008) further states that for large catchments it is not feasible to explicitly represent landscape heterogeneity thus calling for more simplification. For the Auob Catchment model is composed of 1 convertible layer with 371 rows and 268 columns. With a grid size of 1 km, model time is in days within the range of 1st September 2012-31st August 2017 and model length unit are in meters.

3.3.3. Driving forces

Driving forces are also known as forcing data. These data, in case of the MODFLOW-NWT, include effective precipitation, potential evapotranspiration (PET) and abstractions. For accurate temporal and spatial hydrological analysis, it is important that the driving force are continuous and consistent. In case of MODFLOW-NWT, the driving forces such as effective precipitation and potential evapotranspiration must be provided on complete-daily basis, i.e. for each day simulated. The processing and use of these driving forces are indicated in section 3.1.3.2 and 3.1.3.3 of this study. Rainfall and potential evapotranspiration was assigned to the model using the UZF package in MODFLOW-NWT, the package has the ability to integrate surface and subsurface processes during the model simulation. The abstraction wells in the study area, as indicated in section 3.1.2.3 of this study, were assigned using the well package. In case of several wells in one cell, the sum of the well discharges was applied for that cell.

3.3.4. State variables (heads)

State variables are also known as the ground truth. They are used as calibration targets during the model calibration process. They also help constrain other adjusted parameters to ensure that the model simulated heads mimic the ground observations. For this study, the remaining 13 monitoring boreholes as stipulated in section 3.1.2.2**Error! Reference source not found.** were used as state variables in the model calibration. The data was not continuous in time, since they were used as state variables their temporal continuity was not a prerequisite for their use. The observation heads that are used in the observation process, were specified under the head observation (HOB) package. The observation analysis under this package was set in relation to all heads.

3.3.5. Model parameterizations

Numerical models are said to be generic in nature, but what brings them to the specification of the geographic area of interest is dependent on the parameterization of the model (Konikow and Bredehoeft 1992), Konikow & Bredehoeft, (1992) further states that when parameters (such as hydraulic conductivity and storativity), grid dimensions and boundary conditions are simplified, it should be in such a way that they represent a particular site, this is what makes a computer program a site specific model. On the contrary Hill, D'agnese, & Faunt, (1999) states that prior information should be omitted since the omission of prior information promotes how well the data constrain the model. For this study both the approaches were evaluated and used to best represent the field observation and assigning realistic boundaries in order to mimic the Auob Catchment in the best possible way.

Table 6: Auob Catchment parameterization. ε-Brooks and Corey exponent; EXTWC- evapotranspiration extinction water content; EXTDP- evapotranspiration extinction depth; Kv- vertical hydraulic conductivity; Kh- horizontal hydraulic conductivity; Sy- specific yield; θs- soil saturated water content; θr- soil residual water content; cond- conductance; UZF1- unsaturated zone flow; UPW- upstream weighting package HFB- flow and head boundary.

Zone	parameters	Minimum value	Maximum value	unit	MOD- package	Source
Unsaturated zone	Infiltration	0.00028	0.000576	md^{-1}	CHIRPS SRE after correction and validation	Images
	PET demand	0.005108	0.006098	md^{-1}	Satellite ETo in combination with the Kc factor map	Images
	ε	3.5	3.5	-	UZF1	Literature
	EXTWC	0.06	0.16	m³m^{-3}	UZF1	Literature

	EXTDP	0	56	m	UZF1	Literature
	Kv	Kh $_{(min)}$/10	Kh $_{(max)}$/10	m d^{-1}	UZF1	Literature
	θ_s	0.37	0.43	m³m^{-3}	UZF1	Literature
	θ_i	0.05	0.15	m³m^{-3}	UZF1	Literature
	θ_r	0.05	0.15	m³m^{-3}	UZF1	Literature
Saturated zone	Sy	**0.15**	**0.24**	-	UPW	Field and literature
	Kh	8	90	m d^{-1}	UPW	Calibrated
	Cond	25	25	m² d^{-1}	Drain	Calibrated
	Specified flux	0.409	0.409	m³ d^{-1}	FHB	Calibrated

Newton (NWT) solver

The Newton solver was used during this study. With the aim of solving the equations that govern the finite difference, during the different stress period of MODFLOW-NWT.

Table 7: MODFLOW solver options used in the model parameterization.

Solver	Parameter value [unit]
Head tolerance (HEADTOL)	0.001[m]
Flux tolerance (FLUXTOL)	100 [m³d^{-1}]
Maximum number of outer iterations (MAXITEROUT)	300
Portion of cell thickness used for coefficient adjustment (THICKFACT)	0.00001
Matrix solver (LINMETH)	Chi MD (2)
Print solver convergence information (IPRNWT)	Active
Correct groundwater head relative to the cell-bottom altitude when the cell is surrounded by dry cells (IBOTAV)	Active
Model complexity	Complex

UZF

Table 8: UZF parameterization, the values assigned to the activated parameters are indicated in Table 6.

Name	Parameter [unit]
Recharge and discharge location (NUZTOP)	Top layer
Vertical hydraulic conductivity source (IUZFOPT)	Specify vertical hydraulic conductivity
Number of trailing waves (NTRAIL2)	15
Number of waves set	20
Simulate evapotranspiration (IETFLG)	Active
Print summary of UZF budget terms (IFTUNIT)	Active
Specify residual water content (SPECIFYTHTR)	Active
Specify initial unsaturated water content (SPECIFYTHTI)	Active

Calculate surface leakage (inverse of NOSURFLEAK)	Active
The average height of undulations in the land surface altitude (SURFDEP)	1[m]

UZF1 package

The UZF1 package is the replacement of the recharge and evapotranspiration package in MODFLOW-2005. The UZF1 package can simulate groundwater flow in terms of runoff, groundwater discharge, evapotranspiration and infiltration both in space and time. The package can account for both groundwater flow and the associated boundary conditions. The rate at which infiltration takes place is influenced by the saturated vertical hydraulic conductivity. The infiltration (effective rainfall), evapotranspiration demand (PET), extinction depth (rooting depth map) and the extinction water content were assigned in support of literature specification (Niswonger et al. 2006).

Extinction depth and extinction water content

The extinction depth is influenced by land cover and soil types. The types of vegetation in the study area influences the soil water fluxes. It is important when modelling evapotranspiration that different evapotranspiration parameters such as rooting depth should be spatially variable in order to account for variability that is associated with the vegetation and soil types (Shah et al. 2007; Liu et al. 2015). The extinction depth for the different vegetation types were assigned based on estimates of rooting depths for different land cover types defined on land cover map. The assigned values were adopted from different literature as indicated in Table 9 below.

Table 9: Extinction depth for different land cover types.

Land cover	Maximum rooting depth/ Extinction depth [m]	Literature
Trees	56	(Shadwell and February 2017)
Shrubs	15	(Le Maitre et al. 2015) and (GGRETA 2016)
Cropland	6.48	(Lu et al. 2011)
Grassland	1.45	(Shah et al. 2007)
Bare land (sand soil)	0.5	(Shah et al. 2007)

The extinction depth was spatially variable and it was influenced by the landcover. These values were assigned based on literature as indicated in Table 9 above. In spite of the 56m rooting depth that can be depicted from Table 9 it should be noted that due to the averaging effect per pixel the dominant species in the pixel contributes more to the averaging and this can be depicted in the high extinction depths are associated with areas that are dominated by shrublands and tree mixtures this could be due to averaging of the land cover features during the resampling process. Therefore, the dominant landcover type per pixels contribute more to the average as indicated in Figure 21 were the high values are associated with areas dominated by shrublands and some patches of trees resulting in the highest extinction depth having a value of 16.94 m instead of 56 m.
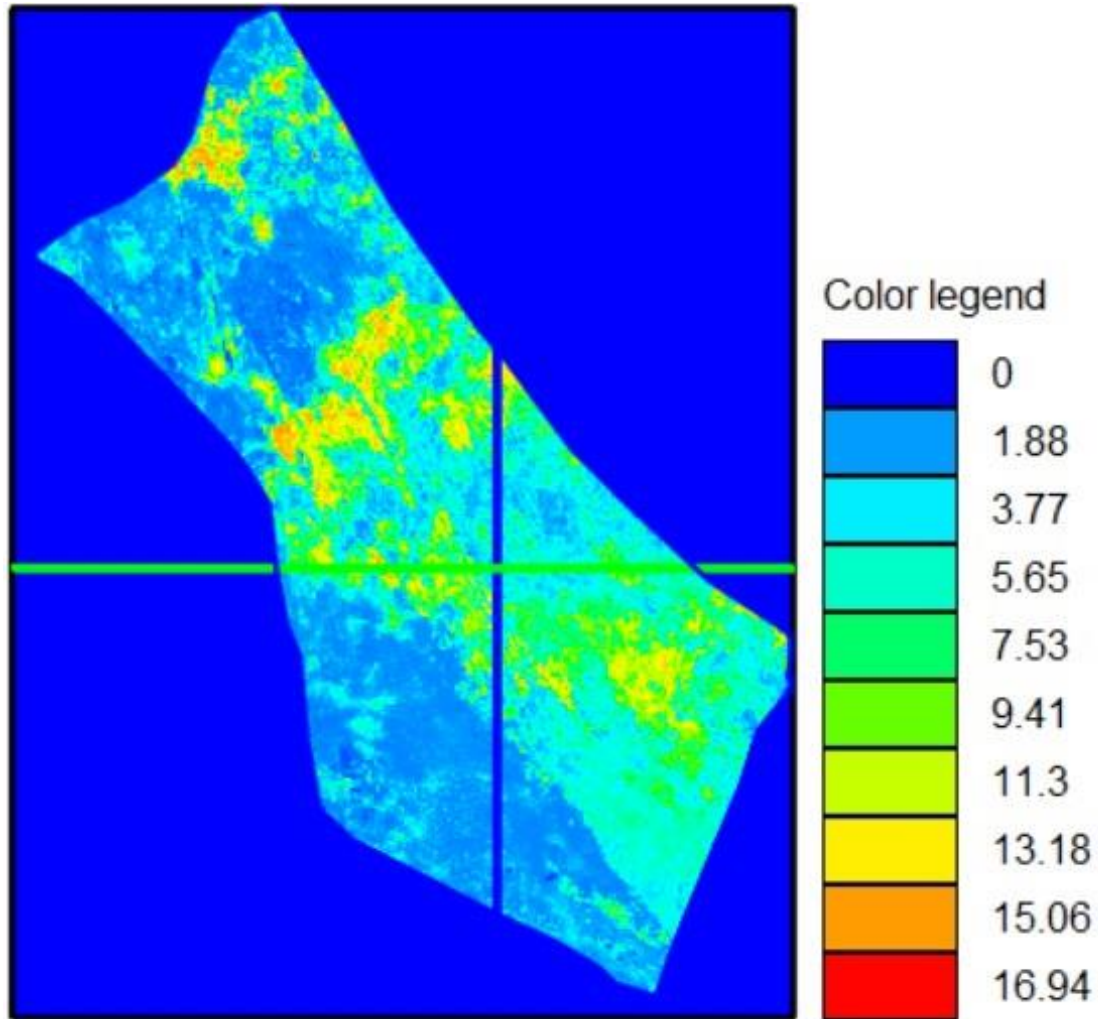
Figure 21: The final model extinction depth after pixel averaging based on the dominant land cover types per pixel.

The extinction water content was assigned as a function of residual water content (residual water content +0.02). As such, it was temporary and spatially uniform. The initial water content was assigned an initial value as indicated in Table 6. The residual water content, initial water content and extinction water content values were adjusted during model calibration.

Hydraulic conductivity and specific yield

The upstream weighting package (UWP) is used for calculating intercell conductance and use a continuous function of groundwater head to treat nonlinearities of cell drying and rewetting. Thus, enabling the application of the Newton formulation for unconfined groundwater flow equation because of smooth conductance derivatives over the full range of head for a model cell (Niswonger & Panday, 2006). Further, it was used for the inputting of the parameters that control the flow between the cells in MODFLOW-NWT (Niswonger and Panday 2011). Thus, the package was used to assign hydraulic (horizontal and vertical) conductivity zones. Both the soil and geology in the different zones were considered when assigning the hydraulic conductivity values. The specific yield was also assigned using this package. The specific yield value was spatially uniform with a value of 0.02. The range of the values assigned to this package is outlined in Table 6.
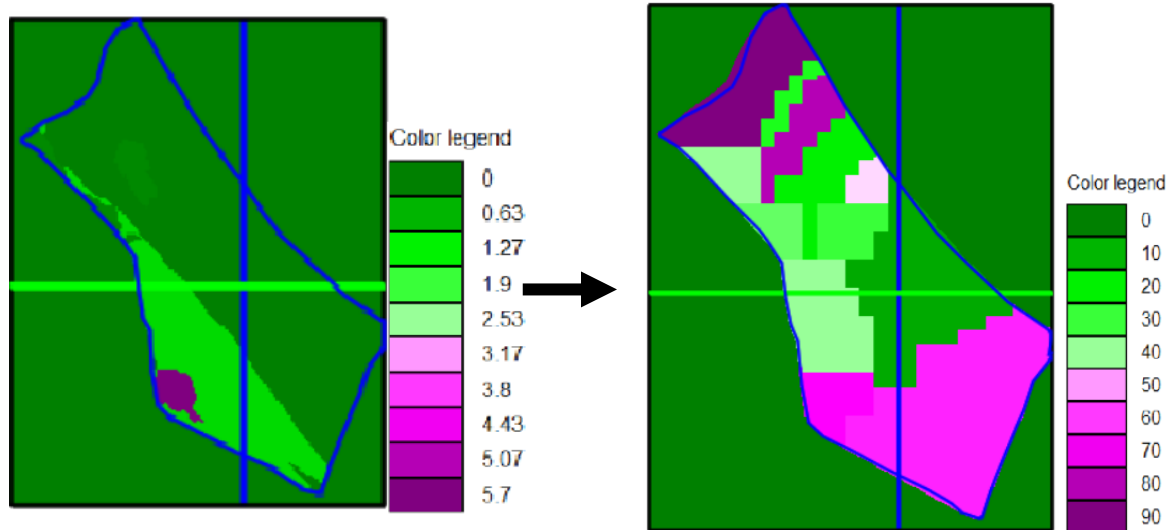
Figure 22: Spatial variability of Kh zones. Initial assigned values and values changed during the calibration.

The initial values were assigned based on borehole data field data and were adjusted during the calibration in order to try and represent the ground truth. The model was simulating a lot of water thus the Kh zone values were increase to try and allow water out of the model as indicated in Figure 22.

3.3.6. Boundary conditions

The study area is typical flow-through area with inflow boundary at the NW outflow at the SE and two no-flow boundaries at the SW and NE. For the NW inflow, General Head Boundary (GHB) Package was proposed, for the SE outflow, Drain Package while the remaining two boundaries were kept as no-flow boundaries. The GHB and Drain Packages are head-dependent flux boundaries. In GHB Package, the inflow (or outflow) fluxes are dependent on the difference between current groundwater head and predefined GHB head of the external source and on the GHB conductance. In the Drain Package, the outflow depends on the head difference between current head and the predefined drain elevation but in the drain package in contrast to GHB, if the current head falls below the drain elevation the outflow is terminated and the inflow is impossible (Harbaugh et al. 2000).

The GHB elevation (identified as the head of the external source of water) was set as 'model top minus 45 m' and the conductance was assigned 20 m^2d^{-1}, both the GHB elevation and conductance was adjusted during model calibration. The drain package was used for the simulation of water outflow of the model domain. The drain elevation was assigned as the model top -30 m. the conductance was set to 30 m^2d^{-1}. Both the drain elevation and drain conductance were adjusted during the calibration of the model.

After some preliminary model runs, it was realised that the model was allowing water out (instead of in) at the GHB inflow boundary. To overcome this problem, the GHB package was replaced by the flow and head boundary (FHB), specified-flow package. For the FHB, a polyline was used to specify the lateral groundwater inflow from the NW. The flow was specified according to Darcy Law (17) based on total rate divided by the object area, multiplied by the object intersected area. As indicated in the formula below;

;

$$Q = K * A * I \qquad\qquad (17)$$

where Q is the is the NW-boundary inflow rate [m³d⁻¹], K is the hydraulic conductivity [md⁻¹], A is the boundary gross cross-sectional flow area [m²] and I is the gradient [-]. Equation (17) can further be presented as follows;

$$Q = K * \left(W_i * \frac{h_1 + h_2}{2} \right) * \frac{\Delta h}{L}$$

(18)

where W_i – the boundary width [m], h_1 and h_2 are the heads [m] at two observational points measured across the boundary along the L, Δh [m]- head difference along the L and L [m] is the flow length along which Δh is defined. See appendix for the calculation of the assigned flow value, it should be noted that the calculated value is the initial assigned value and this value was adjusted during the calibration process based on changes in the hydraulic conductivity.

No flow boundaries

ModelMuse automatically treat the area with no assigned external boundary conditions as no flow boundaries. Thus, after assigning the general head (which was later substituted by the flow and head boundary) and the drain boundaries the rest of the study grid was not set to any external boundary and they were treated as a no flow boundary.3.3.5.2.

3.3.7. Model calibration

The model was calibrated in transient state. The initial conditions of the model were set to steady state to aid in the model initialization. The given variables for the steady state simulation were mainly averages of PET, effective rainfall (P_e), average piezometric heads. During the model spin up period, some of these variables such as P_e and PET were adjusted based on the minimum to the maximum range of the inputs until the best fit response in the model warming up was met. 1 year data was used for the warming up of the model and then discharged as it was not used in the analysis process as per the approach by El-Zehairy et al. (2018). The transient model had 1826-time steps. During the model calibration, the aim was to find a good match between the water balance (WB) components and have a match between the field observed heads and the model simulated heads. The calibration process was executed via trial and error, these method of model calibration enables the modeller to acquire knowledge about the modelled site and the behaviour of the model (Hassan et al. 2014). Moreover, the model calibration was based on the adjustment of certain parameters such as the hydraulic conductivity, specific yield, initial water content, residual water content, maximum saturated water content, extinction water content, drain conductance, drain elevation and specified flow flux as per Table 6 .

3.3.8. Model performance evaluation

The model's performance was evaluated by computing the residual at each calibration target by determining the mean error (ME), mean absolute error (MAE) and the root mean squared error (RMSE) (Anderson et al. 2015). The formula listed below were used for computing the residual at each calibration target;

$$ME = \frac{1}{n} \sum_{i=1}^{n} (h_{obs} - h_{sim})i$$

(19)

$$MAE = \frac{1}{n} \sum_{i=1}^{n} |(h_{obs} - h_{sim})i|$$

(20)

$$RMSE = \sqrt{\frac{1}{n}\left(\sum_{i=1}^{n}(h_{obs} - h_{sim})_i^2\right)} \qquad (21)$$

where n, h_{obs} and h_{sim} are the number of observations, observed heads(m) and simulated heads (m) respectively. Obtaining a good fit does not necessarily mean that the match is acceptable, the match is only acceptable if the parameters and the water balances assumptions used in obtaining this match are realistic. During model performance evaluation, both the hard (history matching) and soft (hydrogeologic reasonableness) knowledge need to be taken into account to best represent the field site (Anderson et al. 2015).

3.3.9. Water balance
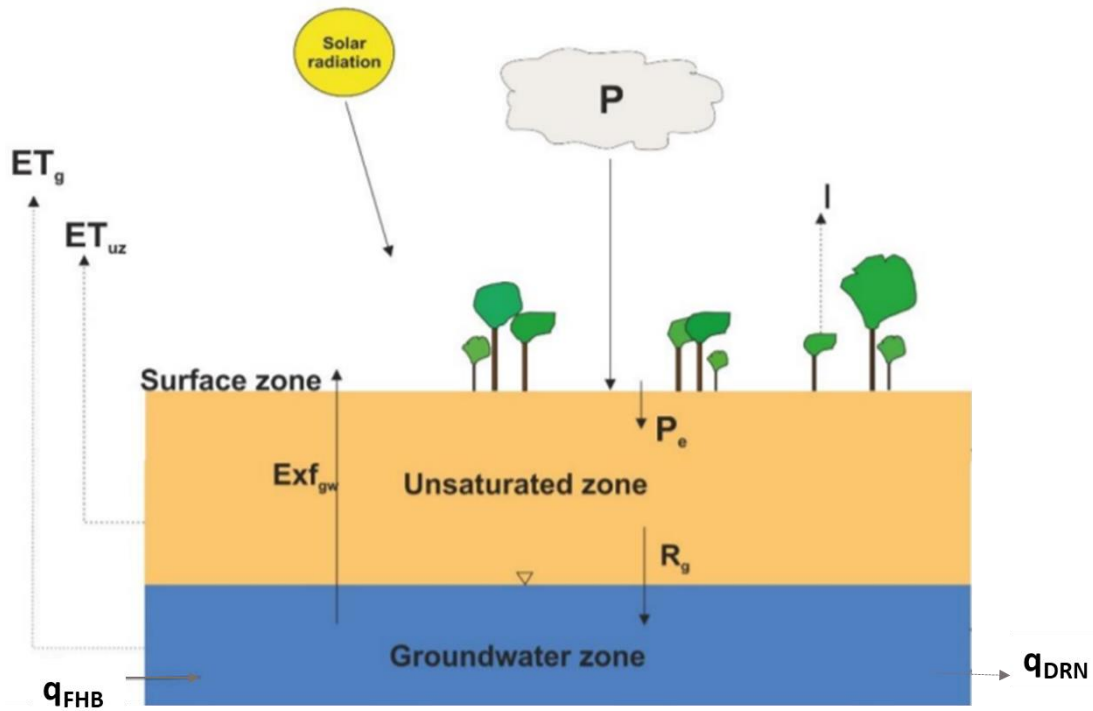
Figure 23: Water balance components map. Source: modified from (Hassan, 2014). The map depicts the different components of the water balance and how the received precipitation can be potentially distributed within the Auob Catchment.

where P is precipitation, I is interception from the canopy, Pe is effective precipitation, Exf_{gw} is groundwater exfiltration, R_g is gross recharge, ET_g is groundwater evapotranspiration, ET_{uz} is unsaturated zone evapotranspiration and q_g is the lateral groundwater outflow.

The water balance for the study area can be presented as follows (Hassan et al. 2014; El-Zehairy et al. 2018; Lekula 2018):

$$P + q_{FHB} + I_g = q_{DRN} + I + q_{ABS} + ET_{ss} + R_o + \pm\Delta S \qquad (22)$$

where: P- precipitation, q_{GHB}- the lateral groundwater flow into the modelled domain across the general head boundary, q_{DRN}- lateral groundwater outflow from the model domain via the drain boundary, I -

interception losses by the canopy, q_{ABS}- groundwater abstraction, ET_{ss}- Subsurface evapotranspiration and ΔS- total change in storage, R_o- runoff and for this study is considered insignificant.

ETss and ΔS can be quantified as follows:

$$ET_{ss} = ET_{uz} + ET_g \tag{23}$$

The subsurface evapotranspiration is composed of the unsaturated zone evapotranspiration and the groundwater evapotranspiration as expressed in the above mention equation.

$$\Delta S = \Delta S_{uz} + \Delta S_g \tag{24}$$

The total change in storage is the combination change in storage in the unsaturated zone and the saturated zone.

Water balance of land surface and unsaturated zone, in this case groundwater runoff is not considered, can be expressed as follow:

$$P_a = P_e + EXF_{gw} = R_g + ET_{uz} \pm \Delta S_{uz} \tag{25}$$

where actual infiltration is a combination of effective precipitation (which is a result of precipitation minus interception) and groundwater exfiltration which is equivalent to the combination of gross recharge, unsaturated zone evapotranspiration and unsaturated zone change in storage.

$$R_g + q_{FHB} = q_{ABS} + q_{DRN} + ET_g + EXF_{gw} \pm \Delta S_g \tag{26}$$

Net recharge is expressed as follows:

$$R_n = R_g - EXF_{gw} - ET_g \tag{27}$$

4. RESULTS & DISCUSSION

4.1. Insitu data

4.1.1. Piezometric data

The figures listed below depicts the temporal distribution of heads, gaps, correction efforts and the response of different piezometric records with in the Auob Catchment.
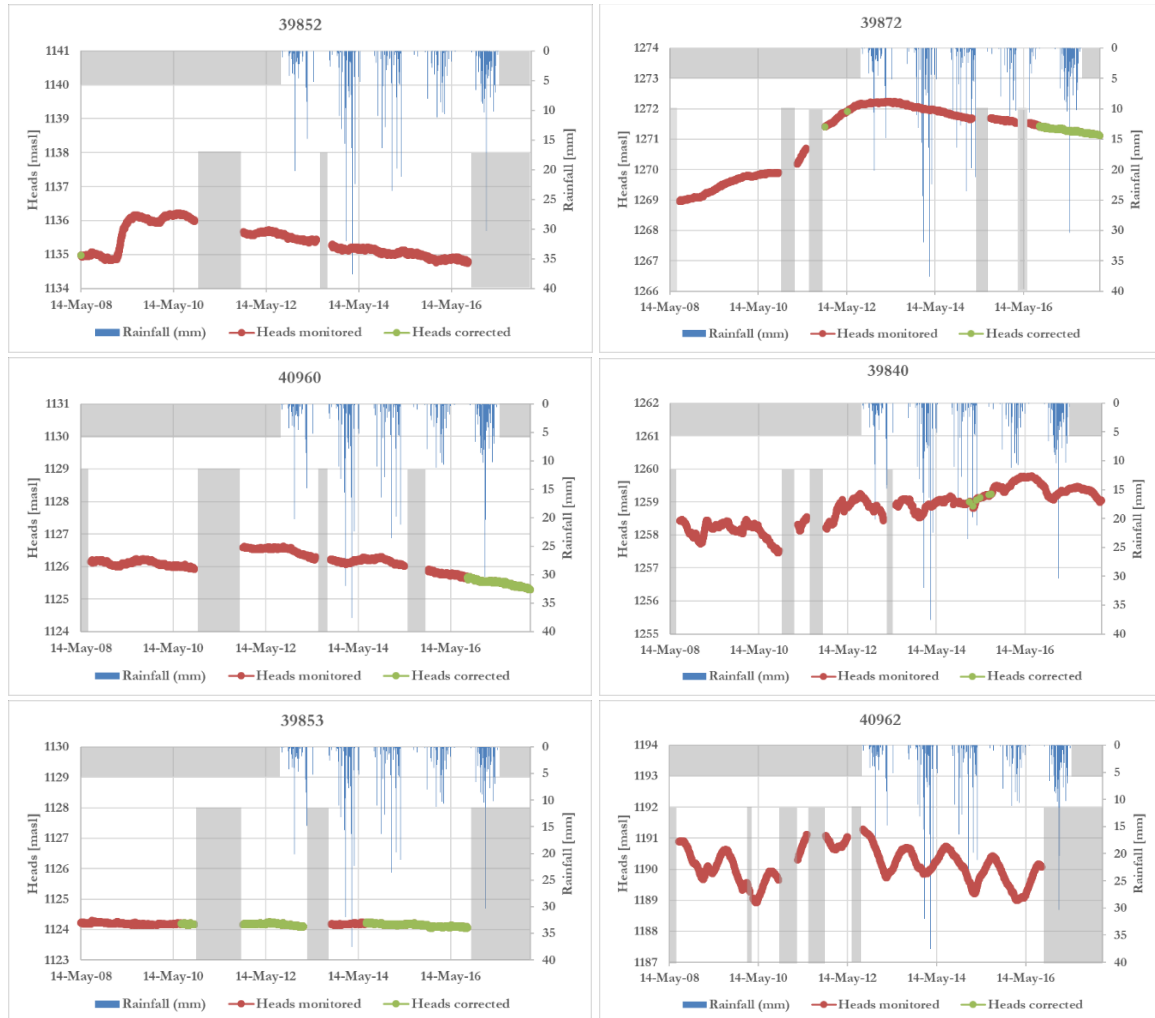
Figure 24: Piezometric heads for the different monitoring boreholes within the Auob Catchment from 14 May 2008 to 14 November 2017. For the reminder of the 16 boreholes as listed in Table 3 please see appendix (Figure 48).

It can be noticed in Figure 24 that the piezometric levels in Kalahari piezometer (40960) show a decreasing trend over time in spite of the rainfall events. The decreasing trend that is noticed in the Kalahari boreholes could be associated with the fact that this boreholes tape into one of the most productive aquifer and most of the abstractions take place in this borehole. This trend is not only common in the Auob Catchment. Studies have revealed that many aquifers around southern Africa have been declining as a result of over pumping of groundwater resources for irrigation (as it can be depicted from Figure 25b, the irrigation water use practice in the Aoub Catchment makes it no exception) and this further reduce groundwater recharge and its replenishing rates (Terrell et al.,2002 in (Adane et al., 2018); Scanlon, Reedy, Stonestrom, Prudic, & Dennehy, 2005). A contrary trend is noticed in the Auob piezometer (39840). Whereas the Nossob

piezometer (39853) shows a fairly stable trend over time. The fairly stable trend in the Nossob boreholes could be a result of its low productivity, low groundwater flux exchange (JICA 2002) and/or very limited human impact.
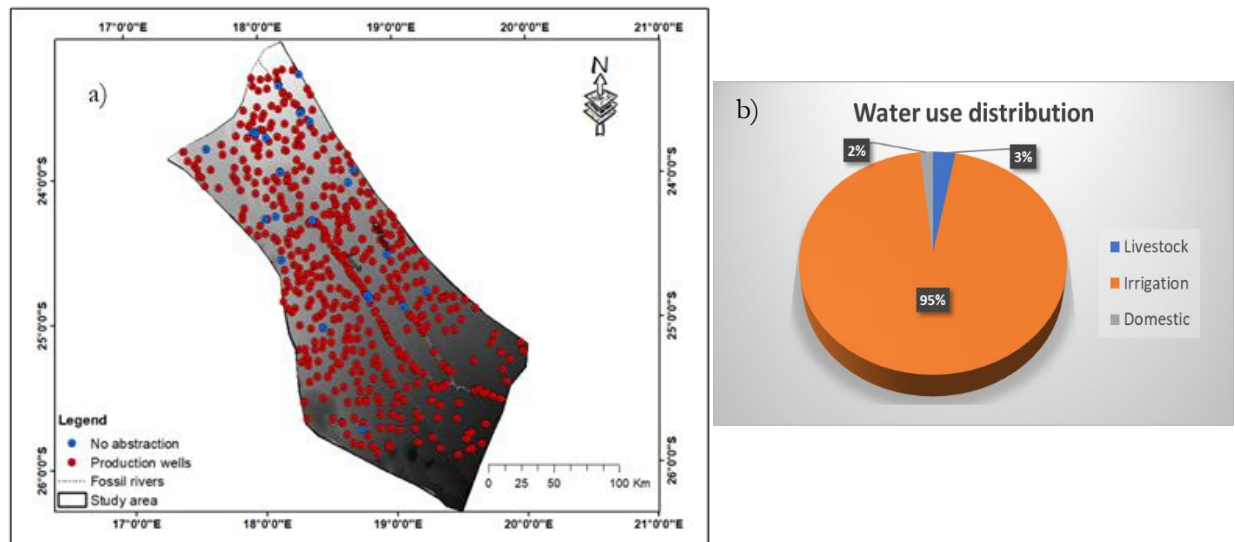
Figure 25: Distribution of abstraction boreholes within the study area. a) Red representing wells that had abstraction and the blue represent wells that had no abstraction and b) represent the percentage of water use.

According to Figure 25 b, 95% of the abstractions within the study area is used for irrigation, 3% is used for livestock and 2% is used for domestic purpose. Abstraction is taking place almost everywhere within the study area (a). An abstraction borehole drilling trend can be noticed along the alluvial streams despite their un frequent flow. This could be due to the relatively shallow water table in these areas and reduced drilling effort along the alluvial strips as well as the related cost. There are spare abstraction wells distribution in the south to the lower south-eastern areas of the study area. The low distribution of the abstraction wells in these areas could be attributed to the presence of the black salt and reduced water quality in this area (JICA 2002; OBASECOM 2009). Additionally, MAWF,(2010) states that the areas in the south to the south-east of the catchment, are dominated by the thick Kalahari sand, making it difficult for successful borehole drilling and setting up. That could have prohibited the placement of boreholes in that area.

4.1.2. Precipitation

4.1.2.1. In-situ rainfall evaluation

The scatter plots represent the relationship between the daily rainfall observed at the Kalahari station in relation to rainfall observed in the other stations surrounding the Auob catchment.
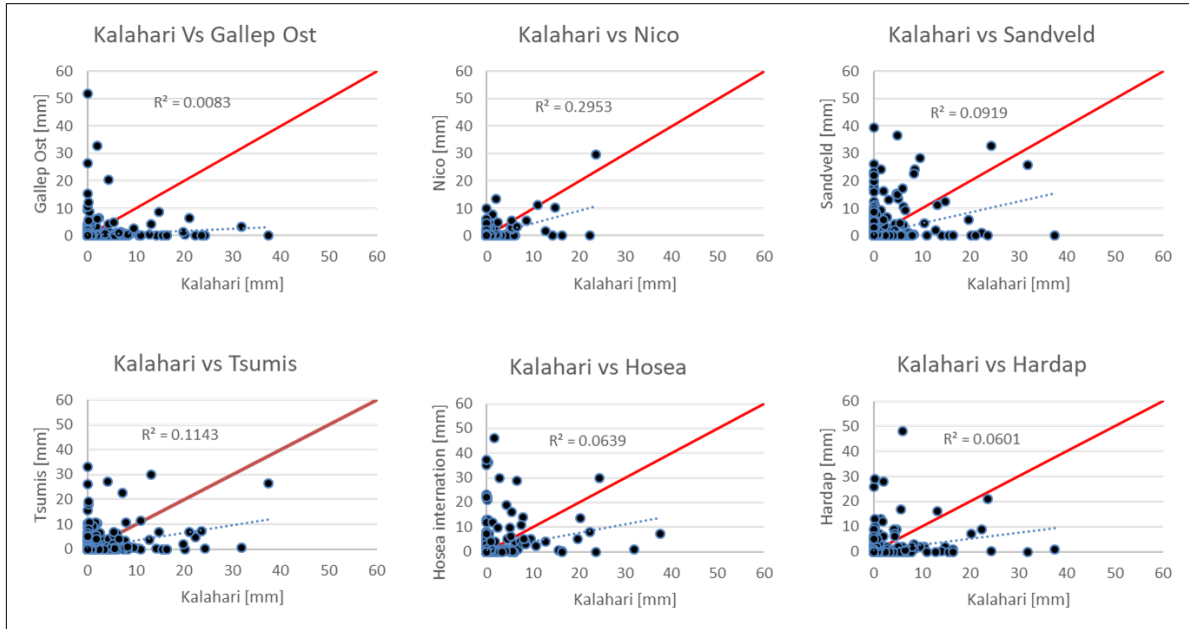
Figure 26: Correlation between the Kalahari station daily rainfall gauge and the daily records from the surrounding rainfall gauges

It can be noticed in Figure 26 that there is a low correlation between the rainfall observed at the Kalahari station and the amount of rain that is observed in the other stations that are outside the study area. This could be attributed to the fact that the other stations are ~250 kilometers away from the main station (Kalahari) which is situated within the study area. Due to the high spatiotemporal variability nature of rainfall and the low rain gauge density (Rahmawati and Lubczynski 2018) satellite rainfall products were used for the estimation of rainfall within the study area.

4.2. Satellite data

Driving forces such as precipitation and evapotranspiration are key contributors to hydraulic modelling. The in-situ data are hampered by the low distribution of gauges especially in developing countries such as Namibia. Satellite products are therefore an attractive option. The determination of which satellite product to use depends on data availability, the objective of the study and the products performance in a given study area.

4.2.1. Precipitation

4.2.1.1. Satellite rainfall evaluation

The scatter plots below display the correlation between the satellite daily rainfall estimates in relation to the in-situ observation at the 5 different station that were incorporated in this study as listed in Table 2.
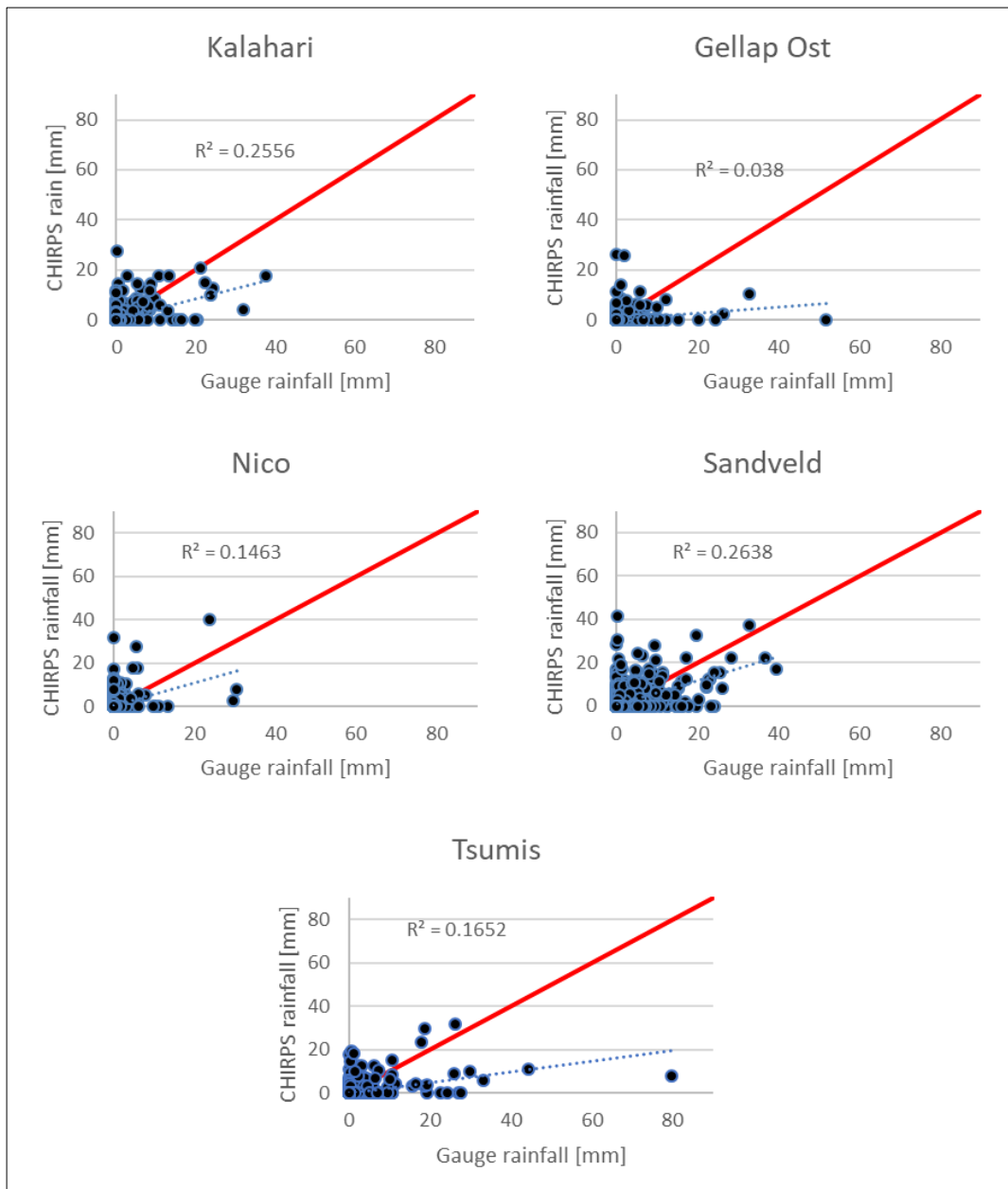
Figure 27: Correlation between daily gauge rainfall and matching pixel of the CHIRPS rainfall product.

According to [Figure 27](#) above, there is a low correlation between the daily satellite products and the in-situ rainfall estimation. This is largely because of daily resolution of the data compared which enhances differences between the two (Rahmawati and Lubczynski 2018), but also due to random errors or systematic bias (AghaKouchak et al. 2012). These errors may be a result of satellite rainfall estimations algorithm as they estimate top of cloud reflectance, infrequent satellite overpass, precipitation retrievals, topography and orbital drift (Joyce et al. 2004; Dinku et al. 2008). Dembélé & Zwart, (2016) and Nicholson et al., (2003) states that bias is mostly reported over the African continent and especially for daily estimation, but it improves for longer timescales as a result of data accumulation.

4.2.1.2.   Satellite product performance before bias correction

Bias detection

The CHIRPS product was used and it has a spatial resolution of 5km x 5km.

Bias detection	Kalahari	Gellap Ost	Nico	Sandveld	Tsumis
POD	0.29	0.17	0.30	0.43	0.24
FAR	0.35	0.46	0.50	0.29	0.28
CSI	0.25	0.15	0.23	0.37	0.22

Figure 28: Bias detection at the 5 different stations within and around the Auob catchment.

Bias decomposition
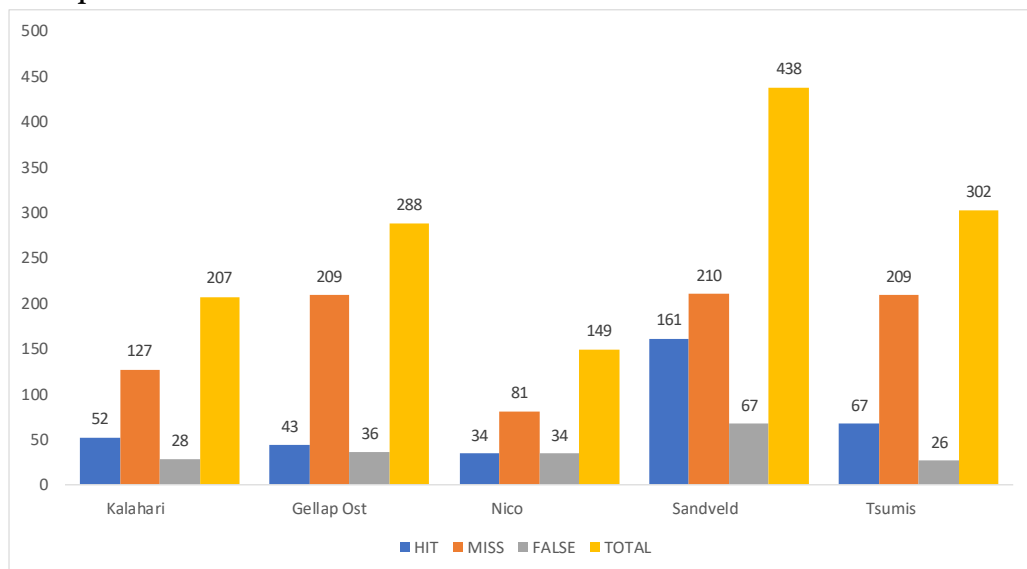
Figure 29: Bias decomposition at the 5 different stations within and around the Auob catchment.

[Figure 29](#) indicates a high miss rainfall volume in all of the stations that are located within and round the Auob Catchment, apart from the Sandveld station. the low miss at the sandveld station as compared to the

rest of the station is probably because it is used in the internal validation or calculation of the CHIRPS product (ftp://ftp.chg.uscsb.edu/pub/org/chg/products/CHIRPS-2.0/diagnostics/list of stations used/monthly/). The general high miss in rainfall could be attributed to the products performance which depends on the retrieval techniques, which determines the restriction and capabilities of precipitation estimation (Stampoulis et al. 2013). Stampoulis et al.,(2013) further states that the satellite performance is also hampered by geographic features such as topographic, climatic conditions and precipitation type. For instance, precipitation type turns to have an effect on algorithm ability to fully capture rainfall. When rainfall rates are low such as in stratiform-type system. The satellites do not capture them well in certain areas. Thus, leading to the high missed rain volumes (Stampoulis et al. 2013). As to the actual cause of the biasness in the products performance for this particular catchment was beyond the scope on this study.

The satellite product performance was evaluated based on different detection and decompositions methods. It can be acknowledged from the figures above that the product is associated with some bias. These biases could be associated with the fact that the comparison made are point to pixel. The rain gauge tipping bucket has approximately 20 cm spatial resolution (Sutron 2015) with effect to ~200 m² while the product has a spatial resolution of 5x5km. Not to mention the algorithm errors that are associated with deriving of the satellite rainfall estimate, which focus on the top of the cloud temperature and the actual rainfall happens at the cloud bottom. All the above mention factors could have contributed to the bias that is being noticed in Figure 28 and Figure 29. Due to the bias that is associated with the satellite products in relation to the insitu estimates, various bias correction scheme were examined as indicated in Figure 30 below.

Bias correction.
The time and space fixed bias correction scheme shows that with increase in rainfall accumulation, the satellite product turns more to mimic the ground truth. During the application of the space fixed and time variable bias factor it can be noticed that over short time window the bias correction scheme is very unstable; it becomes more stable with an increase in accumulation of data. An underestimation of the product was noticed over a two-week window and a better trend was observed during the longer period window such as the thirty-day time steps. The similar trend was observed by Dembélé & Zwart, (2016) and Nicholson et al., (2003), who stated that satellite products turn to perform better with the increase of accumulated rainfall as compared to shorter time spans such as daily data observation.

The time and space fixed bias factor assessment resulted in a correction factor of 1.5. This meant a 50% increase on the actual recorded precipitation value. This bias correction factor over estimated rain at lower limits and mimic only the station value after longer accumulation. This means for the single values the correction factor is exaggerating the estimated rain. For this reason, all the tested bias correction factors were neglected and not used in this study. The satellite product was taken as it was originally presented and was introduced into the model in its original state. This product is already inherently corrected after data acquisition so the attempt in correcting it could make it more erroneous.
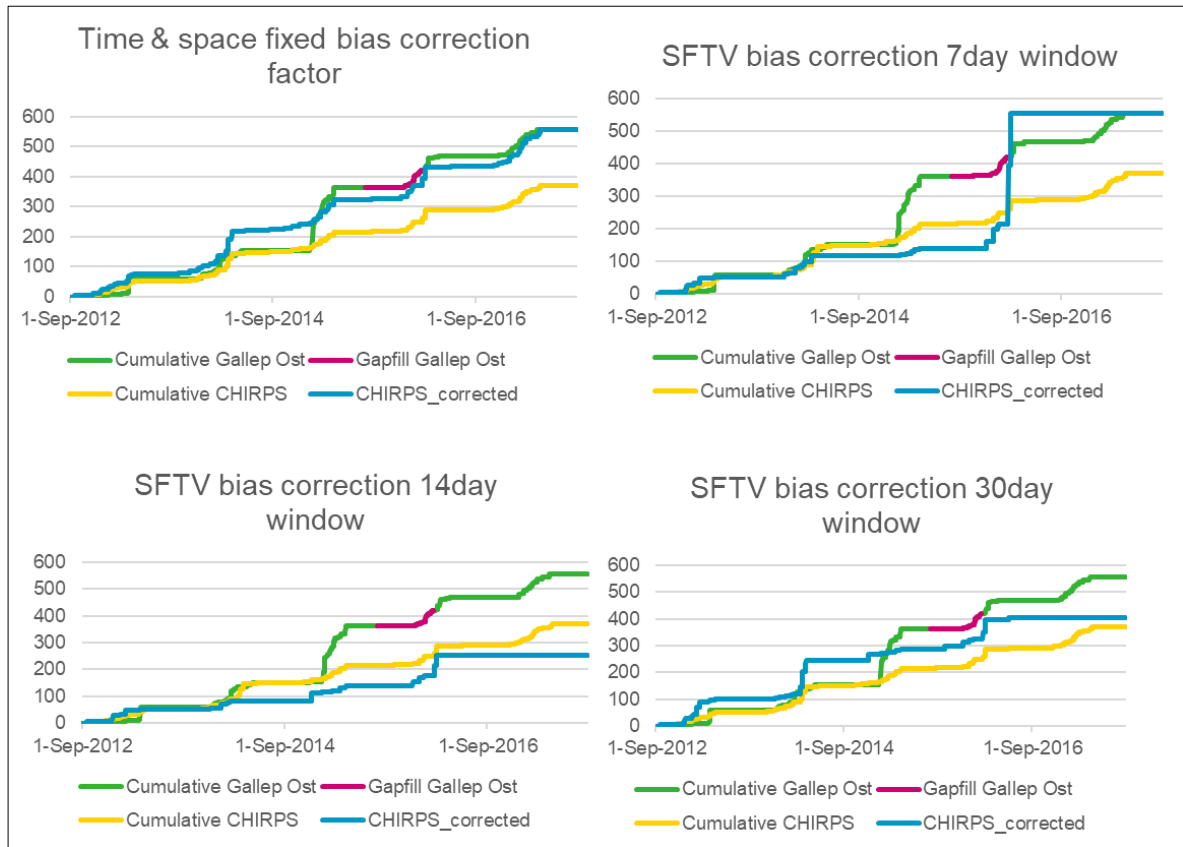
Figure 30: The bias correction schemes. The application of the bias correction schemes where based on the space fixed and time variable bias factor performance in comparison to the performance of the space and time fixed bias factor.

Rainfall distribution within the Auob catchment
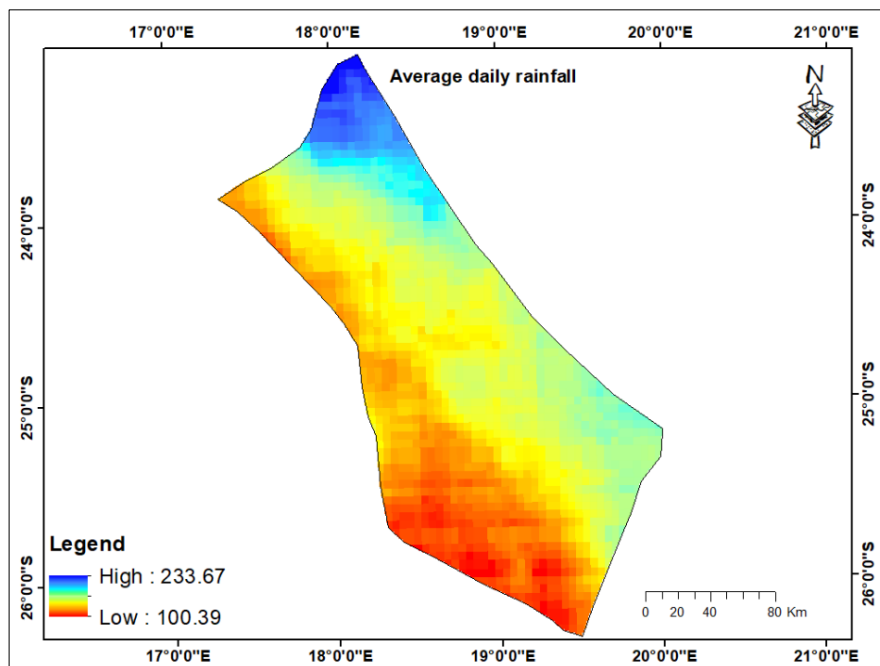
Figure 31: 5 year (1/9/2012-31/8/2017) daily average rainfall distribution of CHIRPS presented in mm yr⁻¹.

The north-western area receives the highest rainfall and the lowest rainfall is received in the southern part of the catchment. The north western regions of the study area are associated with mountainous reliefs and the southern part of the study area is dominated by flat lands that are covered by the thick Kalahari sand. On average the daily rainfall over the study area range from 0.28 to 0.64 mm/day during the 5 year simulation period.

4.2.2. Potential evapotranspiration

4.2.2.1. ETo insitu measurement evaluation

Consistency check using double mass curve technique
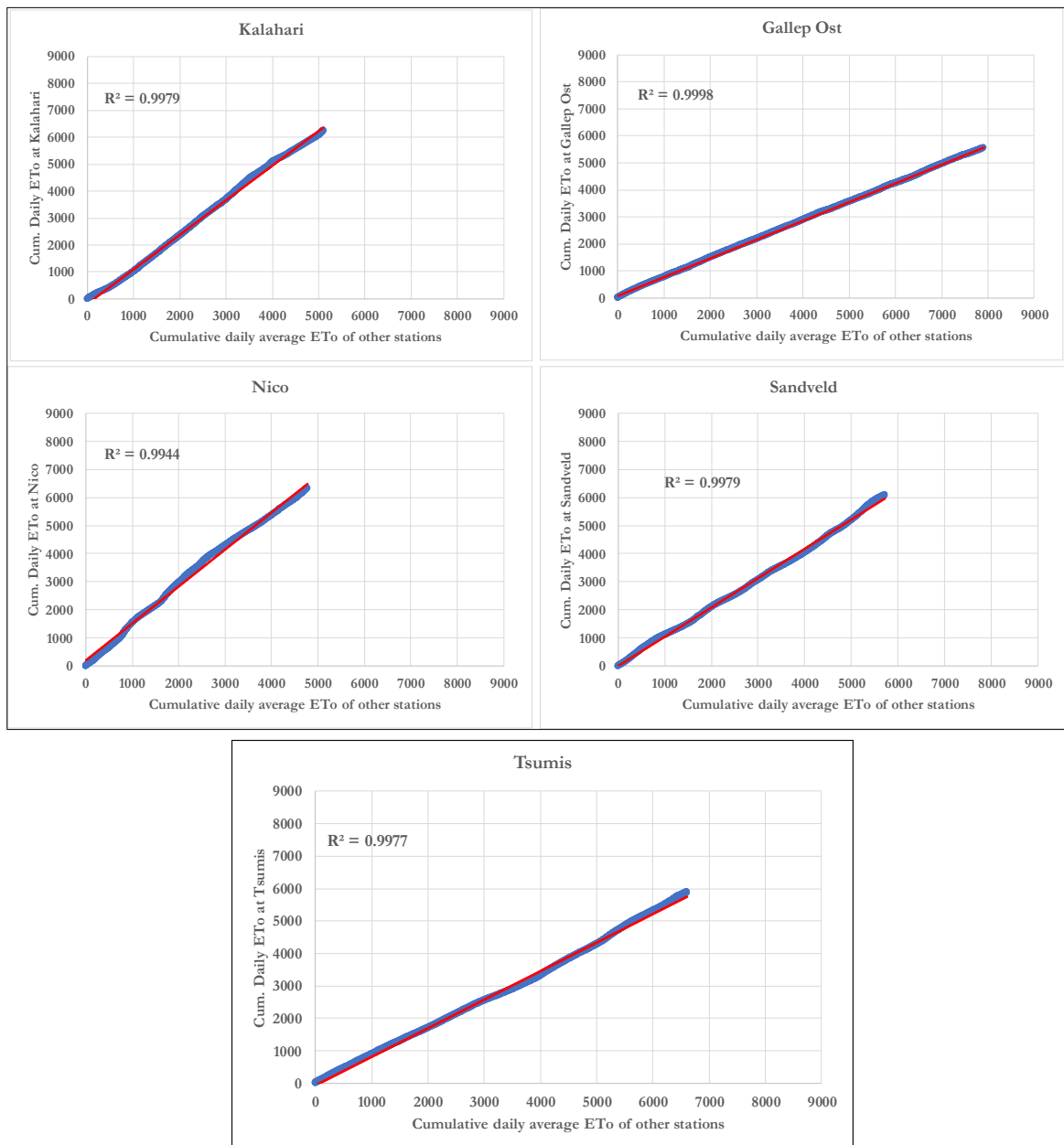
Figure 32: Cumulative daily ET_o time series for each in-situ station verse cumulative daily average ETo of the remaining insitu stations.

The double mass curve results indicate a coefficient of determination that is higher than 0.99, due to the high determination of coefficient and absence of breaks in cumulative curves between the different stations ET_o. There was no need for the further correction of the data as indicated in section 3.1.3 of this study. Moreover, the high coefficient of determination suggest a good agreement between each station relative to the average of the other stations (Bhatti et al. 2016). A smoother curve, with the highest coefficient of determination, is noticeable in the Gallep Ost station. This could be due to the fact that during the gap filling processes for the different variables that were used in the ET_o calculation, this was the only station which had complete data and did not require any gap filling. For this reason, this station ET_o will be used for the validation of the ET_o (US-based GMAO GOES-5 model) from the remote sensing product.
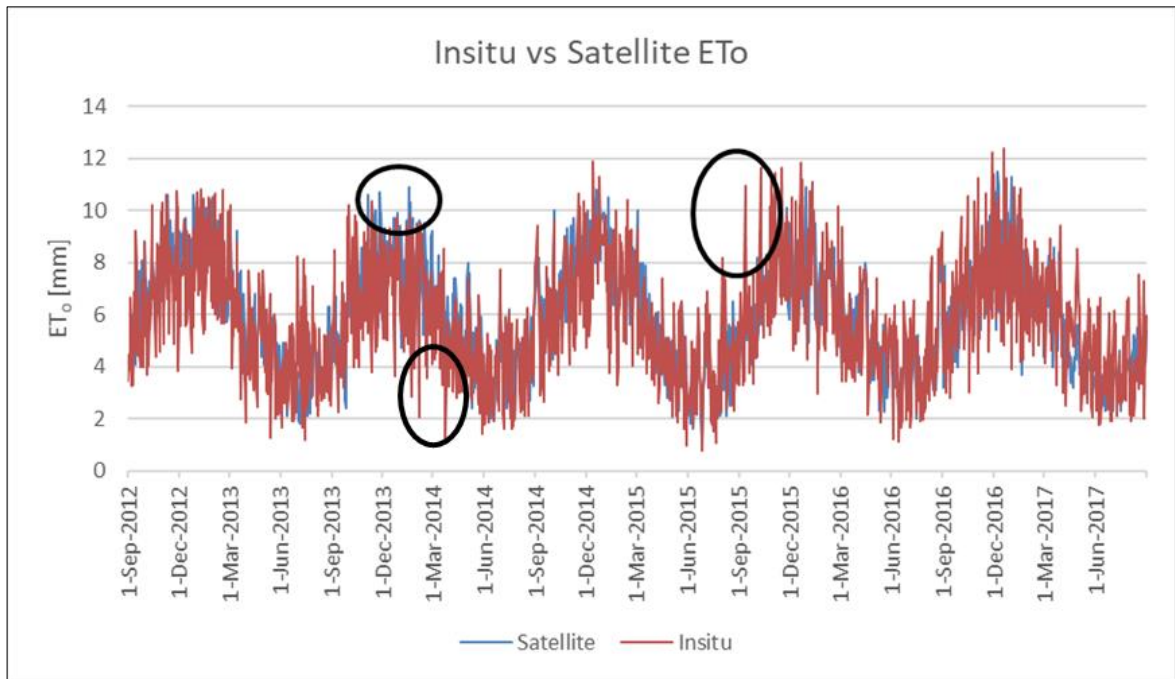
Figure 33: Gallep Ost in-situ against Gallep Ost satellite ET_o.

According to Figure 33 a fairly similar trend can be depicted in the calculated insitu and the satellite observed ET_o. Even if there are some miss match between the peaking of these products as indicated by the circular rings on Figure 33. However, the miss match between the satellite and the insitu data are minor and will not have much influence on the data set as they will cancel each other out over a long period of observation. The seasonal variation of evapotranspiration can be noticed from the two products. Evapotranspiration is higher during the wet season and lower dry season. The high evapotranspiration during the summer months are connected to the high net radiation resulting in high temperatures, low relative humidity and high vaper pressure gradient which increases the evapotranspiration demand.

Scatter plot
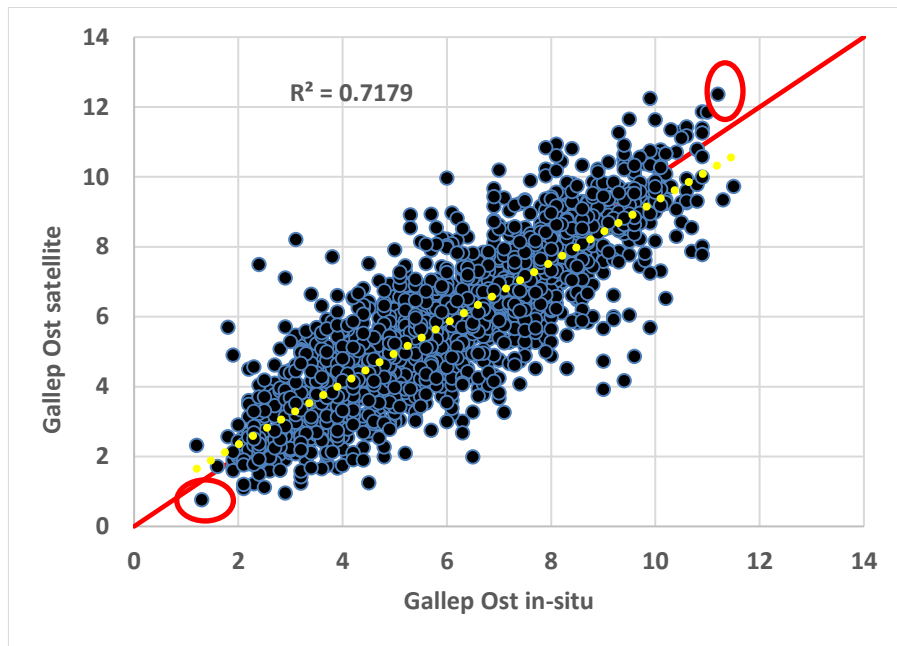
Figure 34: ETo scatter plot of Gallep Ost in-situ against satellite.

The scatter plots display a strong correlation between the statellite and insitu ETo estimates. With a coefficient of determination of ~0.72. At lower readings, the station seem to overestimate ET_o compared to the satellite estimates and a vise versa trend can be noticed at higher readings as indicated with the red circles on Figure 34. Majority of the recordings are correlated thus making the product suitable for use.

Cumulative curve
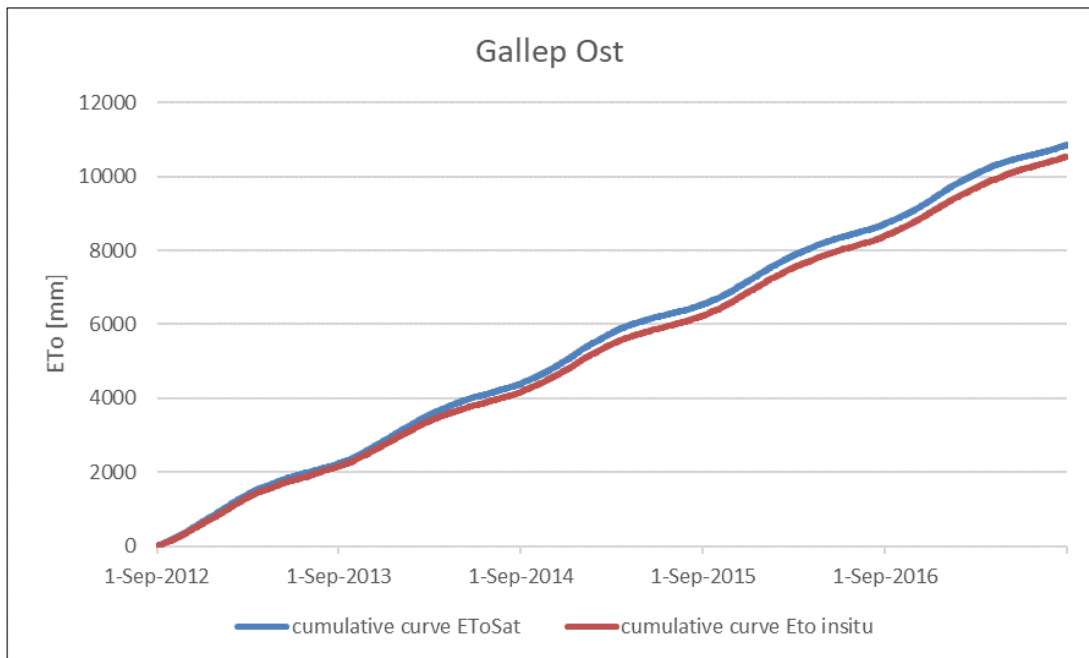
Figure 35: Cumulative curve for Gallep Ost insitu vs Gallep Ost satellite.

From Figure 35 it can be observed that around 3500 mm accumulation of ET_o the satellite and the in-situ calculations begin to vary, the variation is relatively low and it is stable over time. The given range when the in-situ and satellite systematic error is low and consistent, the data in that range can be used for the correction in case need arise. From the scatter plot coefficient of determination, it can be noticed that there is a high degree of correlation, the calculated Pearson correlation shows 0.8556 of correlation as indicated in the Appendix. Thus, there is no need for further correction of this product. Hence, making its adoption for use as a driving force in the numerical model feasible. The spatial distribution of average daily ET_o during the simulation period is indicated in Figure 36 below;

Spatial distribution of evapotranspiration
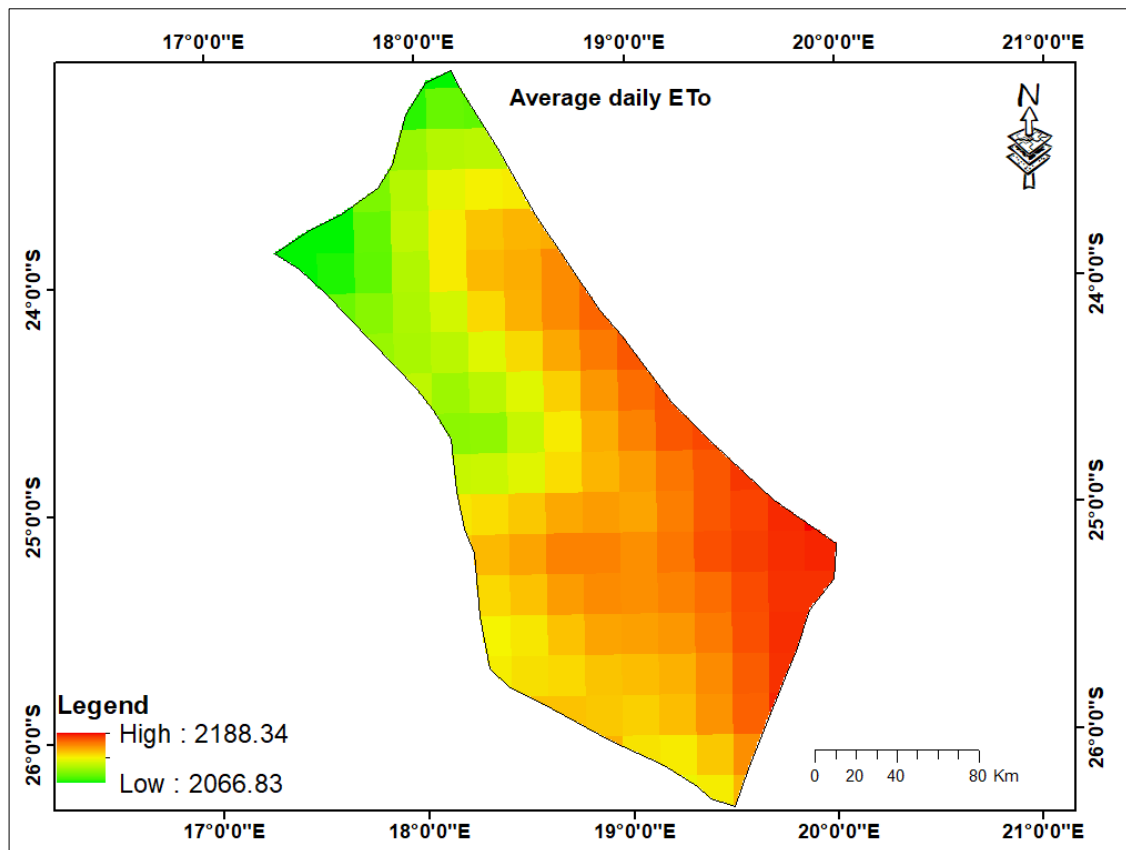
Figure 36: Spatial variability of the 5-year (1/9/2012-31/8/2017) daily average reference evapotranspiration from US-based GMAO GOES-5 model presented in mm yr-1.

There is a relatively minor spatial variability of the average daily reference evapotranspiration (ET_o) at the Auob catchment within the 5 year period of simulation; the lowest values are noticed along the high lands and a gradual increase is noticed in the south to the southeast of the study area. The highest ET_o is noticed in the southeastern regions where the thick Kalahari sands are located. It can also be noticed that evapotranspiration decreases with an increase in elevation. This is due to the fact that at higher elevations the temperatures are lower and less water is lost by plants.

4.2.3. Interception
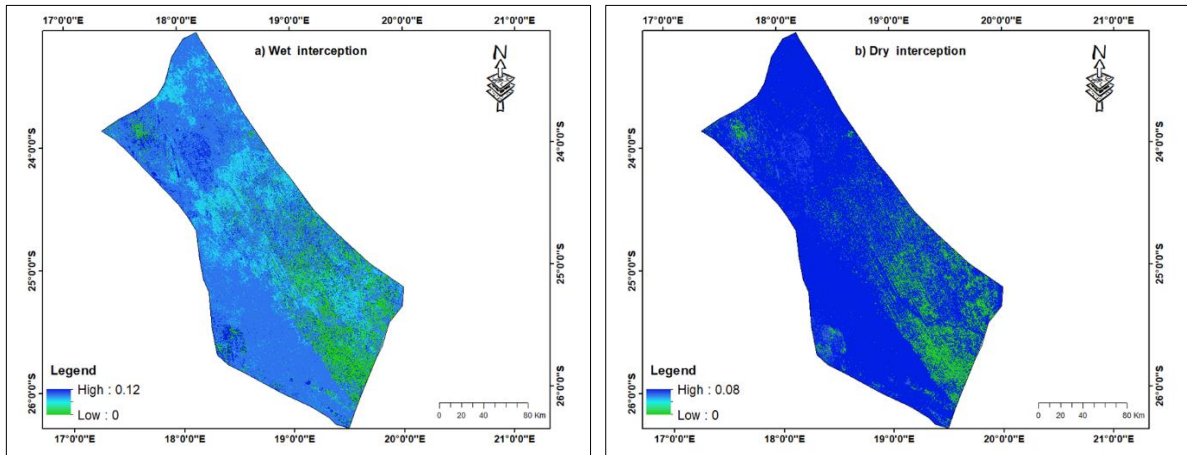
Figure 37: Wet and dry interception rates (% of rainfall) based on the landcover map.

The interception map was created based on the land cover map as stipulated in section 2 of this study. The dry season had low values of interception compared to the wet season. From Figure 37 it can be notice that there is a spatial variation in interception as well. High interception is noticed in areas dominated by trees this trend could be link to the leave area index and canopy cover (Adane et al. 2018).

4.2.4. Rooting depth and Kc factor
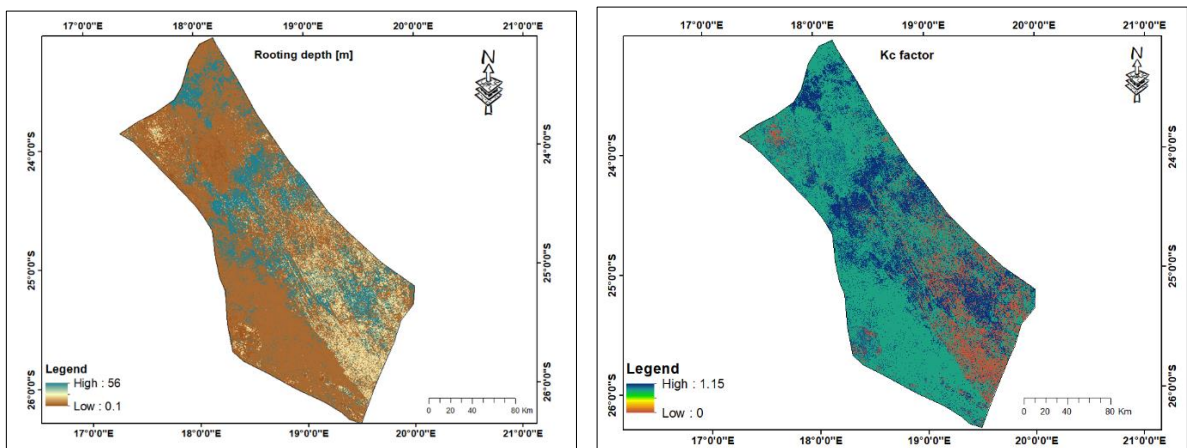
Figure 38: Extinction depth and Kc factor based on land cover map and soil

 According to Figure 38 the study area have the highest extinction depth of up 56m. This means that evapotranspiration can take place at depths up to 56 m below the water ground surface and in areas where the water table rise to this depth the plant species have the ability to tap this water. It should be noted that due to the averaging effect per pixel the dominant species in that particular area contributes more to the averaging. Thus, reducing the highest extinction depth to 16.94m as indicated in Figure 21. The high extinction depths are associated with areas that are associated with shrublands and tree mixtures. Therefore, the dominant landcover type per pixels contribute more to the average as indicated in Figure 38 were the high values are associated with areas dominated by shrublands. Majority of the study area is dominated by grassland, thus most of the area is coved by relatively low extinction depth. Apart from the south eastern part that is dominated by cropland and shrub species (mainly the *Prosopis sp.* that have depths up to 15 m in this area). In terms of Kc, a similar trend can be observed whereby the dominated species with the high Kc

factor trees and shrublands which are reflected with the blue in Figure 38. They are followed by the cropland and the lowest Kc factor is noticed in areas associated with bare and built up areas, which are situated in the south and the north western part of the study area.

4.2.5. Conceptual model

Conceptual models are an iterative simplified schematic representation of reality. Their adjustment are depended on the numerical model response during the setting up, warming up and calibration process.
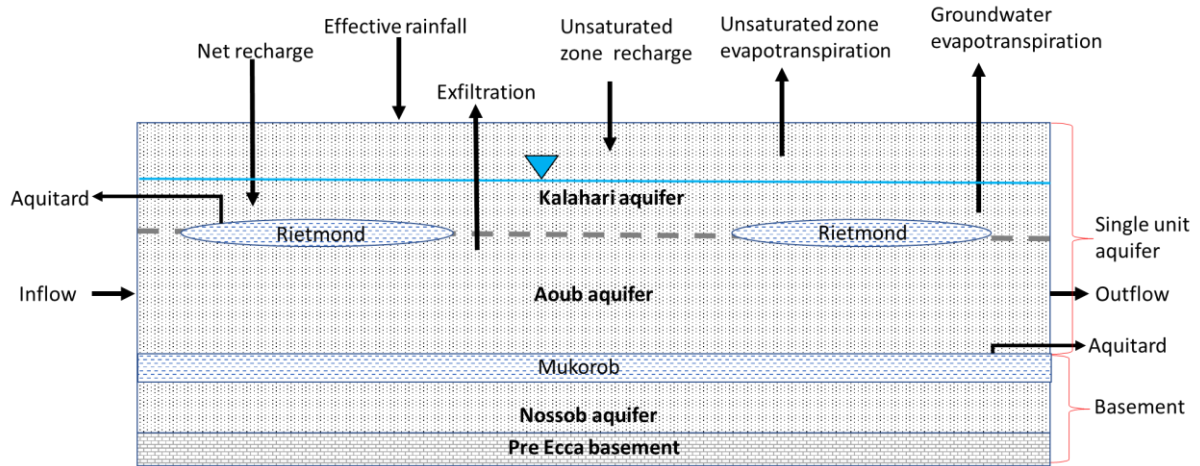
Figure 41: Schematic representation of the Auob catchment (not to scale).

The Auob Catchment can be simulated as a single hydro-stratigraphic unit in a form of an unconfined aquifer when simulating for groundwater recharge and spatio-temporal variation of the groundwater fluxes. The performance of the numerical model greatly influences the conceptualization of the study area. Even though before the implementation of the numerical model it is important to have a well conceptualized study area in order to translate it into a numerical model. Both the conceptual model and the numerical model are interconnected and influence each other. Hence, the response of the numerical model triggers some adjustment in the conceptual model. For instance, the initial proposed general head boundary was allowing outflow of water from the inflow boundary. Thus, it was not a good representation of what was happening on the ground. For this reason, the general head boundary was replaced with a head and flow boundary (specified flux) as indicated in section 3.3.6 of this study. As to whether the Kalahari and Auob Aquifers should be represented as a single unit is not yet clear due to the poor response of the groundwater heads (state variables to the calibration process).

4.2.6. Numerical model findings

Model calibration

The Figure 41 shows the responses of the hydraulic heads to the parameterization of MODFLOW-NWT, after the parameterization and calibration of the model.
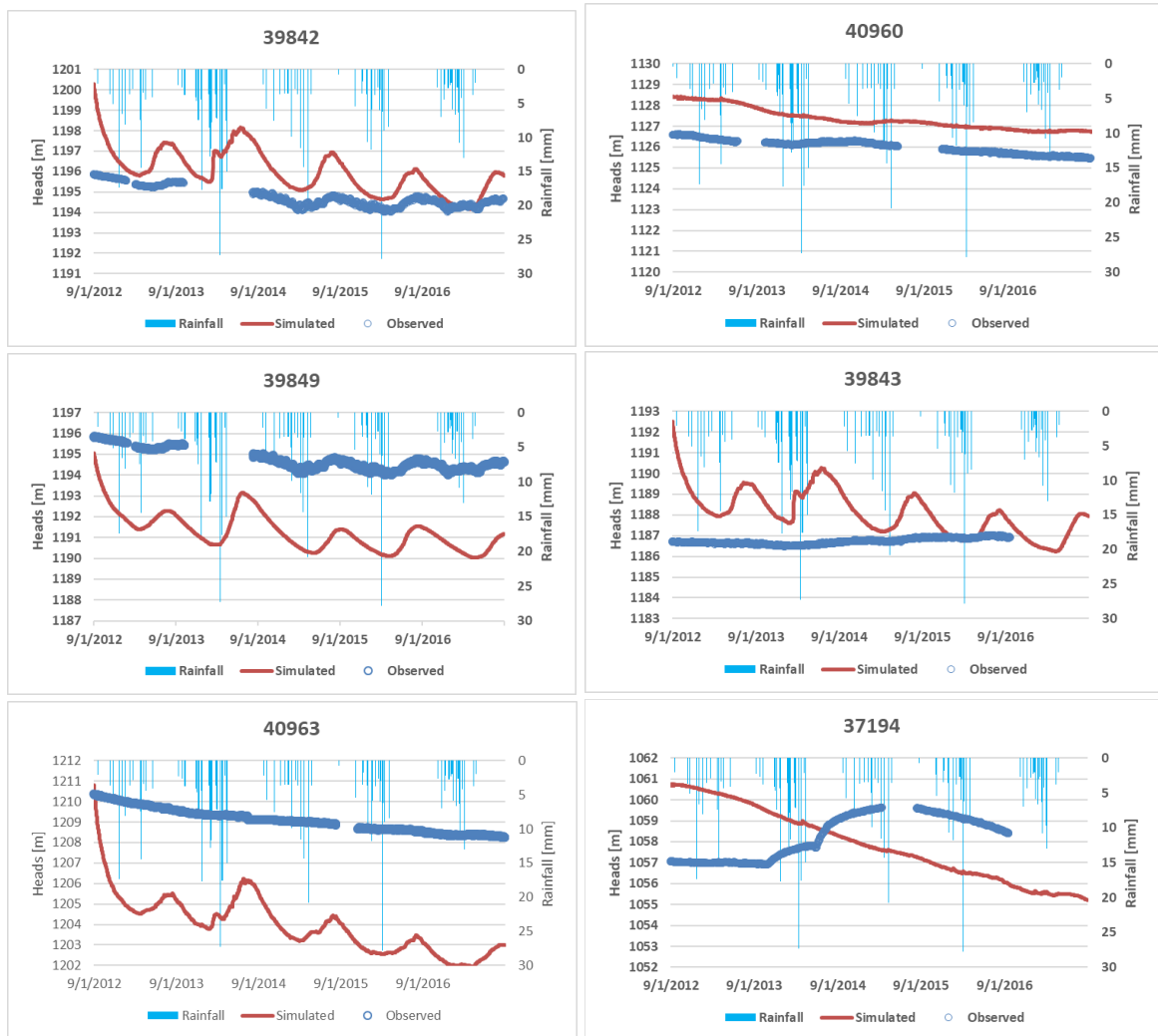
Figure 42: Observed and simulated heads during the model calibration period.

From Figure 42, it can be depicted that most of the simulated heads showed a response to the rainfall. That water table response which particularly can be seen in Kalahari boreholes 39842 and 39849 is a delayed by several month with respect to peak rainfall and occurs in dry season. Such delayed response is because of the time laps before the water reaches the water table through infiltration and percolation. After some time of no rainfall, the water table begins to drop as evapotranspiration and exfiltration takes its course. Furthermore, it is observed that only a few boreholes (BH39842 and BH 39849) showed a similar trend as what is being observed on the ground. Also the third Kalahari less responsive borehole BH40960 showed similar, gently declining simulated trend similar to the measured.

Besides the response of the boreholes to rainfall in BH 39843 and BH 40963, the observed head seemed to be stable over time and were not as responsive as the simulated heads. A contrary trend is observed in BH 37194 were the observed piezometer responded but the simulated showed a continual decline in the trend. Proper representation of heads is dependent on correctness of driving forces, model parametrization, model simplifications made and the reliability of the reference heads. Some boreholes during the data cleaning

processes had records that were marked as unreliable data due to faulty loggers this could also be one of the reason why the state variables were not well imitated by the model. Apart from that, the poor response of the head could be due to poor parameterization of the model due to lack of calibration time, model implementation short coming as most time was invested into trying to set up the model and the inability of the model to simulate the whole date set (it was experiencing dis-convergence after running 2 years 4 months). This problem took up more than 50% of the study allocated time. Which after overcoming it let the calibration process to little time. Thus limiting the proper parameterization of the UZF. This further let to more water being simulated in the model. Some cells indicated less water being simulated while others indicated more water as compared to the observed. Efforts were carried out to best represent this ground truth but time still remained a limiting factor. During the manual adjustment of the data set some boreholes still appeared to have trends that showed problems and they were used for the simulation this could also explain why they were not properly represented.

Considering the continual declining water table it is a result of; large ET_g even if the water makes its way to the water table and activate a rise in response to precipitation. A large portion of water is lost via ET_g in Auob Catchment due to the presence of phreatophytes with roots up to 56 m according to Shadwell and February (2017).

Table 10: Model performance evaluation. The table depict the performance of the model during the model calibration.

BH No.	ME [m]	MAE [m]	RMSE [m]
39843	-1.64	1.65	1.95
39842	-1.11	1.12	0.87
40960	-1.32	1.32	0.91
40963	5.10	5.11	13.54
39849	3.50	3.50	6.28
37194	-0.33	2.28	3.03

The RMSE ranged between 0.87 to 13.54 [m] as indicated in Table 10. The probable explanation for high RMSE is the result of the mismatch between the observed and simulated heads resulting in the discrepancies of the residuals. The mismatch could be a result of uncertainty in the measured water level, the unrepresented heterogeneity that is associated with the 1km² model grid, errors in model parameterization and system conceptualization errors (Hassan et al. 2014; Lekula 2018).

Spatial variability of groundwater components and the effect of catchment characteristics on their distribution.
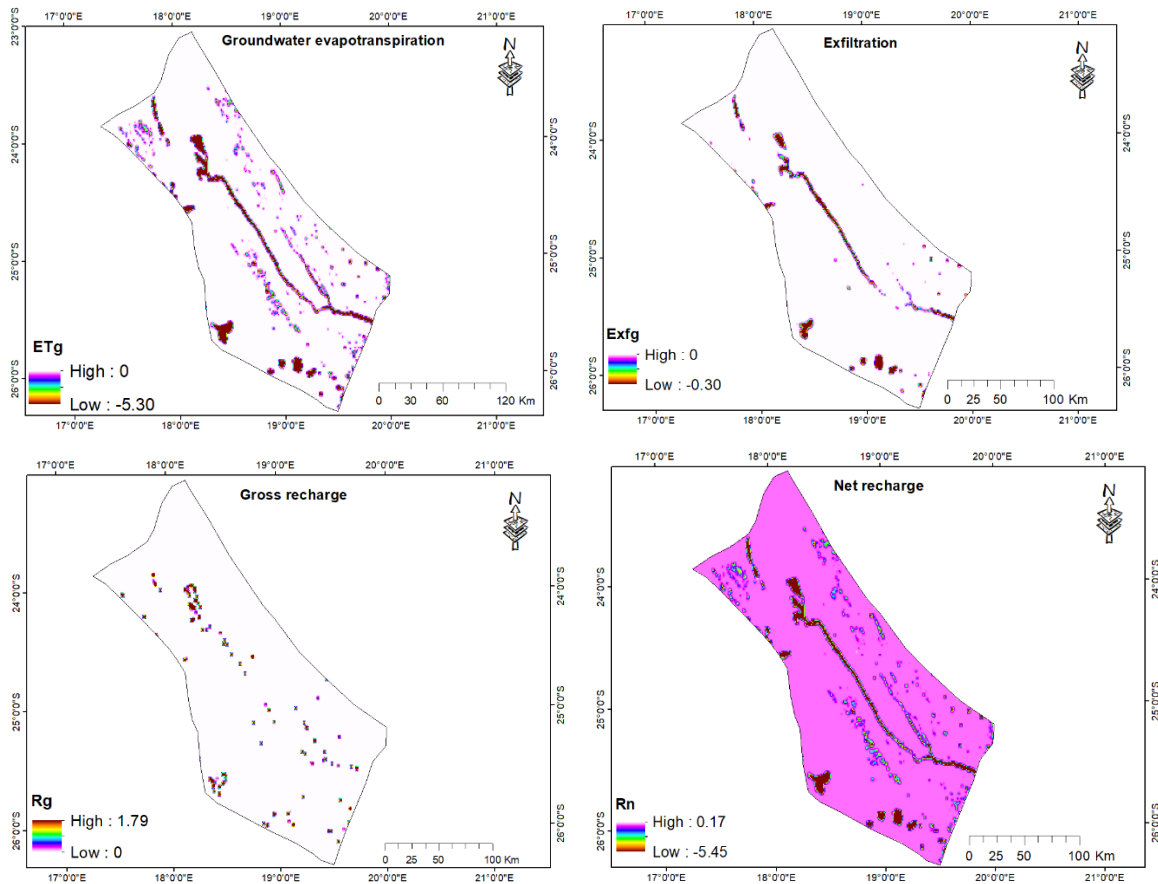
Figure 43: Spatial variability of sub-surface evapotranspiration, net recharge, gross recharge and exfiltration in mmd^{-1}

The negative sign on the fluxes is an indication of groundwater losses and it is depicted on fluxes such as evapotranspiration, exfiltration and net recharge whereas the positive is a sign of groundwater gains and it is depicted in gross recharge. Catchment characteristics play an essential role in groundwater flux distribution. The above listed flux distribution are influence by interception, plant root depths, topographic relief and climatic factors such as rainfall and evapotranspiration (Grinevskii 2014; Adane et al. 2018; Li et al. 2018). Subsurface evapotranspiration is experienced almost everywhere within the Auob Catchment, it is highest along the Auob and the Olifants fossil rivers. This could be due to the relief depressions along the streams and the infestation of the deep rooted vegetation along the dry river beds as observed by Shadwell & February, (2017). The high ET$_g$ along the streams could be attributed to more water close to the surface in this area, hence the high exfiltration as indicated in Figure 43. Grinevskii, (2014) states that mostly water is distributed at the slope and settles at hill feet and this is where groundwater recharge occurs, he further states that the foot of slopes that are associated with recharge are also the same zones that are associated with high potential evapotranspiration. Thus the moisture that finds itself in this area could be influenced by the PET and not necessarily find its way to the groundwater table, especially in arid environments. This trend can be noticed with the distribution of fluxes within the Auob Catchment. The lower areas are found the the south-eastern of the Auob catchment which are away from the mountainous areas and they are associated with high zones of evapotranspiration loses as it can be depicted from Figure 43. Traces of gross recharge are found along the fossil river that are associated with high exfiltration and

evapotranspiration. A simliar trend of high fluxe ditribution along the fossil streams were found in a study by Lekula (2018) who conducted a study in compareable environments. The brow patches in the lower end of the ET_{ss} and Exf_g map as indicated in Figure 43 could be attributed to the presence of the salt block in the lower south eastern part of the Auob Catchment (JICA 2002). In this area since fresh water is less dense as compared to salt water, this causes an upward movement of this water into the Kalahari sand thus further exposing it to evaporation and exfiltration.

Temporal variability of groundwater components
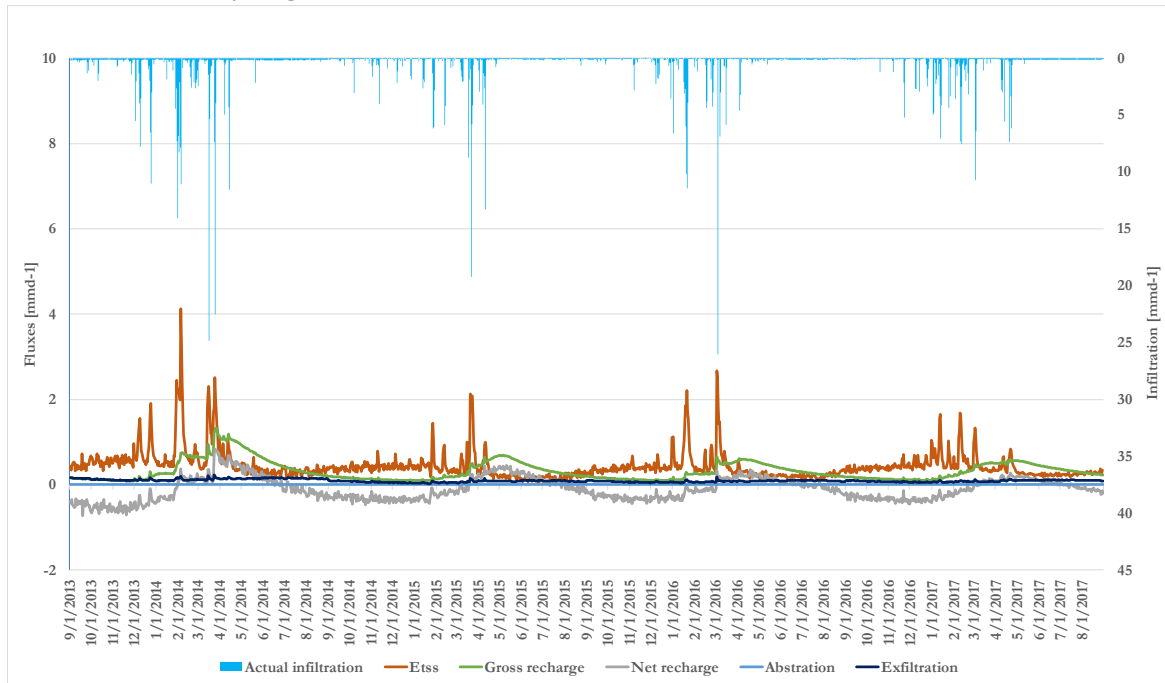
Figure 44: Depicts the temporal variation of groundwater fluxes within the Auob Catchment.

The responses of groundwater fluxes are influenced by the amount of infiltration received in the area. It can be noticed that the first wet season (2013/2014) of simulation had the highest precipitation, consequently high infiltration and the highest evapotranspiration. During the simulation period it can be noticed that there is a delayed response in the gross recharge to infiltration. This could be because of the time lapse taken for the water to reach the water table a similar delayed trend can be depicted from the model simulated groundwater heads in Figure 42. Most of the time the model was losing water due to the continual negative R_n. The net recharge was only found to be positive after the rainfall events. During the wet season most of the water is lost via evapotranspiration and during the dry season gross recharge is almost equal to evapotranspiration as indicated in Figure 44). The generally high negative net recharge in the Auob aquifer could be attributed to the high ET_{ss} due to the presence of deep rooted vegetation and of the thick Kalahari sand that are associated with high evapotranspiration. A similar trend was also observed by Lekula, (2018) who conducted a study in a comparable environment and noticed that catchments with a thick unsaturated zone are associated with high ET_{uz}.

Flux distribution over the Auob Catchment
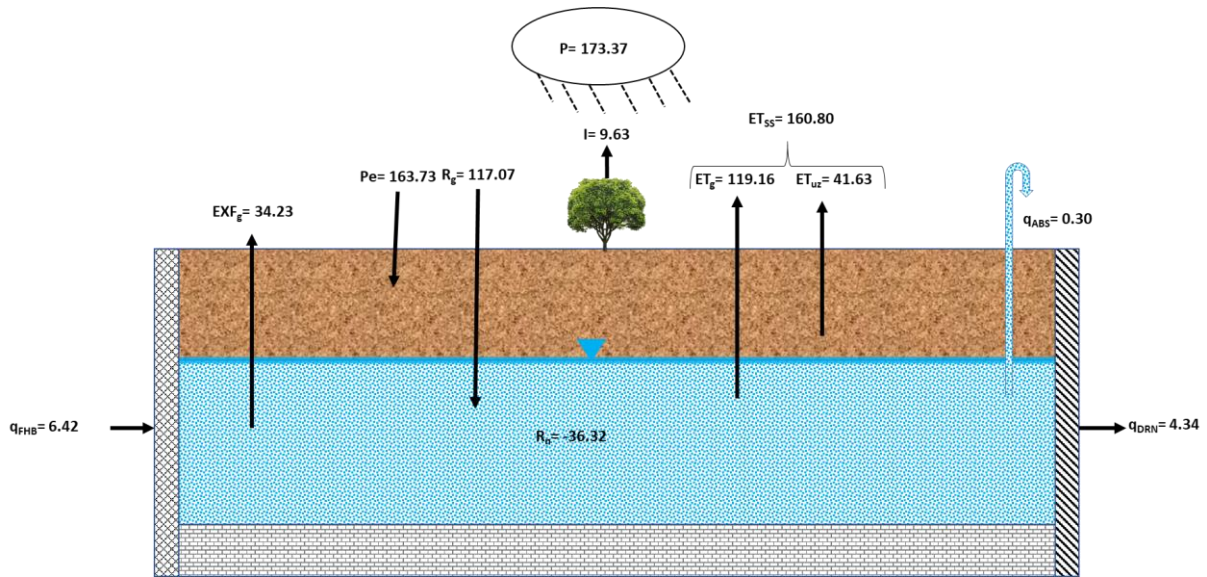
Figure 45: Average distribution of groundwater components during the analysis period (as per Table 11) over the Auob Catchment in mm yr^{-1}.

Water balance

Table 11: Annual water balance of the Auob catchment, the values are expressed in mm yr^{-1} and they are expressed as per equation ((23), and ((27) during the hydrological year start on the 1st September the precous year to the 31st August of the analysed year.

| Year	P	I	FHB	q_{DRN}	Pe	q_{ABS}	ET_{ss}	ET_{uz}	ET_g	EXF_{gw}	R_g	R_n	ΔS_g	ΔS_{uz}	ΔS
2014	247.00	13.71	6.42	4.73	233.30	0.30	217.26	69.58	147.68	48.75	158.39	-38.04	0.04	5.33	5.37
2015	142.08	7.89	6.42	4.42	134.19	0.30	132.74	29.15	103.59	26.91	100.85	-29.66	0.04	4.20	4.24
2016	149.31	8.30	6.43	4.19	141.01	0.30	142.40	35.66	106.73	29.38	101.85	-34.27	0.03	3.50	3.54
2017	155.07	8.63	6.42	4.02	146.44	0.30	150.79	32.14	118.65	31.86	107.18	-43.33	0.03	7.11	7.14
Statistics															
Mean	173.37	9.63	6.42	4.34	163.73	0.30	160.80	41.63	119.16	34.23	117.07	-36.32	0.04	5.03	5.07
SD	42.76	2.37	0.01	0.26	40.40	0.00	33.22	16.30	17.39	8.57	23.98	5.02	0.01	1.37	1.36
Min	142.08	7.89	6.42	4.02	134.19	0.30	132.74	29.15	103.59	26.91	100.85	-43.33	0.03	3.50	3.54
Max	247.00	13.71	6.43	4.73	233.30	0.30	217.26	69.58	147.68	48.75	158.39	-29.66	0.04	7.11	7.14
P%	100.00%	5.56%	3.70%	2.50%	94.44%	0.17%	92.75%	24.01%	68.74%	19.74%	67.53%	-20.95%	0.02%	2.90%	2.93%

Precipitation is the main source of water into this catchment. Over the 4 year of analysisi it can be noticed that on average the catchment receive P= 173.37 mm yr^{-1}, interception is 9.63mm (5.56% of P), the specified flux as lateral inflow into the Auob Catchment is 6.42 mm yr^{-1} (3.70% of P), q_{DRN}=4.34 mm yr^{-1} (2.5% of P), q_{ABS}=0.30 mm yr^{-1} (0.17 % of P), ET_{ss}=160.80 mm yr^{-1} (92.75% of P) and net recharge=-36.32 mm yr^{-1} (-20.95% of P).

From Table 11 it can be depicted that 94.44% of the received precipitation is received in the catchment as effective precipitation, whereas 67.53% of P further percolates as gross recharge. Once ET_g and Exf_{gw} have taken their course, the net recharge accounts for -20.95% of precipitation. This is an indication of a losing aquifer due to the high rates of ETg and can further be depicted in the declining heads during the model simulation. The abstraction in the area accounts for the 0.17% of P. apart from the evapotranspiration which accounts 92.75% of P, out of which 68.74% comes from groundwater evapotranspiration and 24.01% from the unsaturated zones. The high ET_g could be attributed to the presence of phreatophytes such as the *Acacia erioloba* and *Acacia haematoxylon* that can tap water up to 56 m depths and the presence of the *Prosopies sp* that abstract up to 50 l d^{-1} per tree (GGRETA 2016; Shadwell and February 2017). About 34.23% of P

is lost via exfiltration, which is further lost as surface evapotranspiration.

In the past, the Auob catchment was associated with many springs, as artesian basin. Due to the infestation of the *Prosopies sp*, the water table in this area has declined over time and streams disappeared as observed by other author (Alker 2008; GGRETA 2016; Shadwell and February 2017). High groundwater evapotranspiration (Table 11) explains that.

Potential natural recharge zones and available injection wells that can be used in artificial recharge scenario analysis in the Auob Catchment.

The declining water levels in the Auob Catchment can be reversed by use of intervention methods such as artificial recharge. Artificial groundwater recharge can help reduce, stop and/or reverse declining groundwater levels (Xu and Beekman 2003). This practices can additionally prevent saltwater intrusion in coastal aquifers (Asano 1985). Correspondingly, it lowers evaporation losses and improves groundwater quality (Xu and Beekman 2003). In arid environments, however, some implications are born in this mechanism resulting from spatial variation of recharge processes. As such, when implementing artificial recharge, it becomes essential to understand the natural recharge processes and aquifer losses. Similarly, understanding the flow rate, duration, channel characteristics, antecedent conditions, sediment texture, among other factors influencing infiltration process is also crucial (Sarma and Xu 2017). Artificial recharge depth misplacement could result in aquifer choking and, thus, an appropriate depth should be identified.
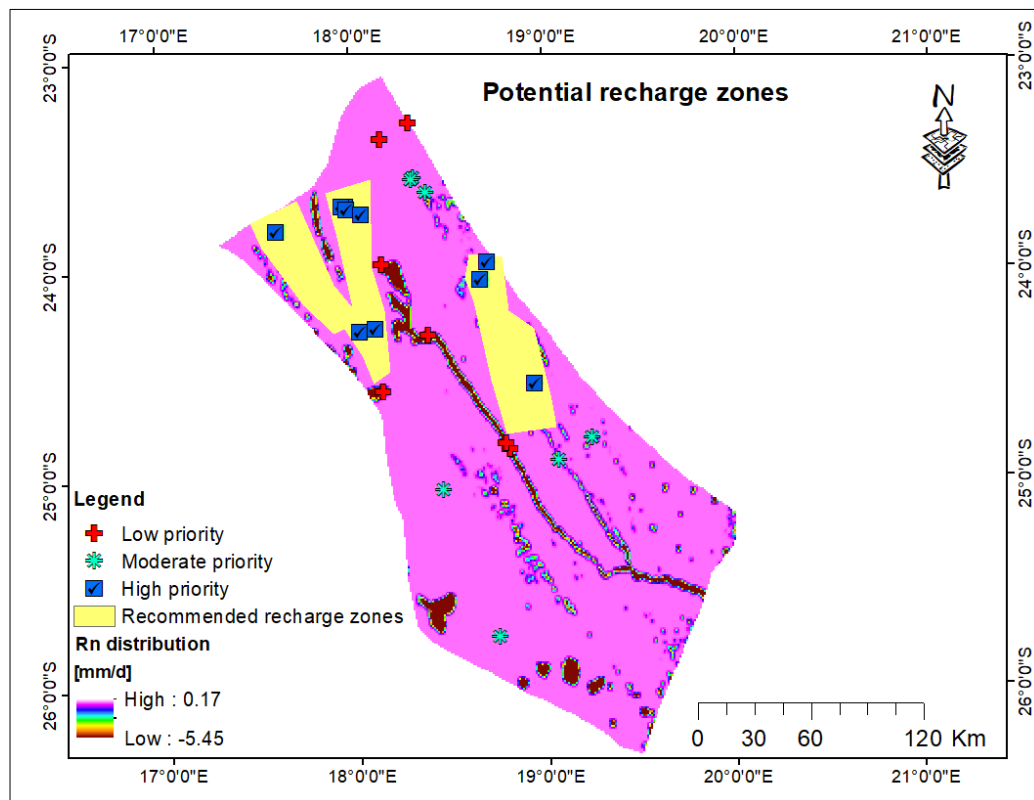
Figure 46: Recommended recharge potential zones and the borehole locations that have no abstraction taking place in them. The priority they can be given during artificial recharge scenario analysis based on the natural recharge distribution of the Auob Catchment.

The current study has to some extent accounted for the natural recharge processes that are associated with the Auob Aquifer and the areas that are prone to losses. Preliminary recharge zones have been identified,

further studies can be conducted in order to simulate the aquifer behaviour in response to injection wells. The injection wells are listed in their order of priority based on zones that are associated with high gross and net recharge. Figure 46 above indicates the zones that could be potential artificial recharge zones and the boreholes are already present in the area. The listed boreholes have no abstractions as indicated in Figure 25 of this study, due to the presence of this unused boreholes no further drilling is required. As the study area is dominated by the agricultural practices (Figure 25b) using 95% of the available water for irrigation, the available agricultural greenhouse roofs can be used for trapping water during the rainy seasons, as source of the water to be channelled to the identified potential injection wells and used to revive the declining water levels. The piezometers that are given low priority in this case as indicated in Figure 46 are either situated at a steep slope, in areas of high ET_{ss} or areas high exfiltration. The zones that are given high priority are associated with high gross and net recharge and fairly gentle slope. The final decision on the adaption of this zones will depend on the scenario analysis and on how the model respond to the injection wells. The proposed zones in this study are just a stepping stone or a recommendation for a detailed study and more detailed analysis need to be conducted.

4.3. Sensitivity analysis

Sensitivity analysis provide insight about model behaviour in response to changes in model parameters. Different parameters such as specific yield, hydraulic conductivity, initial water content, extinction depth and extinction water content caused the model respond differently in terms of gross net recharge, groundwater evapotranspiration, net recharge and groundwater exfiltration.
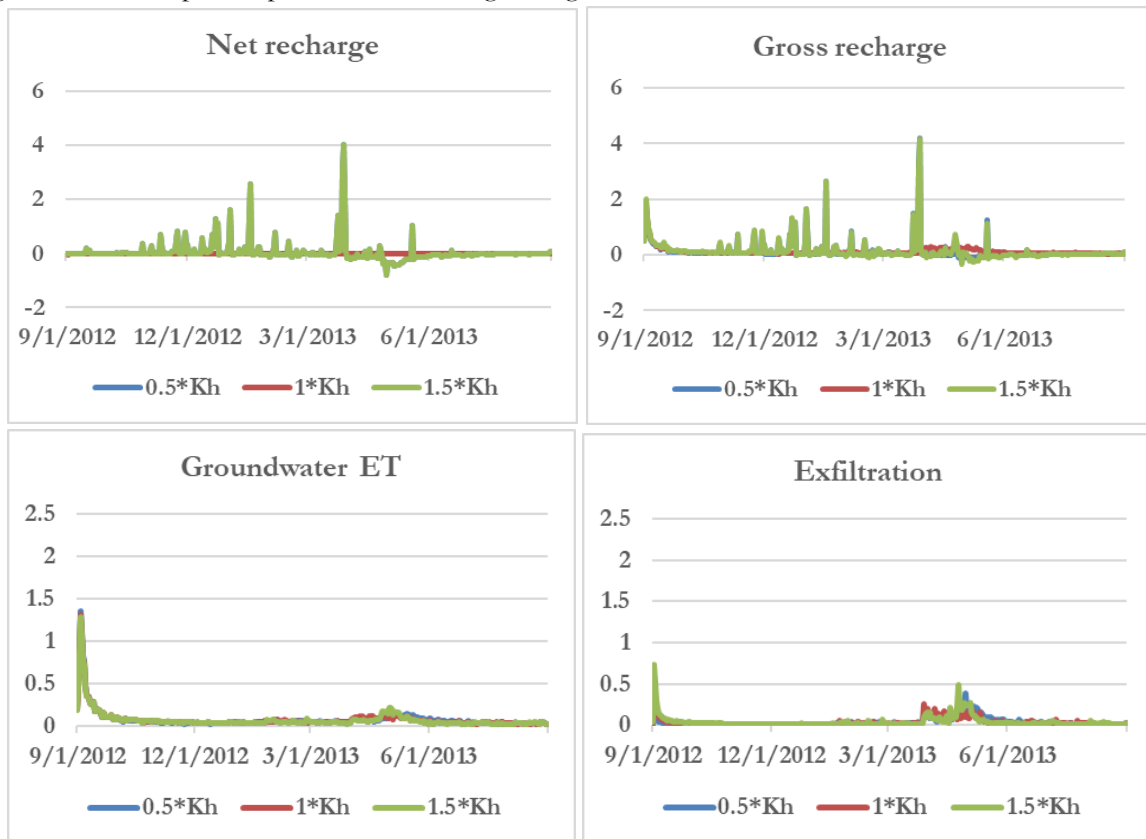

Figure 47: Sensitivity analysis of the hydraulic conductivity and response of groundwater fluxes to changes in hydraulic conductivity. For the remaining sensitivity maps please see in the appendix.

The increase of hydraulic conductivity have an effect on the net recharge as well as the gross recharge. While, not much variation is being notice on groundwater evapotranspiration. A temporal shit in the net peak of exfiltration is being depicted with increase in hydraulic conductivity. The decrease in hydraulic conductivity does not cause much variation in the groundwater fluxes. It should be noted that the sensitivity analysis was done in the middle of the model calibration with intensions of; understanding the response of the different fluxes in response to change in model parameters and the general model behaviour to changes in these parameters, in order to optimise the model calibration. The behaviour of the model fluxes in response to change in the remaining model parameters is indicated in Figure 50 of the appendix.

4.4. Model validation

Validation and verification are no longer critical elements in groundwater modelling. Due to many parameters that are involved in most field-based groundwater models recommended that all data available should be used in the calibration process, instead of splitting it. Thus generally groundwater model validation is not necessary (Anderson et al. 2015). This statement was further supported by Konikow, (2003) who says that model validation requires long-term monitoring data. Moreover, history matching is a bias for model validation, not to mention the parameter uncertainty associated with modelling and solution non-uniqueness. Thus "declarations of validation of a model is not meaningful". What could be verified is a new code or if any of the provided codes are modified. Otherwise, there is no need for code verification when already existing model codes are used. Since these code are already verified by the developers and their verification are usually present in user manuals. Due to the fact that groundwater model cannot make an accurate forecast, it cannot be validated. Thus it is recommended that the word validation should not be used in reference to the groundwater model (Anderson et al. 2015). Furthermore, groundwater models are embodiments of a scientific hypothesis, thus they cannot be proven or validated. even knowing that groundwater models are valuable tools for analyzing groundwater system their predictive accuracy is limited. The use of words like validation and verification are misleading and their use in groundwater modelling should be abundant for more meaningful model-based assessment descriptors (Konikow & Bredehoeft, 1992).

5. CONCLUSIONS AND RECOMMENDATIONS

5.1. Conclusions

The main purpose of the study was to assess groundwater recharge from precipitation and evaluate groundwater resources within the Auob Catchment. In order to achieve this there was a need to organize the hydrological data base of the system, conceptualize it, set up and calibrate a distributed numerical model and evaluate the spatio-temporal distribution of groundwater recharge and groundwater resources.

- The hydrogeological data base in the Auob Catchment consisted of in-situ data, archive data, ancillary data and satellite data. The integrated hydrological modeling, as it is typical for developing countries, also in this case was hampered by data availability. To overcome that challenge satellite products were incorporated into the study. The temporal continuity of the in-situ data (at least for a station) turned to be important in validating the satellite products.

- The Auob catchment was conceptualized as a single hydro-stratigraphic unit. It is a typical flow-through with an inflow boundary at the NW and outflow at the SE. Two no-flow boundaries were assigned at the SW and NE. For the inflow boundary a flow and head boundary (FHB) was used (as specified flux) the outflow boundary was simulated using the Drain package. The ability of this single unit to represent the reality is influenced by its parameterization and assigned boundary conditions.

- The presented IHM of the Auob Catchment is fully operational and convergent. However, the calibration of the presented model, due to the time constrain, should be continued as the model still involves substantial head discrepancy and the water exchange across that model still seems to be too large. These deficiencies are not only because of the time limitations and calibration challenge that turned to be very high, but also because the original data had to be reprocessed due to unacceptable errors and because of some calibration constraints that were associated with model non-convergence after 2 years 4 months, that left only a small amount of time to the final calibration process. This further affected the optimal parameterization of the UZF Package that in turn affected the behavior of the state variables.

- The success of the model to represent the state variable and reality, depends on parameterization of a model. Especially the UZF parameters as the they were noticed to have a great influence on how the model reacts and controls the response of heads and the amount of water available in the model. They also control weather the model is flooded with water or not especially the initial water contents. The UZF parameters also played an imported role in influencing the amount of water that was held or availed for evapotranspiration. The success of model calibration is depended on time availability and the quality of the data set.

- The temporal distribution of the groundwater fluxes in the Auob Catchment is depended on the model forcing and system parameterization. The years of high precipitation resulted in high effective precipitation that further triggered high gross recharge and evapotranspiration. It was noticed that there was a delayed response of gross recharge during the simulation period as

compared to the rainfall events. This could be linked to the slow pace at which the water infiltrates and percolates into the groundwater table, triggering a response in the rise of the water table. A similar trend was also noticed in the response of the attempted calibrated heads that were simulated by the model.

- In terms of the spatial distribution of groundwater resources it was noticed that evapotranspiration exfiltration and gross recharge are high along the fossil rivers. Due to the presence of deep rooted vegetation along the dry river beds that result in high evapotranspiration while the high exfiltration is a result of the relief depression along the fossil rivers, whereas, gross recharge could be a result of the temporal increase of the water levels and high soil moisture associated with this areas.

5.2.   Recommendation

- Care should be taken when conducting groundwater sampling as these data is of great importance to the evaluation of the model performance as this data is treated as the ground truth.

- The 1 km grid is course and can cause under representation of the heterogeneity that is associated with the model. When using super computers a finer grid can be recommended.

- It should be noted that the proposed artificial recharge zones are based on natural recharge distribution of the system and it is not known how the system will react to artificial groundwater recharge. Thus, scenario analysis need to be carried out in order to test the behavior of the aquifer to the presence of injection wells.

- In terms of groundwater management strategies in this area and how best to conserve this precious natural resource. The Auob Catchment is situated in a part of a larger transboundary (SAB) basin as narrated early in this study. Therefore, transboundary water resources management laws on the management water resource can be taken by the three countries and see how best they can partition this resource and sustainably use it.

LIST OF REFERENCES

Adane ZA, Nasta P, Zlotnik V, Wedin D (2018) Impact of grassland conversion to forest on groundwater recharge in the Nebraska Sand Hills. Journal of Hydrology: Regional Studies 15:171–183. doi: 10.1016/j.ejrh.2018.01.001

AghaKouchak A, Mehran A, Norouzi H, Behrangi A (2012) Systematic and random error components in satellite precipitation data sets. Geophysical Research Letters 39:n/a-n/a. doi: 10.1029/2012GL051592

Alker M (2008) The Stampriet Artesian Aquifer Basin A case study for the research project

Allen RG, Pereira LS, Raes D, Smith M (1998) Crop evapotranspiration-Guidelines for computing crop water requirements-FAO Irrigation and drainage paper 56

Anderson MP, Woessner WW, Hunt RJ (2015) Applied Groundwater Modeling : Simulation of Flow and Advective Transport. Elsevier Science & Technology

Anuraga TS, Ruiz L, Kumar MSM, et al (2006) Estimating groundwater recharge using land use and soil data: A case study in South India. Agricultural Water Management 84:65–76. doi: 10.1016/j.agwat.2006.01.017

Asano T (1985) Artificial Recharge of Groundwater. Elsevier Science

Baalousha HM (2016) Groundwater pumping versus surface-water take. Modeling Earth Systems and Environment 2:78. doi: 10.1007/s40808-016-0133-7

Bhatti H, Rientjes T, Haile A, et al (2016) Evaluation of Bias Correction Method for Satellite-Based Rainfall Data. Sensors 16:884. doi: 10.3390/s16060884

Condon LE, Maxwell RM (2015) Evaluating the relationship between topography and groundwater using outputs from a continental-scale integrated hydrology model. Water Resources Research 51:6602–6621. doi: 10.1002/2014WR016774

Corbett ES (1968) Rainfall interception by annual grass and chaparral . . . losses compared. Califonia

Dehotin J, Braud I (2008) Hydrology and Earth System Sciences Which spatial discretization for distributed hydrological models? Proposition of a methodology and illustration for medium to large-scale catchments. Hydrol Earth Syst Sci 12:769–796

Dembélé M, Zwart SJ (2016) Evaluation and comparison of satellite-based rainfall products in Burkina Faso, West Africa. International Journal of Remote Sensing 37:3995–4014. doi: 10.1080/01431161.2016.1207258

Dinku T, Chidzambwa S, Ceccato P, et al (2008) Validation of high-resolution satellite rainfall products over complex terrain. International Journal of Remote Sensing 29:4097–4110. doi: 10.1080/01431160701772526

El-Zehairy AA, Lubczynski MW, Gurwin J (2018) Interactions of artificial lakes with groundwater applying an integrated MODFLOW solution. Hydrogeology Journal 26:109–132. doi: 10.1007/s10040-017-1641-x

FAO (2016) AQUASTAT - FAO's Information System on Water and Agriculture. http://www.fao.org/nr/water/aquastat/countries_regions/Profile_segments/NAM-IntIss_eng.stm. Accessed 31 Jul 2018

February E, Shadwell E, Viljoen S, Hattas D (2017) Feeding choices and impacts of extralimital giraffe on two keystone tree species in the Kgalagadi National Park. Koedoe 59:. doi: 10.4102/koedoe.v59i1.1454

Francés AP, Lubczynski MW (2011) Topsoil thickness prediction at the catchment scale by integration of invasive sampling, surface geophysics, remote sensing and statistical modeling. Journal of Hydrology 405:31–47. doi: 10.1016/j.jhydrol.2011.05.006

García Petillo M, Castel JR (2007) Introduction Water balance and crop coefficient estimation of a citrus orchard in Uruguay

GGRETA (2015) Governance of Groundwater Resources in Transboundary Aquifers (GGRETA) project OVERVIEW AND RESULTS OF THE ASSESSMENT PHASE (2013-2015) International Hydrological Programme United Nations Educational, Scientific and Cultural Organization

GGRETA (2016) Stampriet Transboundary Aquifer System Assessment. Paris

Goudie A, Viles H (2015) Landscapes and Landforms of Namibia. Springer Netherlands, Dordrecht

Grinevskii SO (2014) The effect of topography on the formation of groundwater recharge. Moscow University Geology Bulletin 69:47–52. doi: 10.3103/S0145875214010025

Habib E, Haile A, Sazib N, et al (2014) Effect of Bias Correction of Satellite-Rainfall Estimates on Runoff Simulations at the Source of the Upper Blue Nile. Remote Sensing 6:6688–6708. doi: 10.3390/rs6076688

Haile AT, Habib E, Rientjes T (2013) Evaluation of the climate prediction center (CPC) morphing technique (CMORPH) rainfall product on hourly time scales over the source of the Blue Nile River. Hydrological Processes. doi: 10.1002/hyp.9330

Haitjema HM, Mitchell-Bruker S (2005) Are Water Tables a Subdued Replica of the Topography? Ground Water 0:050824075421008. doi: 10.1111/j.1745-6584.2005.00090.x

Harbaugh AW, Banta ER, Hill MC, Mcdonald MG (2000) MODFLOW-2000, THE U.S. GEOLOGICAL SURVEY MODULAR GROUND-WATER MODEL-USER GUIDE TO MODULARIZATION CONCEPTS AND THE GROUND-WATER FLOW PROCESS. CO 4 McDonald Morrissey Associates

Hassan SMT, Lubczynski MW, Niswonger RG, Su Z (2014) Surface–groundwater interactions in hard rocks in Sardon Catchment of western Spain: An integrated modeling approach. Journal of Hydrology 517:390–410. doi: 10.1016/j.jhydrol.2014.05.026

Hill MC, D'agnese FA, Faunt CC (1999) Guidelines for model calibration and application to flow simulation in the Death Valley regional groundwater system. In: Calibration and Reliability in Groundwater Modelling . IAHS Publ, Zurich, Switzerland

Jacobson PJ, Jacobson KM, Seely MK (1995) Ephemeral-rivers-and-their-catchments. Desert research foundation of Namibia, Windhoek

JICA (2002) DEPARTMENT OF WATER AFFAIRS MINISTRY OF AGRICULTURE, WATER AND RURAL DEVELOPMENT THE REPUBLIC OF NAMIBIA THE STUDY ON THE GROUNDWATER POTENTIAL EVALUATION AND MANAGEMENT PLAN IN THE SOUTHEAST KALAHARI (STAMPRIET) ARTESIAN BASIN IN THE REPUBLIC OF NAMIBIA

Joyce RJ, Janowiak JE, Arkin PA, Xie P (2004) CMORPH: A Method that Produces Global Precipitation Estimates from Passive Microwave and Infrared Data at High Spatial and Temporal Resolution

Kang Y, Wang Q-G, Liu H-J (2005) Winter wheat canopy interception and its influence factors under sprinkler irrigation. Agricultural Water Management 74:189–199. doi: 10.1016/j.agwat.2004.11.004

Kimani M, Hoedjes J, Su Z (2018) Bayesian Bias Correction of Satellite Rainfall Estimates for Climate Studies. Remote Sensing 10:1074. doi: 10.3390/rs10071074

Kipyegon S, Lubczynski, M W. Parodi G, Lekula M (2018) Modelling Groundwater Resources of Transboundary Okwa Basin. University of Twente

Knowling MJ, Werner AD (2017) Transient Recharge Estimability Through Field-Scale Groundwater Model Calibration. Groundwater. doi: 10.1111/gwat.12526

Konikow LF (2003) Validation of Groundwater Models: Meaningful or Meaningless? In: American Geophysical Union, Fall Meeting 2003, abstract id. H11E-0895. http://adsabs.harvard.edu/abs/2003AGUFM.H11E0895K. Accessed 27 Aug 2018

Konikow LF, Bredehoeft JD (1992) Ground-water models cannot be validated. Advances in Water Resources 15:75–83. doi: 10.1016/0309-1708(92)90033-X

Kozak JA, Ahuja LR, Green TR, Ma L (2007) Modelling crop canopy and residue rainfall interception effects on soil hydrological components for semi-arid agriculture. Hydrological Processes 21:229–241. doi: 10.1002/hyp.6235

Kumar CP (2015) Modelling of Groundwater Flow and Data Requirements

Le Maitre DC, Gush MB, Dzikiti S (2015) Impacts of invading alien plant species on water flows at stand and catchment scales. AoB Plants 7:plv043. doi: 10.1093/aobpla/plv043

Lekula M (2018) Multiple data sources and integrated hydrological modelling for groundwater assessment in the Central Kalahari Basin. University of Twente

Lekula M, Lubczynski MW, Shemang EM, Verhoef W (2018) Validation of satellite-based rainfall in Kalahari. Physics and Chemistry of the Earth, Parts A/B/C 105:84–97. doi: 10.1016/j.pce.2018.02.010

Li H, Si B, Li M (2018) Rooting depth controls potential groundwater recharge on hillslopes. Journal of Hydrology 564:164–174. doi: 10.1016/j.jhydrol.2018.07.002

Liu T, Lai J, Luo Y, Liu L (2015) Study on extinction depth and steady water storage in root zone based on lysimeter experiment and HYDRUS-1D simulation. Hydrology Research. doi:

10.2166/nh.2015.191

Lu N, Chen S, Wilske B, et al (2011) Evapotranspiration and soil water relationships in a range of disturbed and undisturbed ecosystems in the semi-arid Inner Mongolia, China. Journal of Plant Ecology 4:49–60. doi: 10.1093/jpe/rtq035

Marklund L, Wörman A (2007) The Impact of Hydraulic Conductivity on Topography Driven Groundwater Flow

MAWF (2000) Ministry of Agriculture, Water and Rural Development Strategic Water Resources Assessment: Theme Report

McMahon TA, Peel MC, Lowe L, et al (2013) Estimating actual, potential, reference crop and pan evaporation using standard meteorological data: a pragmatic synthesis. Hydrology and Earth System Sciences 17:1331–1363. doi: 10.5194/hess-17-1331-2013

Mehreteab YW, Lubczynski M. W, Becht R (2016) INTEGRATED NUMERICAL MODELING APPLYING STRATIFORM HYDROGEOLOGICAL CONCEPTUAL MODEL, SARDON CATCHMENT STUDY CASE, SPAIN

Mendelsohn, J. Jarvis, A. Roberts, C. and Robertson T (2002) Average and median annual rainfall - source data. Cape Town

Mulokoshi G (2016) REPUBLIC OF NAMBIA MINISTRY OF AGRICULTURE, WATER AND FORESTRY DIRECTORATE OF WATER RESOURCE MANAGEMENT DIVISION GEOHYDROLOGY STAMPRIET ALLOCATION REPORT

Muzylo A, Llorens P, Valente F, et al (2009) A review of rainfall interception modelling. Journal of Hydrology 370:191–206. doi: 10.1016/j.jhydrol.2009.02.058

Nicholson SE, Some B, Mccollum J, et al (2003) Validation of TRMM and Other Rainfall Estimates with a High-Density Gauge Dataset for West Africa. Part II: Validation of TRMM Rainfall Products

Niswonger RG, Panday, Sorab. Motomu I (2006) MODFLOW-NWT, A Newton Formulation for MODFLOW-2005 Section A, Groundwater Book 6, Modeling Techniques Groundwater Resources Program

Niswonger RG, Panday S (2011) MODFLOW-NWT, A Newton Formulation for MODFLOW-2005 Section A, Groundwater Book 6, Modeling Techniques Groundwater Resources Program

Niswonger RG, Prudic DE, Regan RS (2006) Documentation of the Unsaturated-Zone Flow (UZF1) Package for Modeling Unsaturated Flow Between the Land Surface and the Water Table with MODFLOW-2005 Section A, Ground Water, of Book 6, Modeling Techniques

Obakeng OT (2007) Soil moisture dynamics and evapotranspiration at the fringe of the Botswana Kalahari, with emphasis on deep rooting vegetation. Vrije Universiteit

OBASECOM (2009) 551Final Report. Gaborone

Rahmawati N, Lubczynski MW (2018) Validation of satellite daily rainfall estimates in complex terrain of Bali Island, Indonesia. Theoretical and Applied Climatology 134:513–532. doi: 10.1007/s00704-017-2290-7

Sarma D (2016) Assessment of sustainable groundwater utilization with case studies from semi-arid Namibia

Sarma D, Xu Y (2017) The recharge process in alluvial strip aquifers in arid Namibia and implication for artificial recharge. Hydrogeology Journal 25:123–134. doi: 10.1007/s10040-016-1474-z

Scanlon BR, Reedy RC, Stonestrom DA, et al (2005) Impact of land use and land cover change on groundwater recharge and quality in the southwestern US. Global Change Biology 11:1577–1593. doi: 10.1111/j.1365-2486.2005.01026.x

Searchy JK, Hardison CH (1960) Double-Mass Curves; Manual of hydrology. General surface water techniques USGeology Survey Part 1:

Serviresa (2018) Namibia Sentinel2 Land Use Land Cover 2016 — GeoNode. http://geoportal.rcmrd.org/layers/servir%3Anamibia_sentinel2_lulc2016. Accessed 2 Dec 2018

Shadwell E, February E (2017) Effects of groundwater abstraction on two keystone tree species in an arid savanna national park. PeerJ 5:e2923. doi: 10.7717/peerj.2923

Shah N, Nachabe M, Ross M (2007) Extinction Depth and Evapotranspiration from Ground Water under Selected Land Covers. Ground Water 45:329–338. doi: 10.1111/j.1745-6584.2007.00302.x

Smith S, Conradie L, Van Eeden B, et al (2014) Kalahari Gemsbok National Park Park Management Plan

Stampoulis D, Anagnostou EN, Nikolopoulos EI (2013) Assessment of High-Resolution Satellite-Based Rainfall Estimates over the Mediterranean during Heavy Precipitation Events. Journal of

Hydrometeorology 14:1500–1514. doi: 10.1175/JHM-D-12-0167.1

Stone A, Edmunds W (2012) Sand, salt and water in the Stampriet Basin, Namibia: Calculating unsaturated zone (Kalahari dunefield) recharge using the chloride mass balance approach. Water SA 38:. doi: 10.4314/wsa.v38i3.2

Strohbach BJ (2008) Mapping the major catchments of Namibia BIOTA-South View project Southern African Science Service Centre for Climate Change and Adaptive Land Management (SASSCAL) - Work package: "Climate data management" View project MAPPING THE MAJOR CATCHMENTS OF NAMIBI

Sutron (2015) Tipping Bucket Rain Gauge 5600-0525. http://labcocomunicaciones.com/resourceUSERCONTENT/catalogos-productos/pluviometro-0525-catalogo.pdf. Accessed 21 Dec 2018

Tashiro Y (2017) Infiltration Rate of Groundwater in Vadose Zone of Uplifted Carbonate Island. American Journal of Water Science and Engineering 3:61. doi: 10.11648/j.ajwse.20170305.12

Teketel AT, Lubczynski MW, Vekerdy Z (2017) INTEGRATED HYDROLOGICAL MODELING OF SURFACE-GROUNDWATER INTERACTIONS The case of Denpasar-Tabanan Basin in the Southern Bali Island. University of Twente

Toba T, Ohta T (2008) Factors affecting rainfall interception determined by a forest simulator and numerical model. Hydrological Processes 22:2634–2643. doi: 10.1002/hyp.6859

Trigo IF, Debruin H (2016) VALIDATION REPORT Reference Evapotranspiration METREF (LSA-303)

Tweed SO, Leblanc M, Webb JA, Lubczynski MW (2007) Remote sensing and GIS for mapping groundwater recharge and discharge areas in salinity prone catchments, southeastern Australia. Hydrogeology Journal 15:75–96. doi: 10.1007/s10040-006-0129-x

Van Der Linden W (2010) Rainfall interception by buildings for urban hydrology modeling. Eindhoven University of Technology

Van Dijk IJMA, Gash JH, van Gorsel E, et al (2015) Rainfall interception and the coupled surface water and energy balance. 402–415. doi: 10.1016/j.agrformet.2015.09.006

World Soil Resources (2006) World reference base for soil resources 2006 International Union of Soil Sciences. Rome

Xu Y, Beekman HE (2003) Groundwater Recharge Estimation in Southern Africa Edited by Printed in Cape Town

6. APPENDIX

Pearson correlation for the validation of ET_o;

$$r = \frac{\sum(x - \bar{x})(y - \bar{y})}{\sqrt{\sum(x - \bar{x})^2 \sum(y - \bar{y})^2}}$$

$$r = \frac{6691.38}{\sqrt{7566.54 * 8083.30}}$$

$$r = 0.8556$$

Head and flow boundary that was used for the specification of flux into the model domain;
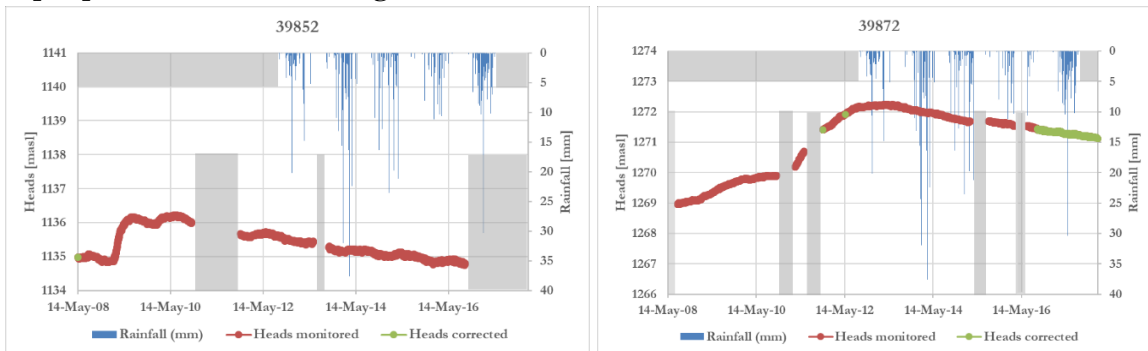
$$Q = K * A * I$$

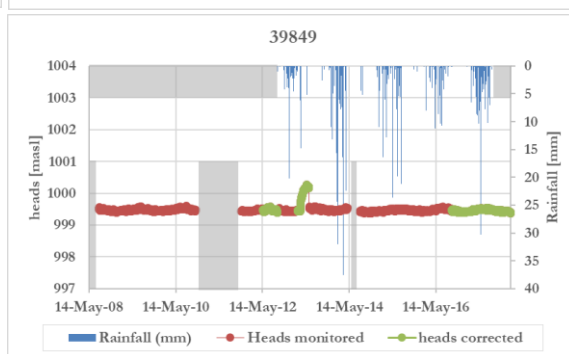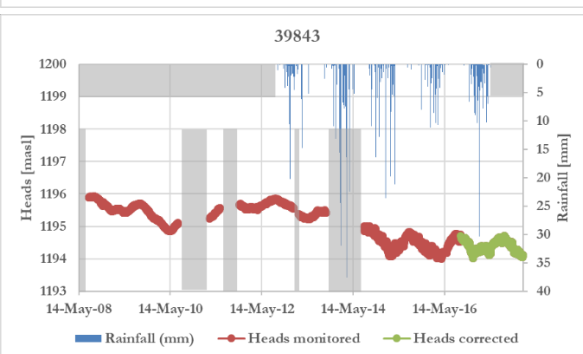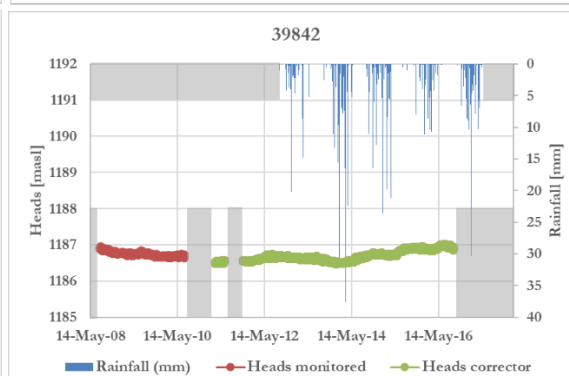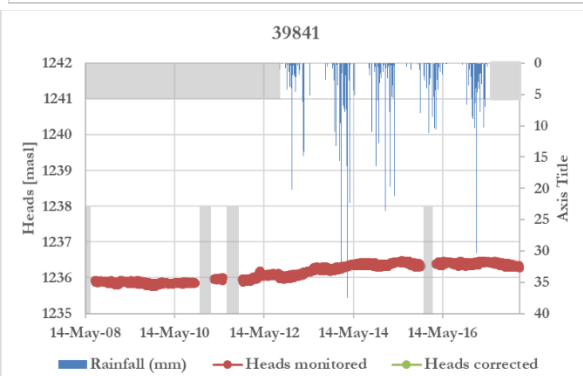$$Q = K * \left(W_i * \frac{h_1 + h_1}{2}\right) * \frac{\Delta h}{L}$$

$$Q = 0.006 * \left(1000 * \frac{150}{2}\right) * \frac{1350 - 1340}{11000}$$

$$Q = 0.409 \text{m}^3\text{d}^{-1}$$

Simulated (Sim) vs observed (Obs) heads and the model performance evaluation calculation.

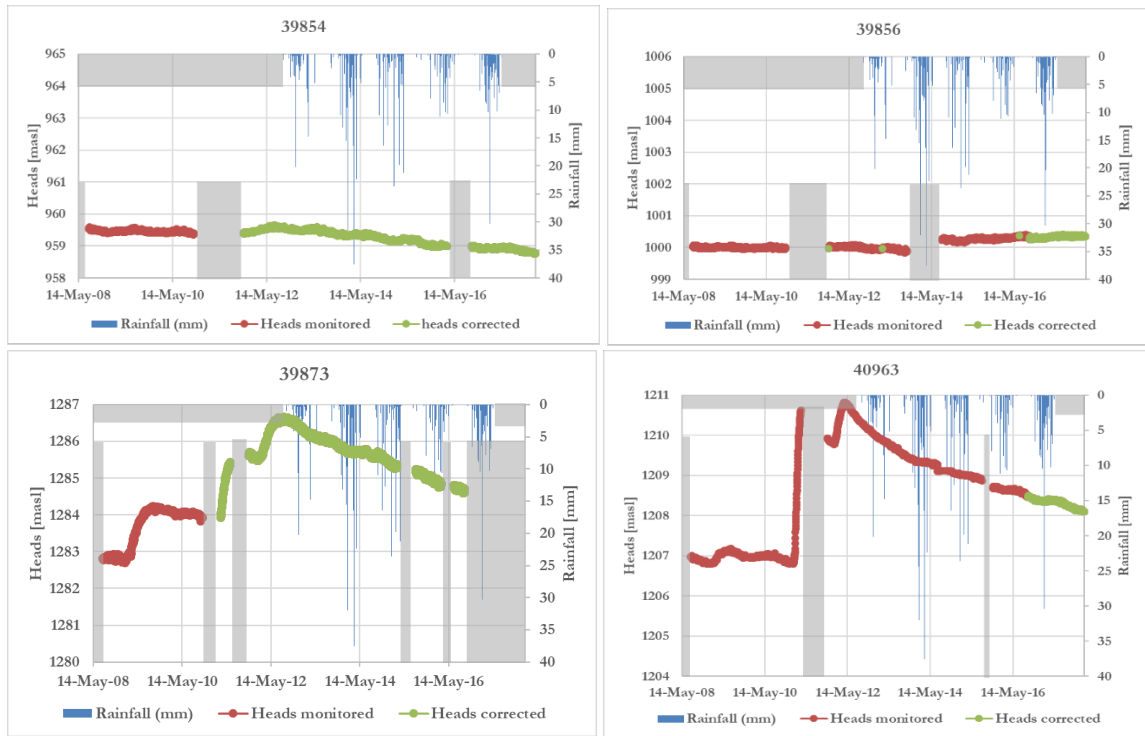**Input piezometers used during the model calibration**
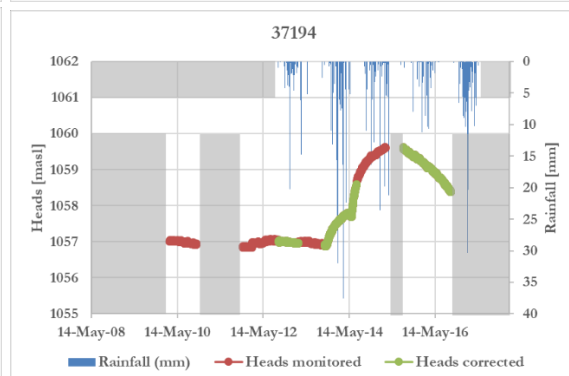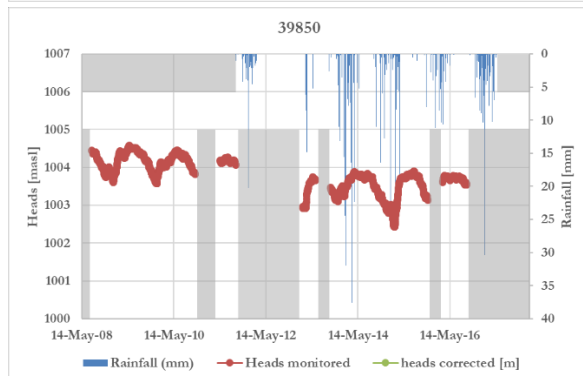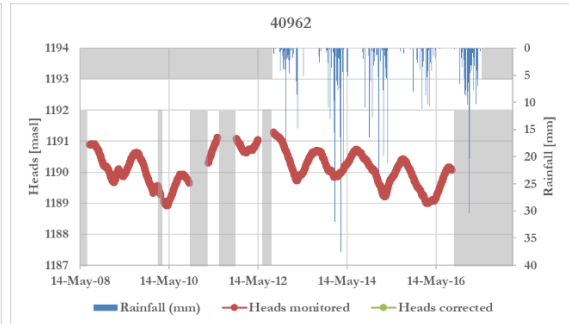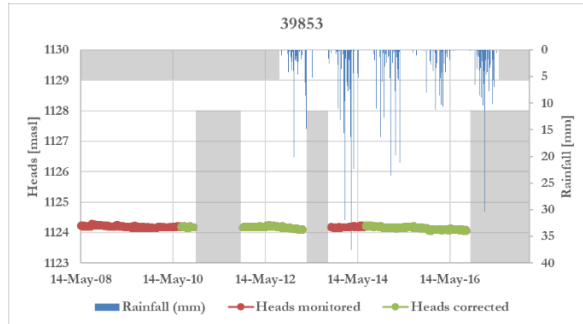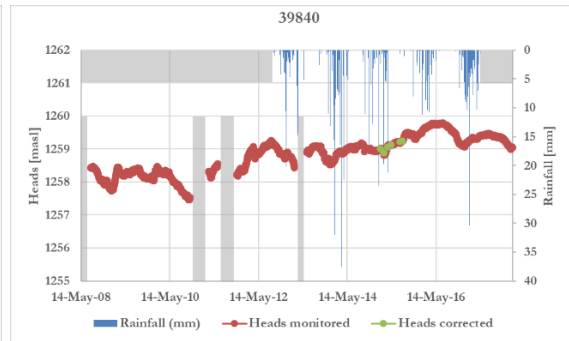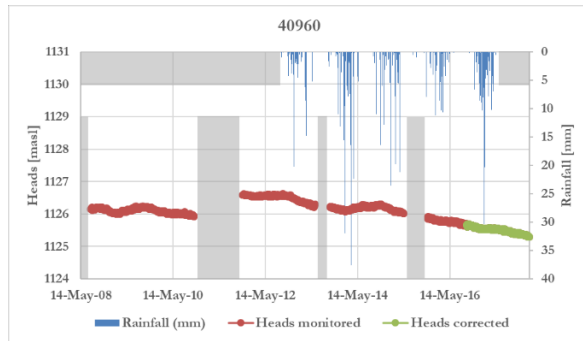
Figure 48: Piezometric heads for the different monitoring boreholes within the Auob Catchment from 14 May 2008 to 14 November 2017 that were used during the calibration of the model.

Land cover variation from the beginning of simulation to end of simulation based on NDVI.
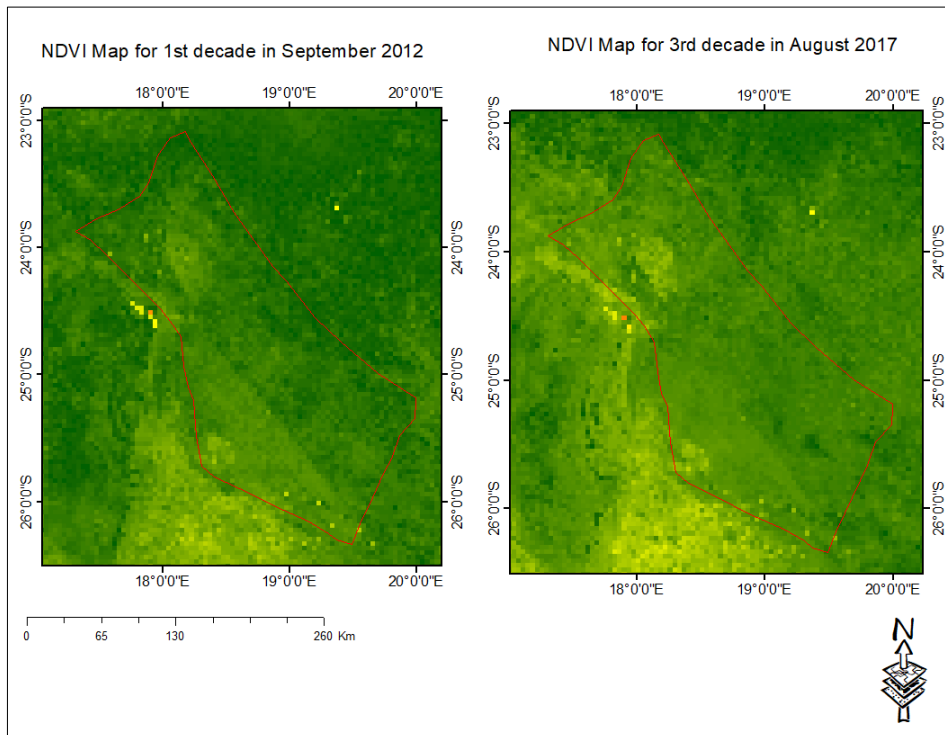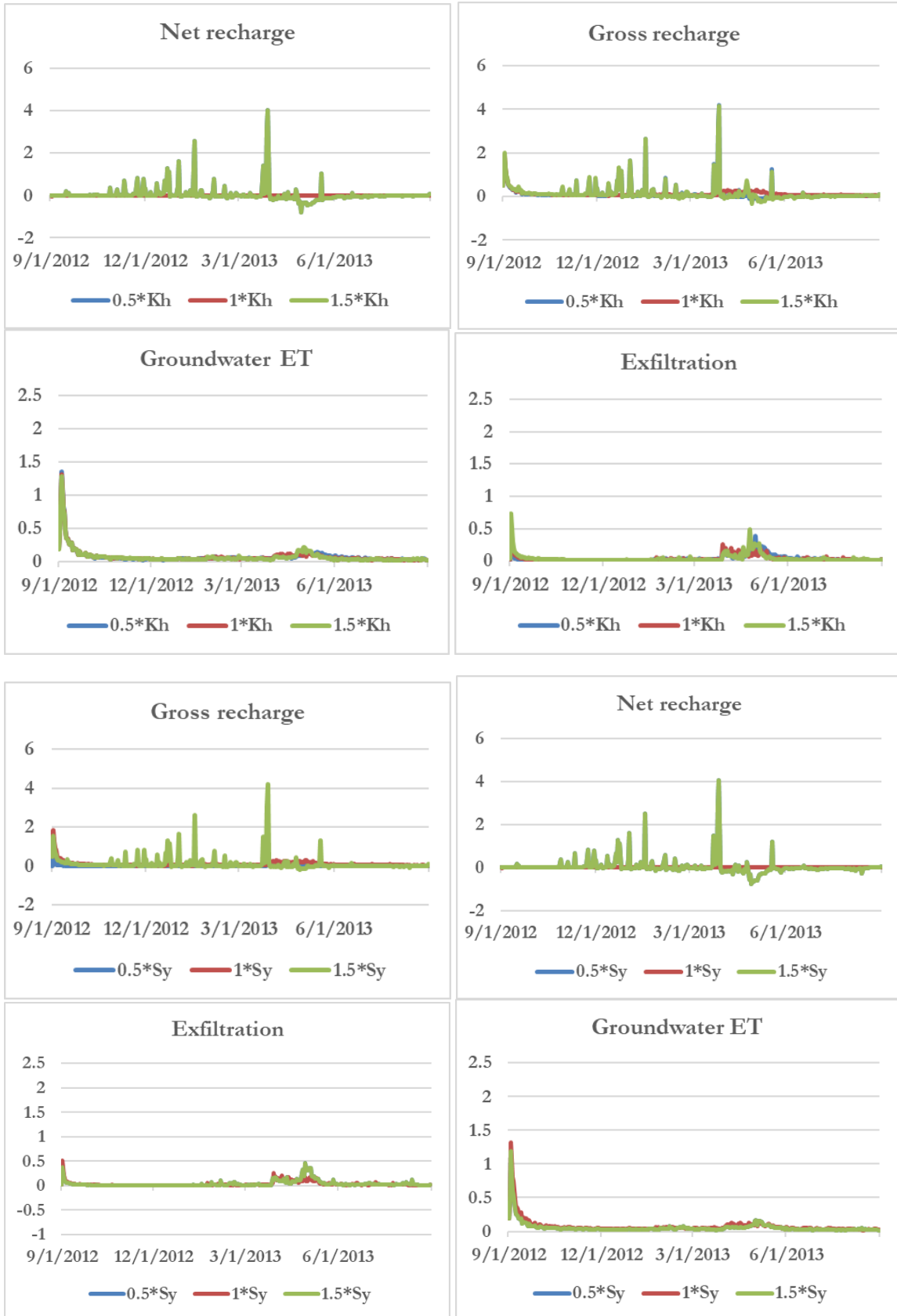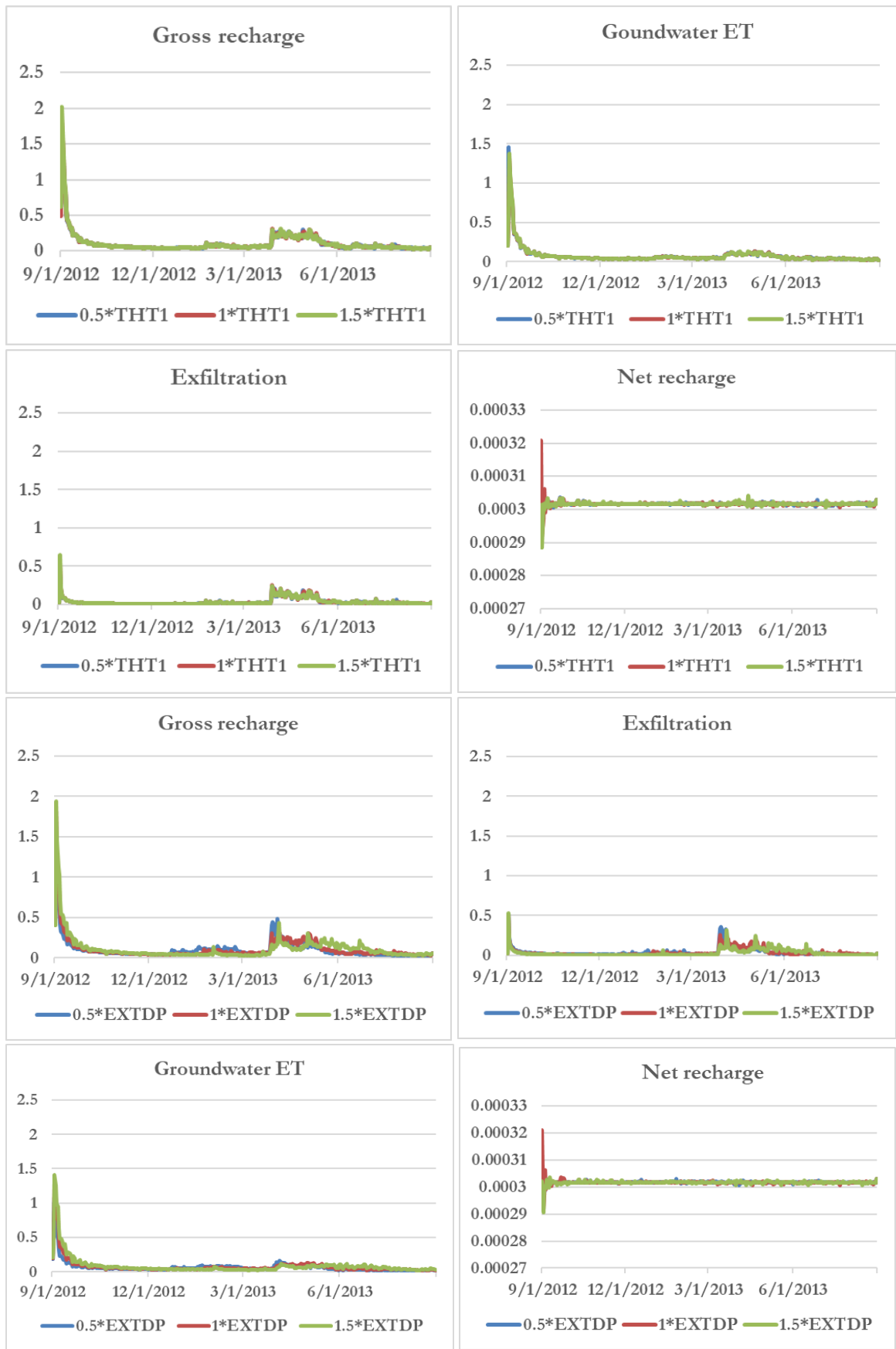

Figure 49: NDVI maps for the beginning and end of the 5 year simulation period conducted during the study. There is no much variation in terms of landcover thus the 2016 map was used during the study period.

Response of different fluxes to the sensitivity analysis

Gross recharge · Groundwater ET · Exfiltration · Net recharge (THT1 sensitivity: 0.5*THT1, 1*THT1, 1.5*THT1)

Gross recharge · Exfiltration · Groundwater ET · Net recharge (EXTDP sensitivity: 0.5*EXTDP, 1*EXTDP, 1.5*EXTDP)
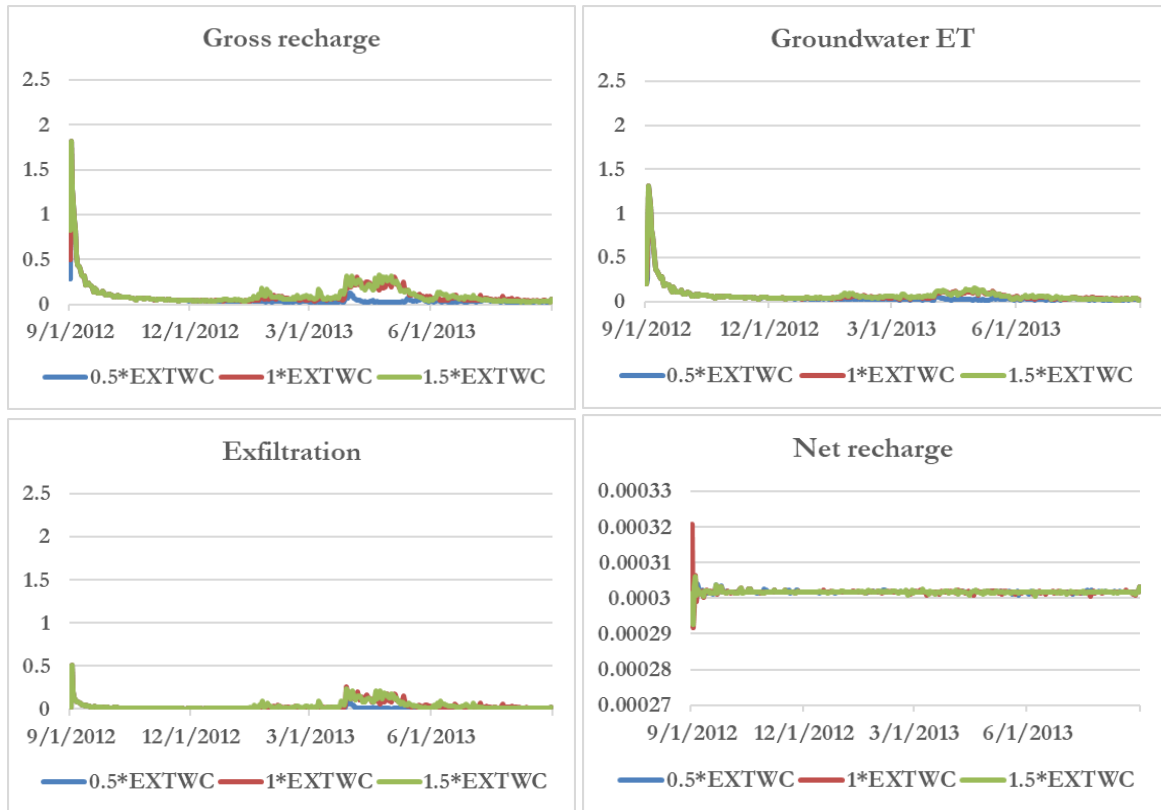
Figure 50: Sensitivity analysis figures. The figures depict the response of model fluxes to changes in different model parameters. This was carried out during the calibration period in an attempted to understand how the model reacts to changes in model parameters and to find means on how to effectively calibrate the model.